FHWA-NJ-2003-016

Development of High-Performance Concrete for Transportation Structures in New Jersey

FINAL REPORT
August 2003

Submitted by

Hani Nassif, Ph.D., P.E.
Assistant Professor

Nakin Suksawang, Ph.D. Candidate
Research Assistant

Dept. of Civil & Environmental Engineering
Center for Advanced Infrastructure & Transportation (CAIT)
Rutgers, The State University of New Jersey
Piscataway, NJ 08854-8014

NJDOT Research Project Manager
Anthony Chmiel

In cooperation with

New Jersey
Department of Transportation
Division of Research and Technology
and
U.S. Department of Transportation
Federal Highway Administration

Disclaimer Statement

"The contents of this report reflect the views of the author(s) who is (are) responsible for the facts and the accuracy of the data presented herein. The contents do not necessarily reflect the official views or policies of the New Jersey Department of Transportation or the Federal Highway Administration. This report does not constitute a standard, specification, or regulation."

TECHNICAL REPORT STANDARD TITLE PAGE

1. Report No.	2.Government Accession No.	3. Recipient's Catalog No.
FHWA-NJ-2003-016		

4. Title and Subtitle	5. Report Date
Development of High Performance Concrete for Transportation Structures in New Jersey	August 2003
	6. Performing Organization Code: CAIT/Rutgers

7. Author(s)	8. Performing Organization Report No.
Hani Nassif and Nakin Suksawang	FHWA-NJ-2003-016

9. Performing Organization Name and Address	10. Work Unit No.
Dept. of Civil & Environmental Engineering Center for Advanced Infrastructure & Transportation (CAIT) Rutgers, The State University of New Jersey Piscataway, NJ 08854	11. Contract or Grant No.

12. Sponsoring Agency Name and Address		13. Type of Report and Period Covered
New Jersey Department of Transportation PO 600 Trenton, NJ 08625	Federal Highway Administration U.S. Department of Transportation Washington, D.C.	Final Report 1-01 to 8-03 14. Sponsoring Agency Code

15. Supplementary Notes

16. Abstract

The primary objective of this research is to identify high performance concrete (HPC) mix proportions that are suitable for transportation infrastructure in New Jersey. Two classes of concrete with compressive strengths ranging from 6 to 12 ksi are developed. Extensive information is available in the literature covering various aspects of HPC. Show case projects have been built in a number of northeast states including New Hampshire and Virginia. The research plan involves: (i) review of existing information, (ii) selection of mix proportions suitable for New Jersey using local aggregates and the proportions in Class A concrete, (iii) evaluation of trial mixes prepared in the laboratory and at least one ready-mix industry, (iv) evaluation of mechanical and long-term properties, and (v) preparation of specifications for the implementation of HPC in future projects.

17. Key Words	18. Distribution Statement
High Performance Concrete, Durability, Silica Fume, Fly Ash	

19. Security Classif (of this report)	20. Security Classif. (of this page)	21. No of Pages	22. Price
Unclassified	Unclassified	124	

Form DOT F 1700.7 (8-69)

Acknowledgements

The authors would like to thank the New Jersey Department of Transportation (NJDOT) as well as Tony Chmiel, NJDOT project manager, Jose Lopez, Nick Vitillo, and Eileen Connelly, for their help and assistance during the period of the project. Also, the assistance of students Kevin Robine, Maqbool Mohamad, David Fusco, Pat Jameison, Amer Mohamad, and Joe Davis is thankfully acknowledged.

TABLE OF CONTENTS

LIST OF FIGURES

LIST OF FIGURES (CONT.)

LIST OF FIGURES (CONT.)

LIST OF FIGURES (CONT)

LIST OF TABLES

SUMMARY

The primary objective of this research is to identify high performance concrete (HPC) mix proportions that are suitable for transportation infrastructure in New Jersey. HPC with compressive strengths ranging from 6 to 12 ksi were developed. Mineral and chemical admixtures were used to develop the HPC mixes. The mineral admixtures were added as cement replacements (by weight) to enhance the durability of concrete and they consisted of silica fume, Class F fly ash, and granulated blast-furnace slag. As for the chemical admixtures, superplasticizer and air entraining agent were also used to obtain good workability and freeze-thaw resistance, respectively.

The research involved (1) review of existing information, (2) development of mix proportions suitable for New Jersey using local aggregates, (3) evaluation of concrete properties, (4) determinant of the effect of various curing methods on early-age and long term performance, and (5) preparation of standard specifications. The review of the existing information consisted of extensive literature reviews on HPC. These literature reviews are summarized in the literature review section of this report. The development of mix proportions, evaluation of concrete properties, and determinant of the effect of various curing methods, are all described in more detail in the research approach section. The properties that are investigated include compressive strength; modulus of elasticity, early-age (autogenous) and drying shrinkage, creep due to compressive load, rapid chloride permeability, scaling, and freeze-thaw. The results of these tests are used for developing standard specifications and recommendations that are summarized in the conclusions and recommendations section.

INTRODUCTION

For many years, scientists and engineers have been improving on the development of concrete technology. Concrete is no longer a simple material that only includes cement, water, and aggregates but a more involved mixture. Many pozzolanic materials (such as silica fume, and fly ash) and chemical admixtures (such as superplasticizer and air entraining agent) are being added to improve the quality of the concrete. Part of this is because of the growing number of deteriorating bridge decks in the northeastern region of the United States where the concrete decks are more prone to a chemical attack from deicing salt. The transition from the cold to hot environment is also another cause of the deterioration of concrete in this region. Hence compressive strength no longer constitutes the only criterion in specifying the concrete, but other factors, such as durability, become more pronounced. HPC has been developed to highlight the durability of concrete.

Scope of the Study

The main objective of this research is to develop HPC mixes using resources readily available in New Jersey. Both mineral and chemical admixtures were used to develop the HPC mixture. The mineral admixture consisted of silica fume, Class F fly ash, and granulated blast furnaces slag. Chemical admixture, superplasticizer and air entraining agent, is also added to obtain good workability and freeze-thaw resistant, respectively. In the development of the mix design, the performance of the concrete is evaluated by measuring its mechanical and durability properties. These properties include compressive strength; modulus of elasticity, early-age (autogenous) and drying shrinkage, creep due to compressive load, rapid chloride permeability, scaling, and freeze-thaw. The results of these tests are used for developing specification and recommendation.

Furthermore, HPC curing practices are also included in this study because poor curing practices may adversely affect both the mechanical and durability performance of HPC. The general curing practices discussed in this study include moist or wet curing; air-dry curing; seal curing by coating the concrete with curing compound, and curing with wet burlap.

General Background

There are many definitions for HPC but one quality that is recognized by all professional organization is durability. HPC must exhibited high durability and therefore HPC usually contained mineral and chemical admixtures. In order to comprehend the used of these admixtures, one must understand the microstructure of concrete. The microstructure of concrete may be divided into three main components—hydrate cement paste, aggregate particles, and the transition zone.

The hydrate cement paste contributes to about 50 to 60 percent of the volume of concrete. It consists of the calcium silicate hydrates (CSH) gel. The main compounds of the CSH gel are tricalcium silicate (C_3S) and dicalcium silicate (C_2S). The CSH gel affects the strength of concrete. The high early strength of concrete results from a higher percentage of C_3S. On the other hand, the later strength gain depends on the percentage of C_2S, provided that there is a presence of water, i.e. moist cured. CSH gel is also the main compound for determining concrete durability since this is the strong bond between aggregate and cement paste it prevent penetration of water or chemical into the concrete.

Aggregate particles of concrete often play a minor role in concrete; they usually influence the modulus of elasticity of concrete. However, for concrete with a low water-to-cement ratio (w/c), they play a bigger role in the mechanical properties of the concrete. Because of the combination of a higher bonding strength between aggregates and hydrate cement paste and weaker fracture strength of aggregates, the concrete fracture strength formerly controlled by the hydrated cement paste is now controlled by the fracture strength of aggregates. In addition, for aggregates with a high alkaline silica reactant, the durability of concrete will be controlled by the reactivity of the aggregates.

The transition zone is a weak link between the aggregate particles and the hydrate cement paste. It is composed of a thin layer of hydrate cement paste. The weakness of the transition zone is linked to the migration of water from aggregates; this water locally increases the w/c ratio and forms calcium hydroxide [$Ca(OH)_2$]. $Ca(OH)_2$ is a relatively weak compound that could be easily attacked by acidic material such as sulfate. Therefore, it is important to eliminate $Ca(OH)_2$ in concrete.

The voids constitute another component that influences the strength and durability of concrete. The voids in concrete could be divided into two types—capillary voids and air voids. Capillary voids are created by the evaporation of excess water in concrete. They are usually found in concrete with a high w/c ratio. Air voids can be classified as either entrap or entrain air in concrete. Entrap air voids are trapped air in concrete created by a poor consolidation process. These voids are usually larger in size and could lead to the premature failure of concrete. On the other hand, air entrain voids are small air voids purposely placed in concrete to resist freezing and thawing.

Pozzolan

Pozzolan by definition is a siliceous or siliceous and aluminous material, which in the presence of moisture chemically reacts with $Ca(OH)_2$ to form strong cementing material (CSH-gel). Hence, pozzolans reduce the weak bonds in concrete, making the concrete stronger, decreasing permeability, and increasing its durability against chemical attack. These materials include fly ash, rice husk ash, silica fume, and granulated blast-furnace slag. Only fly ash and silica fume will be discussed extensively because the mix designs in this study are developed using these two pozzolanic materials.

Fly Ash

Fly ash is considered a pozzolanic material because it is composed of a high portion of silica and alumina that react with $Ca(OH)_2$ to form cementitious material. Fly ash has fine particles with sizes ranging from 1 to 100 μm. The average size of fly ash is in the range of 9 to 15 μm. Fly ash could be divided into two categories.

The main difference between them is the calcium contents or, more specifically, the lime (CaO) contents. The first category is referred to as high-calcium fly ash, which contains between 15 to 35 percent of CaO. This ash is generally obtained from the combustion of lignite and bituminous coals. The ASTM C 618 [1] also refers to it as Class C fly ash. The second category is low-calcium fly ash, which usually contains less than 5 percent of CaO. Low-calcium fly ash is a product of the combustion of anthracite and bituminous coals. The ASTM C 618 specifies it as Class F fly ash. Besides the difference in calcium contents, high-calcium fly ash also contains a lower amount of unburned carbon. It usually contains less than 2 percent whereas low-calcium fly ash contains between 2 to 10 percent.

Because of the difference in calcium content, the reactivity between the two types of fly ash is different. Low-calcium or Class F fly ash is less reactive and needs about 2 weeks to hydrate. Its reactivity depends largely on the composition and mineralogy of portland cement, as well as the fly ash particle size. The finer the size of the particles, the more reactive the ash becomes. The optimum size of the particle for Class F fly ash is 10 μm. The fine particle also contains a lower amount of carbon. On the other hand, high-calcium or Class C fly ash is more reactive and needs about 3 days to hydrate. In some cases it could be reactive enough to possess hydraulic properties.

Effect of Fly Ash on Fresh Concrete

The effect of fly ash on fresh or hard concrete depends on the composition, fineness, and consistency of the fly ash. The high level of variation in fly ash composition from different sources creates a problem. Fly ash is an industrial by-product, or in other words, it is the waste product collected during the coal combustion; therefore no quality control exists for the ash added to concrete. The quality control is also very hard to achieve because of the irregularity of the power consumption throughout the days and from place to place. Today, some suppliers treat and classify fly ash used in concrete to improve the quality of fly ash.

One of the most important characteristics of freshly mixed concrete is the water requirement of the matrix. Concrete containing fly ash will either increase or decrease the water requirement of concrete. Researchers generally agree with Minick et al [2] that the increase or decrease in the water requirement is based on the loss of ignition or carbon content and the fineness of fly ash. The increase in the water requirement of concrete could be explained by the absorption of moisture by carbon particles and the interference between coarse fly ash particles, as well as the aggregates that cause the matrix to be more viscous. Therefore, some low-calcium or Class F fly ash could decrease the flow ability of concrete because the carbon content could be as high as 12 percent. Notably, the high carbon content in fly ash is caused by the large and coarse particles in fly ash.

The lower water requirement phenomenon of fly ash is debatable. However, one widely accepted explanation is the increase in paste volume [3]. The paste volume increases because in practice fly ash is added to the mix as a portland cement replacement by weight and not by volume. Because portland cement is denser than fly ash, the volume of the paste increases; this contributes to the increase in flow ability. Also, fly ash particles, which are smooth and spherical in shape, act as a ball bearing between the cement particles; this increases the workability and mobility of the concrete.

Another factor that effects the water requirement of fly ash is its particle size. Fly ash with a small particle size improves the workability as well as the quality of fly ash [7, 23]. Fly ash with a small particle size contains higher volume of both the glass contents and spherical particles. Thus it reduces superplasticizer, improves workability, and improves the strength development of concrete. Fly ash with a nominal size of 10 micron or less performs the best.

Bleed-water is another important characteristic of fresh concrete. Excessive bleeding could cause segregation and delamination of the top layer of the concrete if the bleed-water is accidentally added to the top surface of fresh concrete during the finishing process. However, if the concrete is not allowed to bleed, plastic shrinkage could occur on a hot windy day. Plastic shrinkage is easily solved by proper protection of the finished concrete; therefore, less bleed-water is warranted. Both Class C and F fly ash decrease the bleed-water in concrete by introducing fine particles that flocculate and obstruct its flow. Class C fly ash reduces the bleed water more than Class F fly ash [18].

Hydration is the chemical reaction between cement and water or (for HPC) mineral admixtures and water. When concrete hydrates it dissipates heat; this is called the heat of hydration. Heat of hydration is very important because, when excessive in concrete, it could lead to thermal cracking. Thermal cracking occurs when the thermal expansion of concrete is greater than its tensile strength. Fly ash reduces the heat of hydration in concrete. This is a result of the slow reaction between the pozzolan (SiO_2, Al_2O_3) and calcium hydroxide ($Ca(OH)_2$). Because of this low heat of hydration, fly ash is often used for mass concrete or as a substitution for Type II and IV portland cement. On the other hand, its slow reaction retards the setting time of concrete [see reference 2, 3, 4, and 5].

The retardation caused by fly ash could be as high as 200 percent more than regular concrete. It depends on the composition, as well the quantity, of fly ash being added to the cement. This is usually the case in the event that low-calcium or Class F fly ash with high carbon content is used to replace a portion of portland cement.
The opposite is also true; in high-calcium or Class C fly ash, the composition could be reactive, leading to a quickly set concrete. Despite the slower setting time, it is still within the 8-hour limit set by ASTM C150[1].

Another factor that effect fly ash concrete at the plastic stage is curing. Killoh et al look at the influence of curing at different relative humidity on the hydration and porosity of a portland/fly ash paste [29]. They use small samples of portland/fly ash (70/30) paste with water binder ratio of 0.59, initially cured for 7 days and then exposed to different relative humidity. At 28 and 91 days a thermogravimetry and methanol absorption are performed to measure the reaction and porosity. The test result shows that the pozzolanic reaction falls when the relative humidity is below 80 percent. The porosity of concrete despite falls slightly under saturated condition, the large diameter porosity is 3 times higher under drying condition than saturated condition. Therefore the relative humidity must be kept at 95 percent, at least in the early curing age, in order to decrease the porosity in concrete.

Effect of Fly Ash on Mechanical Properties of Concrete

The compressive strength of concrete containing fly ash is generally lower than that of regular concrete, especially in its early ages [see reference 3, 11, 16, 17, and 18]. The 1-day strength of concrete containing fly ash could be as low as 50 percent of the 1-day strength of regular concrete. This is more prominent when using low-calcium or Class F fly ash because the rate of the alkaline-to-silica reaction is slower. As for high-calcium or Class C fly ash, the results are two-fold depending on the reactivity of the lime particles in the ash. If the lime content is highly reactive, the compressive strength could be higher than regular concrete even at 1 day and vise verse [18]. Despite the lower early-age compressive strength of fly ash concrete, the long-term compressive strength for both low- and high-calcium fly ash is comparable with regular concrete after 90 days; this is because of the late (usually after 2 weeks) hydration of fly ash. Both laboratory and field data confirm the long-term strength increase of fly ash. Dunstan et al have investigated the long-term effect of concrete with a high volume of fly ash by coring samples from different 10-year-old concrete pavements in the United Kingdom [6]. They established that the concrete strength is still increasing. In some cases the strength increases up to 50 percent higher that obtained at 28 days.

Because of the early-age strength reduction of fly ash concrete, attempt has been made to minimize the strength loss. Berry et al try to diminish the strength reduction by classifying fly ash into different fractions [7]. From their study they find the compressive strength reduction decreases as the material fraction of fly ash becomes smaller. Fly ash with 10 μm particle size or with a smaller fraction has the lowest compressive strength reduction at an early age and a surplus of the regular concrete compressive strength at a later age. Another method for reducing the strength loss is an addition of silica fume [3] or by using Type III portland cement [24]. Bilodeau and Malhotra discovered that there is a strength increase of about 1,160-psi over Type I portland cement.

However, Type III cement shortened the setting time of high-volume fly ash and increased the autogenous temperature of concrete (but the temperature rise is still lower than Type III cement alone). The drying shrinkage remains the same as Type I cement. Moreover, using heat curing could also reduce the early-age strength loss. Carette et al study the development of heat-curing cycles for concrete containing fly ash for the precast industry [28]. The heating cycles use in the study were 2 or 4 hours preset time, follow by heat curing for a period of 8, 12, 16, or 20 hours at curing temperature of 55, 70 or 90^{O}C. The specimens are then left to cool at room temperature for 2 hours. They determine that heat curing could increase the early age compressive strength of concrete and therefore fly ash could be used for precast elements. In the investigation, two heat cycles is suggested, 12 hours heat curing at 90^{O}C with a preset time of 2 hours or a 24 hours cycles at 55 to 70^{O}C with a preset time of 4 hours. However for other mix proportion other heating cycles need to be modified in the lab.

The strength reduction also directly causes the modulus of elasticity of concrete containing fly ash to be lower than that of regular concrete. However, based on compressive strength criteria, the modulus of elasticity of concrete containing fly ash is comparable with that of regular concrete having the same strength. It is also observed in many research projects that the modulus of elasticity increases parallel to the compressive strength. Only one difference exists between concrete containing fly ash or any other pozzolanic material and regular concrete; in the latter the transition zone is less dense, and, thus, the cement paste dictates the mechanical properties. On the other hand, in concrete containing pozzolanic material the transition zone is denser. Hence, the cement paste becomes stronger than the aggregate, which alter the failure criteria from cement paste to aggregate. As a result, the mechanical properties are controlled by the properties of the aggregates at low water-to-binder (w/b) ratio. As mentioned earlier, dense microstructures are caused by the calcium hydroxide in cement reacting to pozzolan to create calcium silica hydrate (CSH-gel) (therefore eliminating the transition zone or weak link between the binder and the aggregates). Many researchers illustrated this by comparing the calcium hydroxide level in concrete with and without a pozzolanic material additive. Their data shows a decrease of $Ca(OH)_2$ in concrete containing pozzolanic material [8, 9, 10].

As far as the effect of fly ash on the creep and drying shrinkage of concrete, the results presented by many researchers contradict each other and are, therefore, inconclusive. The main reason for this is the inherent sensitivity of the test. Both creep and drying shrinkage depends on the exact chemical composition of the matrix. Generally, concrete containing less than 20 percent of fly ash will have a creep strain either lower or comparable with that of regular concrete in the long run. The justification for this effect is the smaller percentage of compressive strength reduction, as well as the late hydration, which increases the rate of compressive strength at a later date.

Some mix results show both increase and decrease of drying shrinkage to concrete containing fly ash in comparison with regular concrete. However, the drying shrinkage property is likely to be affected in a manner similar to creep [3].

Nasser and Al-Manaseer looked at the shrinkage and creep of concrete containing 50 percent fly ash [20]. The shrinkage result showed about 11 percent higher than ordinary portland cement concrete. Whereas the creep is lower for concrete containing fly ash, 13 percent for unsealed and 39 percent for sealed specimens. Furthermore, the creep of concrete has a linear relationship with stress to compressive strength ratios. Luther and Hansen also compare the creep and shrinkage of high-strength silica fume concrete with fly ash concrete with similar strength [33]. The result shows that there is no significant different in creep of silica fume concrete with fly ash concrete. On the other hand the shrinkage of silica fume concrete is equal or better than fly ash concrete. Other mechanical properties, tensile strength, modulus of rupture, and modulus of elasticity of the concrete are the same.

Other mechanical property that has been studied is the effect of fly ash on the fatigue behaviors. Tse et al study the fatigue behavior of concrete containing fly ash [19]. In their study they subjected specimens of different percentage of fly ash of either Class C or F to fatigue load. The results show that Class C fly ash with less than 50 percent portland cement replacement performed better than plain concrete. However, the reverse effect is true for Class F fly ash. The reason for this is due to the lower compressive strength of concrete with Class F fly ash.

The effect of curing on the mechanical properties of concrete is also examined. Swamy and Mahmud study the mechanical properties of concrete containing 50 percent Class F fly ash with low water-cement ratios of 0.32 to 0.42 [21]. Furthermore they also investigated the curing on concrete containing fly ash. The result showed that high early strength could be obtained with slump in excess of 150 mm. The concrete containing fly ash had a higher strength gain of 50 to 100 percent from 28 days to one year than ordinary portland cement concrete that has a strength increase of 18 to 25 percent under wet curing. Also under air curing, the strength development of concrete containing fly ash was steadier and reaches the target strength but for ordinary portland cement concrete the strength were below the target strength of 25 to 35 percent. Nevertheless, air curing has a negative on mechanical properties of concrete for both ordinary and fly ash concrete.

Overall, the effect of the mechanical properties of fly ash on concrete is highly dependent on the composition and the fineness of the fly ash. Fly ash with a higher calcium level tends to be more effective in the compressive strength largely because of the accelerated rate of hydration. Interestingly, the loss of ignition or carbon content in fly ash has no direct effect on the mechanics of concrete.

The fineness of fly ash is also very important. Fly ash particles of 10 μm or smaller tend to perform better than large-sized particles. After all, the enhancement of concrete with fine particles and higher lime content makes the concrete denser and also reduces its pores sizes.

Effect of Fly Ash on Durability

Despite several negative effects of fly ash on the mechanical properties of concrete, its advantages cannot be denied. Fly ash makes concrete denser and therefore improves its durability. One of the most important characteristics of concrete durability is the impermeability of the concrete. Concrete must be impermeable to water and mineral admixtures that could damage the steel rebar within. Such damage would lead to a structure failure. In New Jersey, the impermeability of concrete to chloride ions is very important because of the cold winter; deicing salt (NaCl) has to be added to the bridge deck to prevent the deck from freezing. If the concrete is permeable, the deicing salt could penetrate through it and indirectly cause the steel rebar to rust.

Many researches have proven that concrete containing fly ash has an improved impermeability [8, 9, 10]. Fly ash strengthens the transition zone in concrete making it denser and more durable. The pores of concrete fill up with fine particles that eliminate water penetration. In the long run, concrete containing fly ash tends to perform better than regular concrete. Different types of permeability tests yield similar results. Using a rapid chloride permeability test, Sivasundaram et al indicated the long-term (1 year) permeability of concrete is substantially low [11]. According to their data, permeability decreases as time increases especially at 90 days. Bilodeau and Malhotra [35] as well as Gebler and Klieger [18] also reported similar results. In both studies, the resistance to chloride-ion penetration of concrete containing fly ash is superior to that of regular concrete. Furthermore, the concrete permeability using ponding test yielded similar results. Marusin investigate the concrete permeability by using the ponding test [34]. He also investigates the effect of curing period where samples were subjected to 7 or 14 days curing before starting the ponding test. The result shows that concrete with Class F fly ash is almost impermeable whether or not it is subjected to different curing. In fact only the 25 mm depth is contaminated above the corrosion threshold level. The curing duration also decreases the permeability.

Furthermore, the effect of fly ash on permeability is also effect by the curing condition. Thomas et al study the effect of curing on the strength and oxygen and water permeability of fly ash concrete [30]. In the study they subject the specimens to 1, 2, 3, or 7 day cured with a control specimens stored in water. The strength and oxygen and water permeability test are performed at 28 days. The result shows that the strength increases as the length of curing increases and this is more noticeable for fly ash concrete than ordinary portland cement concrete.

The same effect is also observed for the oxygen and water permeability. Longer curing is needed to obtain lower permeability in concrete.

Another important durability factor for concrete is the ability to resist chemical attacks. Chemical attacks such as sulfate cause the concrete to deteriorate and rupture because of the expansion of concrete from the alkaline-silica reaction, which produces ettringite and gypsum. This occurs when a substantial amount of sulfate exists in the aggregates or the soil within the area. The addition of fly ash improves the concrete resistance to sulfate. The resistance depends on the type and the amount of fly ash used. Generally, Class F fly ash performs better than Class C fly ash because of the high-calcium content, which is more reactive with the sulfate. This is supported by numerous literatures. Freeman and Carrasquillo look at the sulfate resistance of fly ash concrete[25]. They use Class C or Class F fly ash to replace 25 to 35 percent of Type II portland cement. For mixtures with Class F fly ash, the sulfate resistance performs equally or better than Type II cement alone. On the other hand Class C fly ash has lower resistance to sulfate resistance. However if the ash is intergounded into the cement, the sulfate resistance improves. Sturrup et al also published similar results in their study of the durability of fly ash concrete [4]. They discover that a replacement of 25 percent of fly ash could reduce alkali silicate expansions. Another, literatures is shown in Ramachandran et al paper where they use high volume fly ash to control alkali-aggregate reactivity [36]. The use of high volume fly ash found to be effective in reducing the expansion due to alkali-aggregate reactivity.

Despite these durability benefits, there are some durability factors that need to be cautious when using fly ash. These durability factors include, deicer scaling and freezing and thawing resistance. These durability factors are very important in New Jersey because of the high temperature changes. The ability of concrete to resist freezing and thawing cycles as well as deicer scaling depends on the entrain air in concrete. Generally, concrete with 6 percent air content performs well in freezing and thawing as well as deicer scaling. Whiting [26] study the resistance of deicer scaling of concrete containing fly ash. The specimens are subjected normal construction curing practice of 7 days moist curing. In his study the result shows that the deicer scaling resistance is reduced with the reduction in portland cement. A fly ash replacement of 50 percent by weight of portland cement performs unsatisfactory in the deicer resistance. Also to increase the resistance to deicer salt the water to binder should be kept low. Barrow et al, who study the temperature of concrete containing either Class C or F fly ash, also supported Whiting conclusion [31]. In their study, the resistance to scaling in the present of deicer salt of fly ash concrete is not as good as regular concrete. Similarly, freezing and thawing resistance of fly ash concrete is also not good as regular concrete. Nasser and Lai study the freezing and thawing resistance of concrete containing high volume of fly ash [27]. They observe that concrete with 50 percent of fly ash perform unsatisfactory.

They suggested the reason that contributes to this is because of the slow migration of portlandite and ettringite crystals from C-S-H to the air voids or in other words, the percentage of entrained air in fly ash concrete decreases. Gebler and Klieger also study the effect of air entraining concrete containing fly ash [12].

In their study they discovered that concrete containing fly ash generally performs well in freezing and thawing, but the fly ash does not improve the freezing and thawing resistance more than regular concrete. They also suggested that Class C fly ash performs better than Class F fly ash. In their study, Class F fly ash concrete samples exhibit a higher weight loss; they suspected the silica content has an adverse effect on the freezing and thawing of concrete. However, concrete containing fly ash performs comparably with regular concrete. Class F fly ash has a negative effect on freezing and thawing because the plastic concrete containing Class F fly ash loses more air than Class C fly ash or regular concrete. The higher organic matter content, carbon content, and loss of ignition in Class F fly ash cause this.

Silica Fume

Silica fume is a highly reactive pozzolanic material primarily composed of silicon dioxide (SiO_2) in noncrystalline form. It is a light to dark gray or bluish green-gray powder produced by an electric arc furnace during the manufacture of silicon or ferrosilicon alloy. It has a spherical like fly ash, but it is 100 times smaller, with an average diameter size of 0.1 μm. Its specific surface area is very large compared to portland cement (20,000 m^2/kg (by nitrogen absorption method) versus 300 m^2/kg, respectively).

Effect of silica fume on fresh mix concrete

Silica fume is a highly active pozzolan; it is essentially silicon dioxide in noncrystalline form, having a large specific surface area. Like other pozzolans, SiO_2 reacts to $Ca(OH)_2$ with the presence of water to form C-S-H. Because of the small size and the large surface area of silica fume, it absorbs a lot of water, making the water-demand for silica fume concrete very high and the setting time of the concrete very fast. In general, concrete containing silica fume has either a superplasticizer or retarder added to it. The superplasticizer increases the flow of concrete without affecting the w/c ratio. Superplasticizer propels the water from the silica fume particles to increase the workability of the concrete for a few minutes; because of this, superplasticizer also retards the mix. On the other hand, when the workability of concrete is not an issue, a retarder is used to slow down the reaction to increase the working time with concrete.

Besides increasing the setting time and workability, these two chemical admixtures offer other benefits. One of the advantages is their effect on the rate of change of heat in concrete. Concrete containing silica fume releases a very high heat of hydration.

As discussed by Roy, the rate of hydration of silica fume is very high because of the intense reaction between the silica fume and portland cement [13]. This high heat could cause microcracking if the concrete is subjected to wind; this is the major disadvantage of silica fume concrete. Another disadvantage of silica fume on concrete is the high viscosity, making the concrete difficult to pump.

An additional advantage of silica fume is the cohesiveness it offers the mix, causing less bleed-water. In fact, silica fume concrete does not release any bleed-water at all. This is a major advantage, as well as a disadvantage. The advantage is the elimination of segregation because no extra water exists on the top surface of the concrete. However, because water is not released, its evaporation could leave pores in the concrete if the concrete is not properly consolidated.

Mechanical properties of silica fume concrete

Silica fume is known for its ability to increase the strength of concrete because of its chemistry and hydration. Silica fume, when added to portland cement, reacts rapidly to form C-S-H. As a matter of fact, for very low w/c ratio concrete, the aggregate, rather than the cement paste, controls the concrete strength. Because of the higher strength of silica fume concrete, other mechanical properties of the concrete also improve.

Charif et al study the mechanical properties of silica fume concrete as part of a vast research program concerning the calculation and the reduction of concrete slab deformations [39]. Their final results indicate concrete containing silica fume can increase the compressive strength by 100 to 150 percent. The elastic modulus can be increased by 20 to 30 percent. The tensile strength can be increased by 40 to 60 percent. The creep deformations can be reduced by 30 to 60 percent.

Creep is a very important concrete property, especially for prestressed concrete. Prestressed concrete is usually designed to have higher compressive strength, thus silica fume concrete is perfect for this application. There are numerous paper published investigating creep and shrinkage of silica fume concrete. Persson correlated laboratory and field tests of creep in HPC carried out between 1991 and 1999 [44]. For this purpose, about 400 cylinders made out of eight mix compositions of HPC were studied in the laboratory. Half the number of HPC was sealed; half of the studies were carried out on air-cured HPC. Parallel tests on strength, internal relative humidity, RH, and hydration were carried out on about 900 cubes made of HPC from the same batch as the cylinders. Fragments from the strength tests were used to observe RH. Shrinkage was studied in relation to creep. The results and analyses of the laboratory studies show a large influence of the maturity, as well as of the mix composition, of the HPC on the measured creep. The creep coefficient of HPC is smaller than in normal concrete. In contrast, shrinkage of HPC is somewhat larger than in normal concrete.

Similar creep result is reported by Al-Khaja, who investigated high strength concrete mixes with and without silica fume in the Arabian Gulf region [40]. In his study, silica fume considerably reduces creep of concrete, given 1 month reduction strain of 18.5-percent for creep. Wiegrink et al, whom study the shrinkage cracking of high strength concrete, show similar shrinkage result [41]. According to their study, silica fume concrete shows higher shrinkage and lower creep.

Cracking for high-strength silica fume concrete develops much faster and is significantly wider than that of normal-strength concrete. Moreover, not only the drying shrinkage increases but also autogenous shrinkage for silica fume is very significant since this could be as high as drying shrinkage. Kanstad et al. perform a study to address the effect of silica fume on the early age crack sensitivity of HPC [43]. Tests were performed on concrete containing silica fume ranging from 0 to 15 percent, with a w/c ratio of 0.40. They canvassed realistic temperatures, tensile strength, modulus of elasticity, and autogenous shrinkage. All tests were conducted under isothermal conditions. Data were collected for 7 days for autogenous shrinkage. They concluded an increase in silica fume content raises the tensile strength and modulus of elasticity but also causes more of autogenous shrinkage.

Despite the higher drying shrinkage, increasing the curing time could reduce this. Hindy et al report the drying shrinkage results of ready-mixed concrete containing silica fume [38]. The concrete containing silica fume and ordinary concrete have a compressive strength of 98 MPa (14,200 psi) and 80 MPa (11,600psi) at 91 days, respectively. The effect of curing time, curing conditions, silica fume content, and w/c ratio were investigated. The drying shrinkage for both concretes decreases as the curing time increases or as the w/c ratio decreases. They also compared the drying shrinkage of small specimens with an actual-sized column made with the two concretes. From the comparison, the shrinkage measured using the small specimens overestimate the drying shrinkage of the actual-sized columns.

In addition to compressive creep, an attempt has been made to study the tensile creep properties of silica fume concrete. Koveler et al study the effect of the tensile creep behavior of concrete at early ages [42]. They found the use of 10 percent silica fume increases the early age tensile creep of high strength concrete in comparison with concrete without silica fume at the same w/c ratio of 0.33.

Durability characteristic of silica fume concrete

Silica fume improves the durability of concrete tremendously because of its denser microstructures. Many researchers [14, 15], including these authors, have observed the permeability of concrete decreases when about 10 percent of silica fume is added to it.

Gagné et al investigate the chloride-ion attack on low water-cement ratio pastes containing silica fume [15]. As it is well established that concrete is more perceptible on chloride-ion attack when the pH of concrete is below 13. This is due to the leaching of calcium ions that facilitates the penetration of chloride ions. In their investigation they subject the specimens that consist of Type III cement, Type III cement with 6 percent silica fume, and French CPA-HPR cement with 6 percent silica fume paste, to 3 percent sodium chloride solution at a pH level of 11.5 and 13.

Mercury intrusion porosimetry, X-ray diffraction, scanning elecron microscopy and electron microprobe measurements are the techniques used for the study. From their result, they concluded that silica fume decrease chloride penetration at the pH level of 11.5.

Another report that shows the superior durability of silica fume concrete is by Berke, who investigates the effect of silica fume on the resistance of steel corrosion, erosion, and chemical attacks [48]. In his study, concrete with embedded steel rebar are produced with varying level of silica fume from 0 to 15 percent by cement weight (0 to 30 percent for chemical testing). Other parameters in the investigation are the water-to-cement ratio and calcium nitrate. Polarization resistance and macrocell corrosion techniques are used to measure the corrosion rate in the steel rebar. The specimens are immersed in 3 percent NaCl solution for both methods. The United States Army Corp of Engineers method CRD-C 63-80 is used to perform the erosion test. The chemical testing is performed in 5 percent acetic acid, 1 percent sulfuric acid, 5 percent formic acid, and mixed sulfates. From his results, silica fume improves the resistance to steel corrosion, erosion, and chemical attack.

Nevertheless, one major disadvantage associated with silica fume concrete is micro-cracks. Silica fume concrete, if improperly cured, will crack while it sets because of the temperature differential that stresses it. The temperature differential results from the heat of hydration, which is relatively high for silica fume concrete.
It causes the concrete to expand whereas the cool ambient temperature causes it to contract. This expansion and contraction could bring about enough stress for the concrete to crack.

Combination of Silica Fume and Fly Ash in Concrete

Silica fume and fly ash are a perfect combination since they complement each other. The advantage of one enhanced the disadvantage of the other. For instant, silica fume increases the strength whereas fly ash decreases the strength of concrete at an early age. Thus, adding silica fume to fly ash concrete would increases the early-age strength. On the other hand, adding fly ash to silica fume concrete would increases the slump and also prevents early-age shrinkage of concrete resulting in a more durable concrete.

Besides an improvement on the concrete mechanical property, there is also an improvement on the durability property. Gautefall, and Havdahl study the effect of silica fume on the mechanism of chloride diffusion into hardened cement paste [14]. The specimens consist of both ordinary and blended cement with 10 percent fly ash. The silica fume is used to replace cement by weight ranging from 5 to 15 percent. They also vary the water-to-cement + pozzolan ratio from 0.5 to 0.9. The specimens are immersed in stagnant seawater at 20 ºC for 6 months and then tested for the chloride diffusion using a potentiometer titration procedure. Fick's second law is used to determine the diffusion coefficient. From their results they conclude that silica fume reduced chloride diffusion. Furthermore, the blended cement specimens out perform the ordinary specimens.

Slag

Alexander tested blended cement concretes incorporating blast furnace slag and condensed silica fume (CSF) for modulus of elasticity, creep, and shrinkage strains, with the intention of comparing their performance with that of plain portland cement concretes [45]. Exposed and sealed specimens were investigated. The results showed the exposure condition of the specimens during testing was critical. The addition of slag possibly caused a small increase in creep and shrinkage at early ages in exposed specimens, but this effect was usually reversed at later ages. Strains were markedly reduced in sealed slag specimens. The addition of CSF effected further moderate reductions in strains. Within-source and between-source variability of portland cement clinkers with regard to movement properties appeared to be considerable. The use of a blended cement resulted in less variability in cumulative strains.

Khatri and Gross studied the effect of different supplementary cementitious materials on mechanical properties of HPC [46]. They studied the mechanical properties, as well as fresh concrete properties, of concrete containing silica fume, ground-granulated blast furnace slag (slag), fly ash, and general-purpose (GP) portland cement.
Concrete mixes were prepared with GP portland cement, high slag cement, and slag cement, and also mixes were prepared with the addition of silica fume and fly ash. The work focused on concrete mixes having a fixed w/b ratio of 0.35 and a constant total binder content of 430 kg/m3. Apart from measuring fresh concrete properties, the evaluated mechanical properties were development of compressive strength, flexural strength, modulus of elasticity, and strain because of creep and drying shrinkage. Results indicated the addition of silica fume to GP portland cement concrete marginally decreased the workability of the concrete but significantly improved the mechanical properties. However the addition of silica fume to high slag cement concrete had a less pronounced effect on the workability and mechanical properties of the concrete.

Li et al. studied the effect of blended cement on early age shrinkage and creep [47]. Cement was blended with silica fume, granulated slag, and their combination. The test parameters were w/b ratio, aggregate content, blended cement, and dry and sealed curing conditions. It was concluded a lower w/b ratio is associated with higher autogenous shrinkage. The drying shrinkage of concrete mixtures with a higher w/b ratio was lower, provided they had a higher aggregate content than mixture with lower w/b ratio. The blended cement concrete gave higher shrinkage results than the ordinary portland cement.

RESEARCH APPROACH

This research is divided into four phases. In phase I, HPC mixes are developed using resources readily available in New Jersey. In phase II the developed HPC mixes are tested for their durability; permeability (rapid chloride permeability), scaling, and freeze-thaw tests are performed on the concrete. In phase III and IV shrinkage and creep of HPC, respectively, are investigated.

Phase I of the program is to establish an HPC mix design with a targeted compressive strength ranging from 6 to 10 ksi. The final mix design incorporates two types of pozzolanic materials, silica fume and fly ash. The pozzolanic materials are used as a direct replacement of cement by weight. The replacement amounts of silica fume and fly ash are between 5 and 15 percent and between 10 and 25 percent, respectively. A total of eight combinations of pozzolanic materials exist for a given w/b ratio (The binder consists of cement and pozzolans.). The w/b ratios investigated consist of 0.44, 0.39, 0.37, 0.35, 0.33 and 0.29. A total of 48 mixes exist. All mixes are tested for their compressive strength. For selected mixes, the drying shrinkage and the modulus of elasticity are tested. In addition, the effect of curing methods on concrete compressive strength is also investigated. The mix proportioning of these mixes are shown in Table 4.

Phase II of the program focused on the durability of the selected mix designs and also the method of curing. The performed durability test consisted of the rapid chloride permeability test (ASTM C1202), the freeze-thaw test (ASTM C666), and the scaling test (ASTM C672). The effect of curing on rapid chloride permeability is also investigated on one mix design.

Phase III consisted of mixes related to autogenous shrinkage. A total of eight concrete mixes (seven normal weights and one lightweight aggregate) were made in the laboratory; their mix proportioning is given in Table 4.1. As shown in the table, four parameters were used in the study, 1) w/b ratio, 2) pozzolanic materials, 3) type of aggregates, and 4) superplasticizer content. The investigated w/b ratio consisted of 0.29 and 0.35.

A low w/b ratio of 0.29 was used to simulate a worst-case scenario for autogenous shrinkage. As for the combination of pozzolanic materials, the mixture containing only silica fume was considered a control. Fly ash was added to reduce shrinkage; granulated blast furnace slag (GBFS) is also added to the control mix. In this phase, three curing methods were applied to all the samples. The curing conditions consisted of curing with burlap, using a curing compound, and air-dry curing.

In phase IV, compressive creep in HPC is studied. The mixes in this phase consist of HPC with compressive strengths ranging from 8 to 12 ksi. The mix design is based on some of the selected mixes, as well as mixes that contain only one pozzolanic material. Furthermore, a w/b ratio of 0.27 is used to obtain a compressive strength of 12 ksi. Other parameters include loading age, aggregates sources, and a percentage of pozzolanic materials.

Phase I

A comprehensive mix design of various research projects is collected and modified to fit with New Jersey resources. The mix design is based on ACI guidelines for high strength concrete. In this phase the mixes are selected based on the early and long-term performance of their compressive strengths.

Properties of Materials

The materials used in this project are readily available in New Jersey— with the exception of fly ash, which is obtained from Pennsylvania or Baltimore. Type I portland cement with a specific gravity of 3.15 was used. The mixing water is readily available from the tap at room temperature. The fine aggregate consists of concrete sand obtained from Weldon's quarry in Fanwood, NJ. The sand has a bulk specific gravity at oven dry of 2.56, a dry-rodded unit weight of 107.17-lb/ft^3, and a rate of absorption of 0.36 percent. Figure 1 shows the gradation of the concrete sand.
The coarse aggregate consist of 3/8- and 3/4-in crushed stones obtained from the same quarry as the sand. They have a bulk specific gravity at oven dry of 2.81 and 2.84, a dry-rodded unit weight of 98.11 and 96.22 lb/ft^3, and a rate of absorption of 1.0 and 1.2 percent, respectively. Figure 2 shows the gradation of the 3/8-in crushed stone. Some of the mix also utilized lightweight aggregate, which consists of shale-type material from New York. The nominal maximum size of the aggregates is 3/4-in. The specific gravity at oven dry is 1.23, the rate of absorption is 9.07 percent, and the dry rodded unit weight is 49.48 lb/ft^3. The pozzolans consisted of silica fume, fly ash and slag. The silica fume, super plasticizer, and air entraining agent are obtained from W.R. Grace. The silica fume (FORCE 10000 D) has a specific gravity of 2.22. The superplasticizer consisted of a product called DARACEM 19 and ADVA 100. A product called DARAVAIR 1000 is used for the air entraining agent. Class F fly ash with specific gravity 2.49 was used.

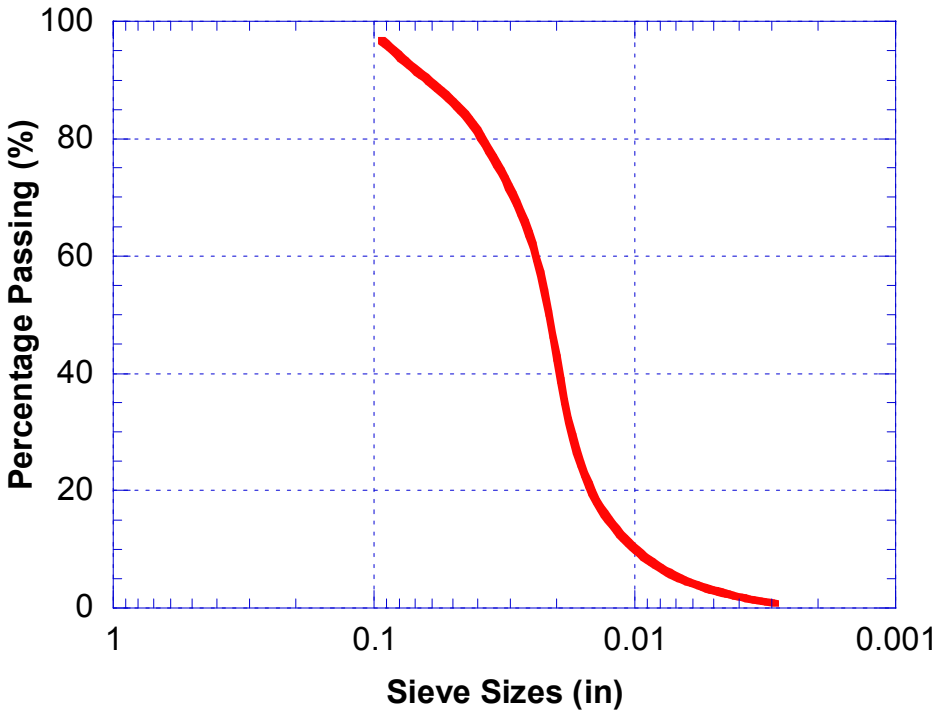

Figure 1. Gradation of fine aggregates

Table 1. Gradation of fine aggregate

Sieve Size	Percent Passing, %
No. 8	96.77
No. 16	85.57
No. 30	62.41
No. 50	24.28
No. 100	3.89
No. 200	0.66
Pan	0.00

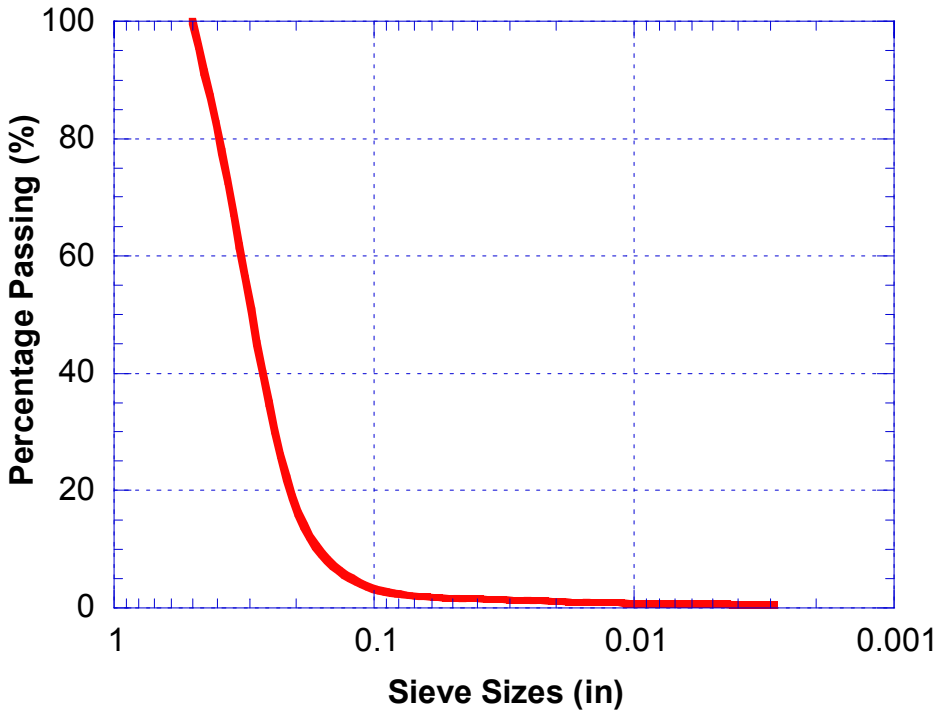

Figure 2. Gradation of coarse aggregates

Table 2. Gradation of coarse aggregate

Sieve Size	Percent Passing, %
No. 1/2	100
No. 3/8	61.71
No. 4	8.69
No. 8	1.85
No. 16	1.17
No. 30	0.92
No. 50	0.66
No. 100	0.42
No. 200	0.27
No. Pan	0

Table 3. The Information of the supplies

ITEM	MODEL	COMPANY NAME	ADDRESS	TEL
Cement	Type I	Lafarge	5160 Main Street Whitehall, PA 18052	(800) 523-9211
Fly Ash	Class F PRO ASH	Separation Technology Inc.		(201) 401-3391
Silica Fume	FORCE 1000D	W.R. Grace & Co. - Conn.	62 Whittemore Avenue Cambridge, MA 02140	(617) 498-4963
Superplasticizer	DARACEM 19			
A.E.A	DARAVAIR 1000			
Coarse Aggregates	3/8-in Crushed Stone	Fanwood Crushed Stone Co.	Office - 141 Central Ave. Westfield, NJ	(908) 233-4444
Fine Aggregates	Concrete Sand			

Mix Proportion

A total of six groups (A, B, BN, C, D, and G) of mixes based on w/b ratio exist. In each group, eight trial mixes were mixed with varying percentages of silica fume and fly ash, as shown in Table 4. Superplasticizer and air entraining agents were also added to every mix to obtain 2 to 5 in of slump and 3 to 7 percent air content, respectively.

Table 4. Mix proportions

Group	Mix ID	Cement (%)	Silica Fume (%)	Fly Ash (%)
A, B, C, BN, D, G (w/b = 0.44, 0.39, 0.37, 0.35, 0.33, 0.29, respectively)	1	78	7	15
	2	85	5	10
	3	80	5	15
	4	75	5	20
	5	70	5	25
	6	74	8	18
	7	70	10	20
	8	65	15	20

Mix Design Procedure

The mix design procedure follows the *"Guide for Selecting Proportions for High-Strength Concrete with Portland Cement and Fly Ash"* [2] and is summarized below.

Step 1: *Select a slump and required concrete strength*—In this study; the targeted slump was between 2- and 6-in.

Step 2: *Select the maximum size aggregate*—The maximum size of the aggregate was selected on the bases of the desired compressive strength of concrete.

Step 3: *Select the optimum coarse aggregate content*—The optimum content of the coarse aggregate depends on its strength-potential characteristics and maximum size. The recommended optimum coarse aggregate contents are expressed as a function of dry-rodded unit weight. In this study, the nominal maximum size was 3/8 and 3/4 in. Therefore, the fraction volumes of coarse aggregate were 0.65 and 0.72, respectively.

Step 4: *Estimate the mixing water and air content*—The quantity of required water per unit volume of concrete to produce a given slump depends on the maximum size, particle shape, grading of the aggregate, the quantity of cement, and type of water-reducing admixture used.

Step 5: *Select w/b*—The w/b ratio was calculated by dividing the weight of the mixing water by the combined weight of the cement and pozzolanic materials. The w/b ratios were varied according to the targeted compressive strength.

Step 6: *Calculate the content of the pozzolanic material*—The weight of the pozzolanic material required per cubic yard of concrete could be determined by dividing the amount of mixing water per cubic yard of concrete (step 4) by the w/b ratio (step 5)

Step 7: *Pozzolan content*—The amount of cement to be reduced by pozzolans depends on the type of pozzolans to be used.. In this study, Class F fly ash and silica fume were used. Therefore, the recommended replacement (percent by weight) is 10 to 25percent and 5 to 15 percent, respectively.

Step 8: *Sand content*—Having found the volume of cementitious material per cubic yard of concrete, the volumes per cubic yard of coarse aggregate, water, and entrapped air, the sand content of each mixture could be calculated using the absolute volume method.

Mixing, (ASTM C 192)

To begin the mixing process, coarse and fine aggregates were added to the mixer. While the mixer was running, one-third of the mixing water was added, followed by air entraining agent. The mixer ran for 30 seconds before the cement, pozzolans, and remaining water were added. The mixer continued mixing for another 3 minutes before resting. The concrete was left to rest in the mixer with the lid closed for another 3 minutes. After that, the superplasticizer was added to the concrete and mixed for another 3 minutes.

Slump Test, (ASTM C143)

The slump of each concrete batch was measured immediately after mixing. The slump test was performed using a slump cone, which was filled with concrete in three layers. Each layer was approximately one third the volume of the cone. Moreover, each layer was rodded with 25 strokes using a tamping rod. The strokes were uniformly spread over the cross section of each layer, and they did not penetrate into the underlying layer. In filling and rodding the top layer, the concrete was heaped above the mold before rodding was started to ensure the cone is fully filled. As soon as the cone was filled with concrete, it was removed from the concrete by raising it in a vertical direction, avoiding lateral or tensional motion. The slump was immediately measured by determining the vertical difference between the top of the cone and the displaced original center of the top surface of the concrete.

Air Content, (ASTM C173)

The air content of each batch of concrete was measured in accordance with the ASTM test method C 173 (volumetric method). The measuring bowl of the air meter was filled in three layers, each approximately one-third the volume of the measuring bowl. Each layer was rodded with 25 strokes using the tamping rod. After each layer was rodded, the side of the bowl was tapped 10 to 15 times with a rubber mallet to close the voids left by the tamping rod and releasing the air that may have been trapped. The excess concrete was struck off until the surface was flush with the top of the bowl. The top section on the bowl was attached, and the funnel was inserted into the opening at the top so the bowl could be filled with water. The air meter was filled with water until the meniscus was leveled with the zero mark. The watertight cap was attached and tightened. The air meter was repeatedly inverted and agitated for a minimum of 45 seconds to free concrete from the base. After that, the meter was tilted at approximately 45 degrees so the dense particles could flow to the bottom of the meter. The meter was rolled and rocked for approximately 1 minute, and it was rested at an upright angle for the air to flow up. Using alcohol could also eliminate the extra air bubbles. However, the number of alcohol shots needs to be recorded and added to the air reading on the meter where one shot of alcohol equals 1-percent of air.

The 1-minute rolling and rocking procedure was repeated until two consecutive readings do not change more than 0.25 percent of air.

Consolidating Method

Three layers of concrete were filled, each approximately one-third the volume of the mold. Each layer was vibrated using a vibrating table to consolidate the concrete. After each layer is vibrated, the outsides of the mold were taped lightly 10 to 15 times with a rubber mallet. The excess surface of the concrete was struck off and the cylinders were covered with plastic.

Curing Method

After 18 to 24 hours the specimens were demolded, carefully labeled, and placed in the curing room for moist curing at a temperature of 73 degree Fahrenheit and a rate of humidity of 97-percent. For the study of the effect of curing, the specimens were subjected to the following curing methods:

Dry Curing (D)—The dry-cured specimens were left untouched after casting. After the specimens harden, they were demolded and stored in the environmental chamber. This curing method was used to simulate a worst-case scenario.

Curing Compound (C)—The exposed surface of the specimens were coated with a thin layer of a commercially available curing compound using a brush, immediately after casting. After the concrete hardens, all the uncoated surfaces were coated using the same method. This method was common practice in industry and sometimes a substitute for moist curing.

Burlap Curing (B)—Burlap cured specimens were covered with wet burlap after casting and wrapped when they harden. The burlap was monitored every 2 days to ensure its wetness. This curing method was used to simulate the best curing condition for concrete. The specimens were wrapped with wet burlap until the targeted time was reached.

Burlap Curing (B) – Burlap cured specimens were covered with wet burlap, after casting and wrapped when they hardened. The burlap was monitored every two days to ensure its wetness. This curing method was used to simulate the best curing condition for concrete. The specimens were wrapped with wet burlap until the targeted time was reached.

Testing Procedures

In this phase, the compressive strength, drying shrinkage, and modulus of elasticity were performed on the concrete. The compressive strength was performed on all of the concrete whereas drying shrinkage and modulus of elasticity were performed on selective mixes.

Compressive Strength of Cylindrical Concrete Specimens (ASTM C39)

The specimens were tested at 1, 3, 7, 14, 28, 56, and 90 days using a 400,000-lb Tinius-Olsen compressive machine. The loading rate of the Tinius-Olsen remained constant. The specimens were either capped using a neoprene pad or capping compound when tested.

Drying Shrinkage (ASTM490-93a)

Drying shrinkage samples were cast the same way as described in the method of consolidation except the gauges studs were screwed into the plate of each end of the specimens. The plates were also attached to the molds with a hex screw from the other sides. After the molds were filled with concrete, the hex screw needs to be removed so it would not create any stresses when the concrete is setting. The specimens were removed at the same time as the other specimens. After stripping the specimens from the mold, they were first placed in water so they have the same temperature. After about 15 minutes, the lengths between the two studs, as well as the length of the reference bar, were measured using a comparator. When making the comparator reading, the specimens were slowly rotated and a minimum reading was recorded.

The length change was calculated by the following formula:

$$L = [(L_x - L_i)100]/G \qquad (1)$$

Where,

- L_x = the difference between the length of the specimens and the reference bar at x days.
- L_i = the difference between the length of the specimens and the reference bar at 1 day.
- G = the total length of the specimen = 10 in.

Stress-Strain Relationship, (Modulus of Elasticity), (ASTM469)

The specimen is placed in the compressive machine with the strain-measuring equipment attached. Two types of strain measuring equipments were used, one consists of a compressometer and the other linear voltage displacement transducer (LVDT). The specimen was loaded at least twice. During the first load, which was primarily for the seating of the gauges, the performance of the gauge was observed. In hydraulically operated machines, the load was applied at a constant rate within a range of 30 to 40 psi/sec, and the load was applied up to approximately 40 percent its ultimate compressive strength. The load and deformation was recorded. To determine the modulus of elasticity, the results are plotted on a graph, in which the slope is the modulus of elasticity. Another method is to directly calculate the modulus of elasticity by using the equation:

$$E = (S_2 - S_1)/(\varepsilon_2 - 0.00005) \quad (2)$$

Where,

E = modulus of elasticity

S_2 = 40 percent of the ultimate stress.

S_1 = stress at 0.00005 strain

ε_2= strain where the stress reaches 40 percent of the ultimate strength

Results and Discussion

Fresh mix concrete

Table 5 a and b show the mix proportions in percentages and the amount of chemical admixture added to each mix, as well as the fresh mix concrete properties.

Table 5a. Fresh mix properties

Mix	w/b	SF (%)	FA (%)	SP (oz/cwt)	AEA (%)	Air content (%)	Slump (in)
A1	0.44	7	15	8	0.1	2.5	1.5
A2	0.44	5	10	8	0.1	4.25	2.25
A3	0.44	5	15	8	0.1	2.5	1.8
A4	0.44	5	20	8	0.1	4	2
A5	0.44	5	25	8	0.1	3.5	2.25
A6	0.44	9	18	8	0.1	3.25	1.5
A7	0.44	10	20	8	0.1	3	1.5
A8	0.44	15	20	8	0.1	3.5	1.5

Table 5b. Fresh mix properties (cont.)

Mix	w/b	SF (%)	FA (%)	SP (oz/cwt)	AEA (%)	Air content (%)	Slump (in)
B1	0.39	7	15	10	0.1	7.5	5.75
B2	0.39	5	10	10	0.1	6.5	4.75
B3	0.39	5	15	10	0.1	5.25	3
B4	0.39	5	20	10	0.1	6	6
B5	0.39	5	25	10	0.1	3.5	3.2
B6	0.39	9	18	10	0.1	3	3
B7	0.39	10	20	10	0.1	3.5	2
B8	0.39	15	20	10	0.1	3	2
B1N	0.35	7	15	20	0.1	5	5.5
B2N	0.35	5	10	20	0.1	4	4
B3N	0.35	5	15	20	0.1	4.5	3
B5N	0.35	5	25	20	0.1	4.25	3.5
B6N	0.35	9	18	20	0.1	4	3.5
B8N	0.35	15	20	20	0.1	2	3
C1	0.37	7	15	10	0.1	1.75	1
C2	0.37	5	10	15	0.1	5	3
C3	0.37	5	15	10	0.1	4	1
C4	0.37	5	20	15	0.1	6	3.75
C5	0.37	5	25	15	0.1	8.5	9
C6	0.37	9	18	10	0.1	4.2	1.75
C7	0.37	10	20	10	0.1	4	0.75
C8	0.37	15	20	13	0.1	4	0.75
D1	0.33	7	15	18	0.1	4	3.5
D2	0.33	5	10	20	0.1	4	4
D3	0.33	5	15	18	0.1	4	3.5
D4	0.33	5	20	16	0.1	3.5	3.5
D5	0.33	5	25	14	0.1	4.5	5.5
D6	0.33	9	18	15	0.1	3.25	0.5
D7	0.33	10	20	15	0.1	3.5	1
D8	0.33	15	20	20	0.1	3	1.5
G1	0.29	7	15	22	0.1	3.5	4
G2	0.29	5	10	20	0.1	3	1.75
G3	0.29	5	15	22	0.1	3	5.375
G4	0.29	5	20	20	0.1	3.5	5.5
G5	0.29	5	25	16	0.1	3	4
G6	0.29	9	18	22	0.1	3	4
G7	0.29	10	20	20	0.1	3.5	3.25
G8	0.29	15	20	22	0.1	3.5	3.5

Compressive Strength

Generally the mix proportion with the combination of 7 and 15, 5 and 10, 5 and 15, and 9 and 18 percent of silica fume and fly ash, respectively, outperform other mixes in the compression test. In addition, the mix with high early strength also has high long-term compressive strength. However, it is important to note that the mix with the combination of 5 and 15 percent of silica fume and fly ash, respectively, has higher workability. Thus lower the amount of superplasticizer and reducing cost. Two sets of mixes are selected from each group based on their compressive strength shown in table 6a and b.

The effect of w/b ratio on compressive strength is also investigated. This effect is plotted on figure 3. From the graph, the compressive strength increases as the w/b ratio decreases. However, no constant relationship exists between the eight combinations. Also some of the 90-day compressive strength decreases. The suspected reason for this is most of the 90-day compressive strengths are very high (roughly 10 ksi). At this capacity, rather than the transition zone between the cement paste and coarse aggregate, the coarse aggregate itself becomes the strength-limited state. Therefore, the cylinder breaks between 10 to 12ksi. Another reason for explaining this is a limitation exists on the available apparatus for testing high strength concrete. Both the capping compound and the metal cap are designed for testing concrete between 4 to 7 ksi.

Table 6a. Selected mix design

(Lb/cu yd.)	**Selected Mix Design**					
	A2	**A3**	**B1**	**B6**	**C2**	**C3**
Portland Cement Type I	85%	80%	78%	73%	85%	80%
Class F Fly Ash	10%	15%	15%	18%	10%	15%
Silica Fume	5%	5%	7%	9%	5%	5%
W/CM	0.44	0.44	0.39	0.39	0.37	0.37
Super Plasticizer (oz/cwt)	8	8	10	10	15	10
AEA (oz/cwt)	1.5	1.5	1.5	1.5	1.5	1.5
Slump	2.25	2.5	4.75	3	3	1
Air Content	4.25	2.5	6.5	3	5	4
28 days Compressive Strength (psi)	6220	6154	6817	7494	8475	7696
28 days Shrinkage (%)	0.053	N/A	0.0437	0.0570	0.03	0.0357

Table 6b. Selected mix design (cont.)

(Lb/cu yd.)	Selected Mix Design					
	B1N	B2N	D1	D3	G1	G2
Portland Cement Type I	78%	85%	78%	80%	78%	85%
Class F Fly Ash	15%	10%	15%	15%	15%	10%
Silica Fume	7%	5%	7%	5%	7%	5%
W/CM	0.35	0.35	0.33	0.33	0.29	0.29
Super Plasticizer (oz/cwt)	20	20	18	18	22	20
AEA (oz/cwt)	1.5	1.5	1.5	1.5	1.5	1.5
Slump	5	3	3.5	3.5	4	1.75
Air Content	5.5	4.5	4	4	3.5	3
28 days Compressive Strength (psi)	9735	9715	10177	9748	10637	10106
28 days Shrinkage (%)	0.05	0.0553	0.0413	0.0413	0.0437	0.0453

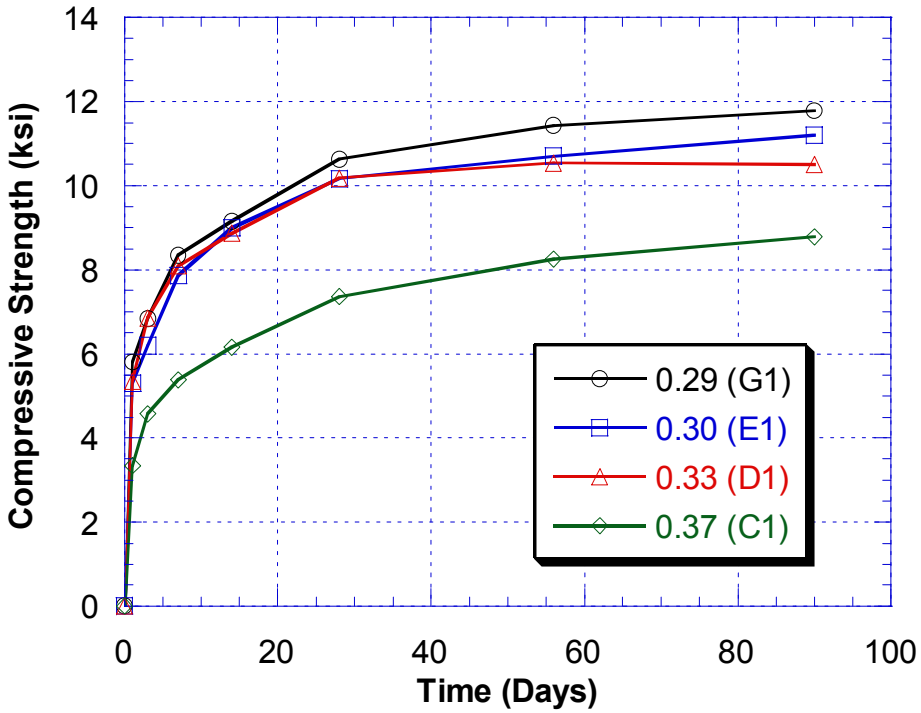

Figure 3. The effect of w/b ratio on the compressive strength of HPC with a combination of 7percent silica fume and 15 percent fly ash

Furthermore, the effect of pozzolans on compressive strength is observed in various mixes. Two parameters are investigated: (i) volume of pozzolanic materials and (ii) w/b ratios. The volumes of pozzolanic materials are investigated by comparing the effects of a single pozzolanic material and a combination of pozzolanic materials on the compressive strength. These comparisons are weighed against a conventional concrete mix (control). Three different levels of each pozzolan are studied; 5, 10, and 15 percent for silica fume and 10, 20, and 30 percent for fly ash. Figures 4a and b summarizes the compressive strength of these mixes. At early age, control or conventional concrete has a higher compressive strength than concrete with fly ash, but at 28 days, the mix containing 10 percent fly ash has a greater compressive strength than the control specimens. The mix containing 20 percent fly ash also has a higher compressive strength than the control mix at 60 days; as a matter of fact, it has the highest compressive strength at 90 days. Regarding the effect of silica fume, all mixes have higher compressive strength than control specimens at all ages; except for the mix containing 15 percent silica fume; it has a strength decrease at 90 days. Figure 5 and 6 illustrate the effect of the combination of pozzolanic materials on the compressive strength. From the graphs, the mix with a smaller combination of fly ash and silica fume performs better in the compressive test than mixes with a high volume of silica fume and fly ash. Generally, mixes that contain more than 25 percent of pozzolanic materials do not yield compressive strengths as high as conventional concrete.

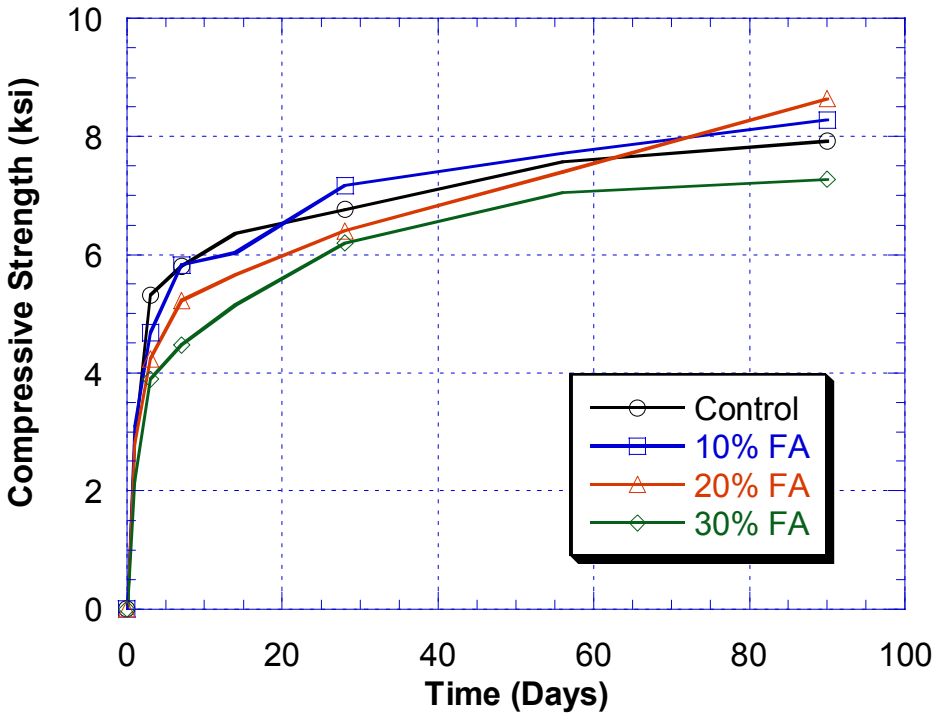

Figure 4a. Effect of fly ash on the compressive strength of HPC with a w/b = 0.39

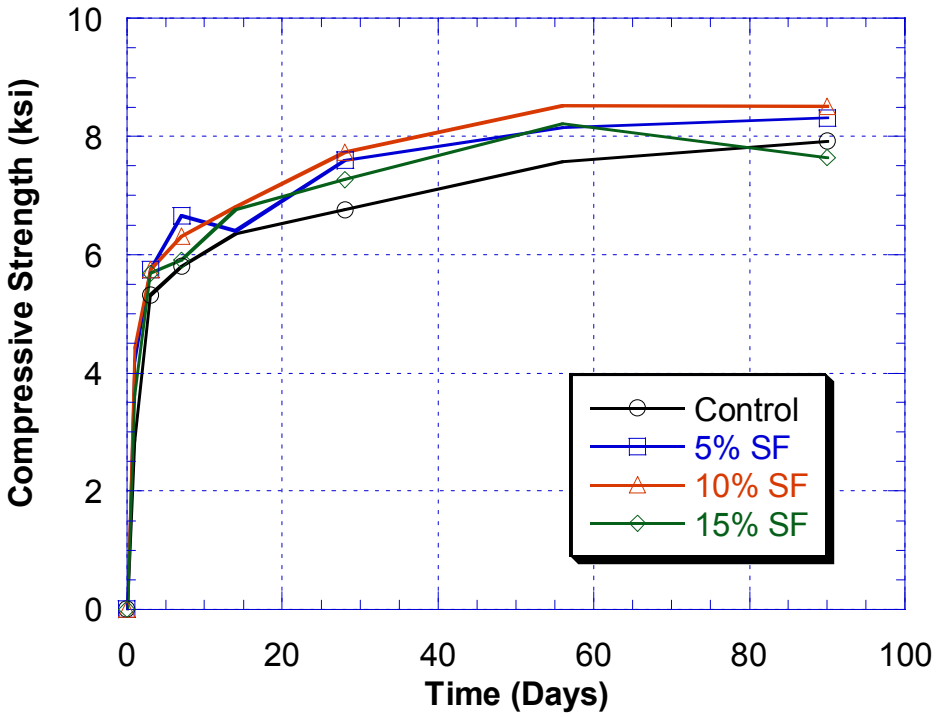

Figure 4b. Effect of silica fume on the compressive strength of HPC with a w/b = 0.39

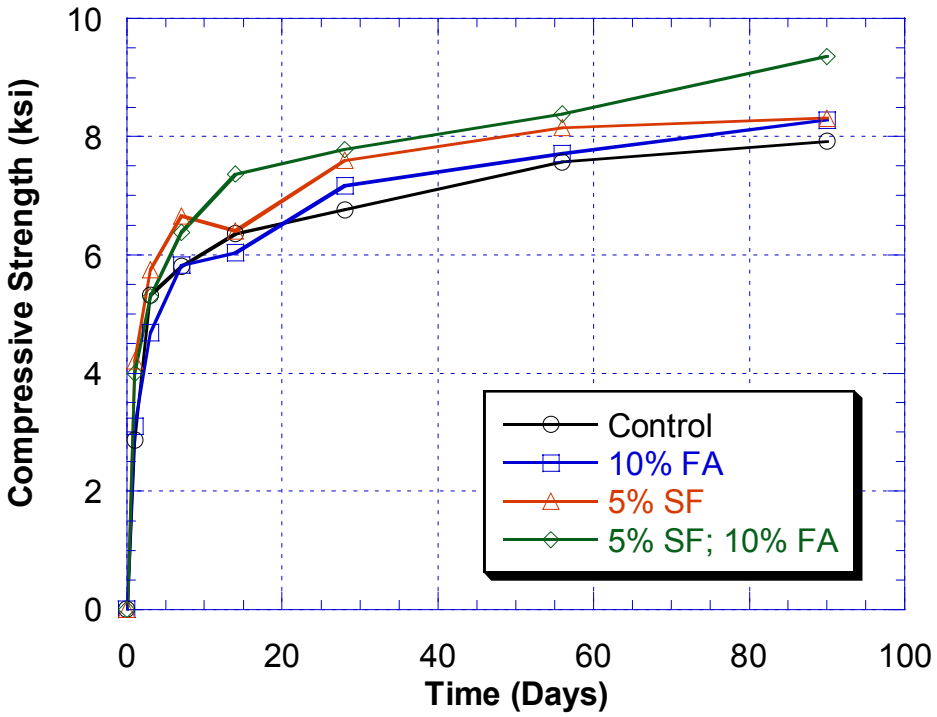

Figure 5. Effect of pozzolans on the compressive strength of HPC with a w/b = 0.39

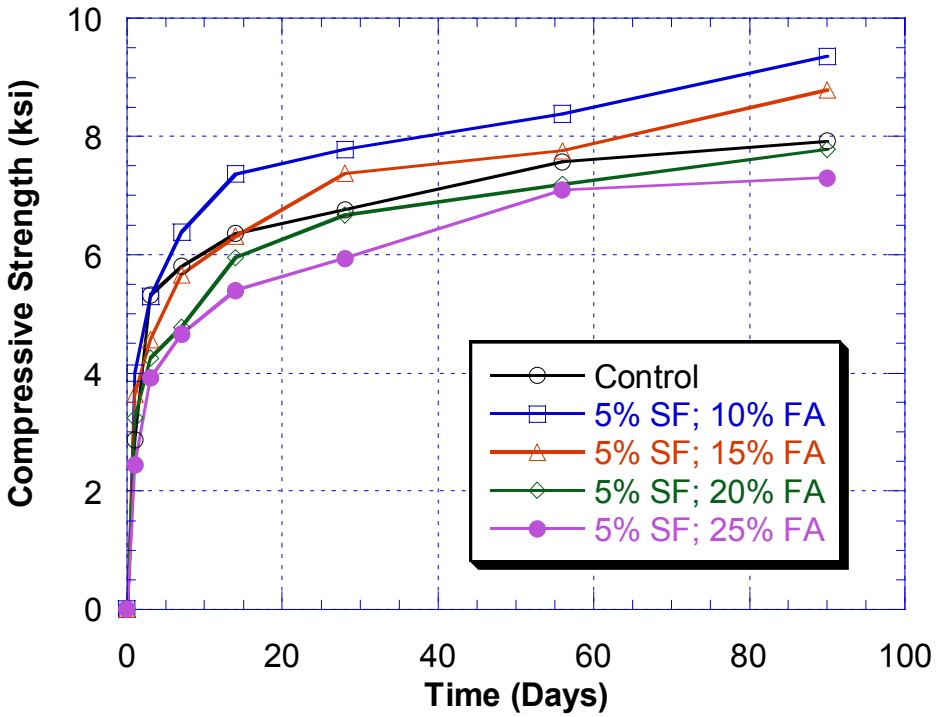

Figure 6. The effect of pozzolans on compressive Strength of HPC with w/b = 0.39

In addition, low strength concrete is developed; the compressive strength results are plotted in figures 7 through 11. The main reason for this development is to create low permeability concrete using a higher w/b ratio to disallow any high strength concrete substitution by the concrete plants. Ready-mix concrete plants often have a misconception that high strength concrete mixes have low permeability and tend to mix regular portland cement concrete with very low w/b ratio instead of concrete with pozzolanic materials.

The effect aggregate has on the compressive strength can be divided into two categories: (i) sizes of aggregate and (ii) sources of aggregate. The aggregate sizes are 3/8 and 3/4 in. The source consists of north and central New Jersey. For the aggregate size study, the mix is based on HPC containing 5 percent SF and 30 percent FA with w/b ratio of 0.40. Figure 10 illustrates the compressive test results of this mix. From the graph, the mix with 3/8-in aggregate performs better than the larger size aggregate.

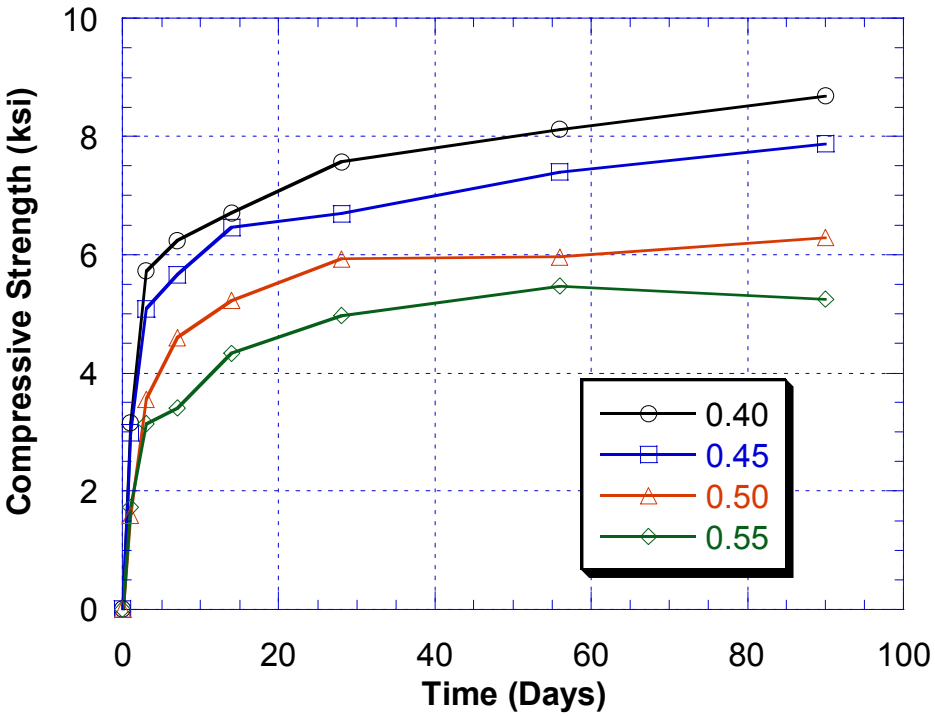

Figure 7. Effect of w/b ratio on compressive strength of low-strength HPC with 5 percent silica fume

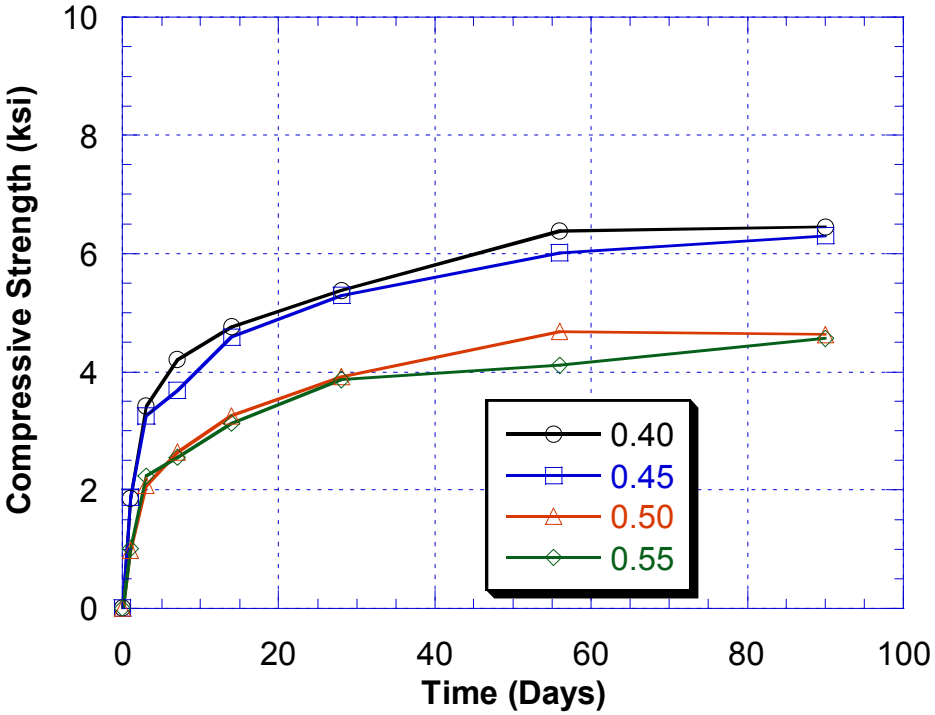

Figure 8. Effect of w/b ratio on compressive strength of low-strength HPC with 30 percent fly ash

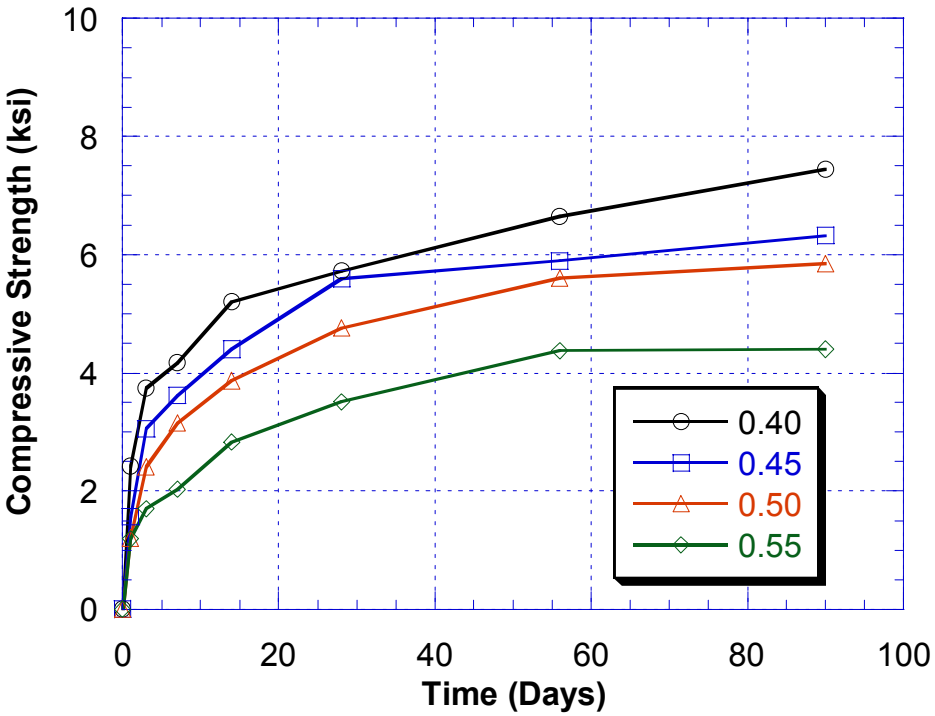

Figure 9. Effect of w/b ratio on compressive strength of low-strength HPC with 5 percent silica fume and 30 percent fly ash

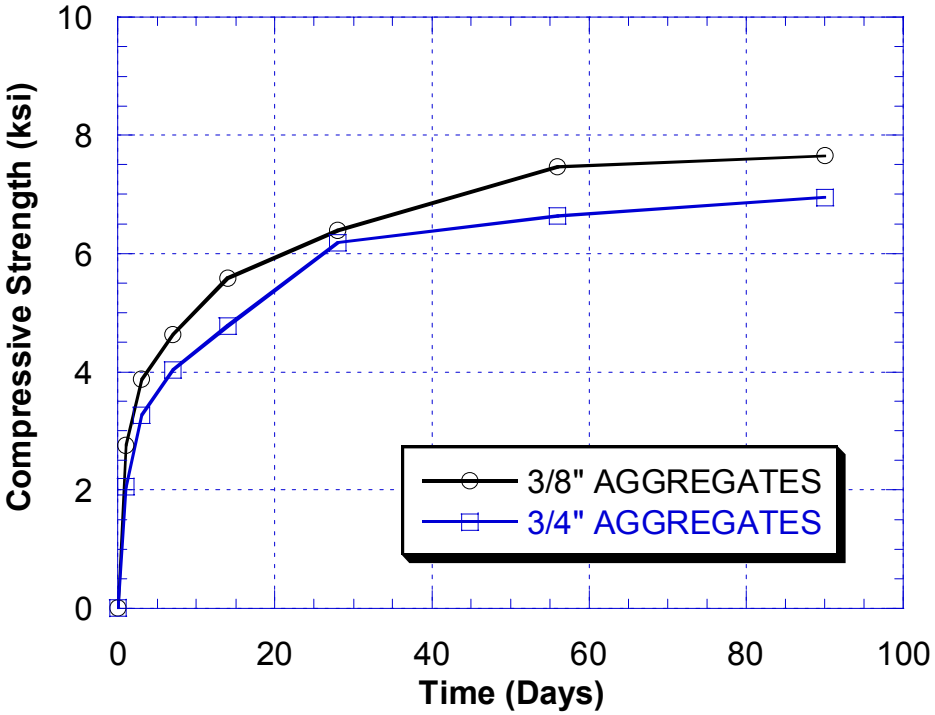

Figure 10. Effect of aggregate on compressive strength of HPC with w/b = 0.39

Drying Shrinkage

For phase I, the drying shrinkage was performed on some of the mixes. The results are shown in figure 11 through 13. From the figures, mix with 5 and 10 percent and 9 and 18 percent silica fume and fly ash, respectively, consistently outperformed other mixes. These were the same mixes that have the highest compressive strength. In general, mix with low w/b ratio had higher the drying shrinkage; however, the amount of pozzolanic materials had more influence on the drying shrinkage. With an exception of the two optimum mixes, an addition of fly ash decreased the drying shrinkage especially the mix with low w/b ratio. Consistently, mix with 5 and 15 percent silica fume and fly ash, respectively, performed poorly and have the highest drying shrinkage.

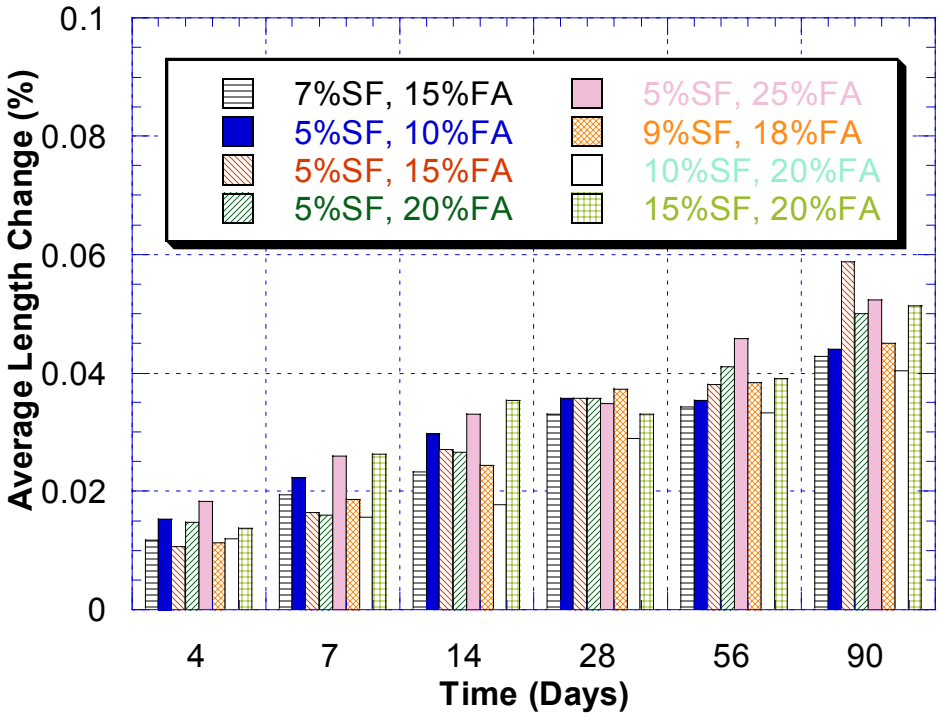

Figure 11. Drying shrinkage of HPC with w/b ratio of 0.37

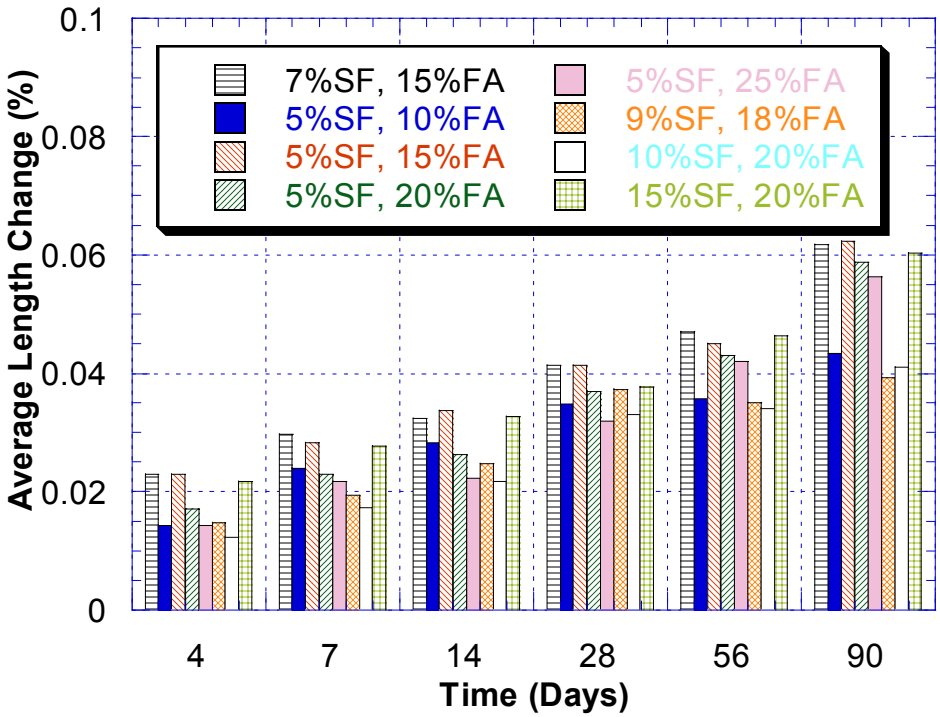

Figure 12. Drying shrinkage of HPC with w/b ratio of 0.33

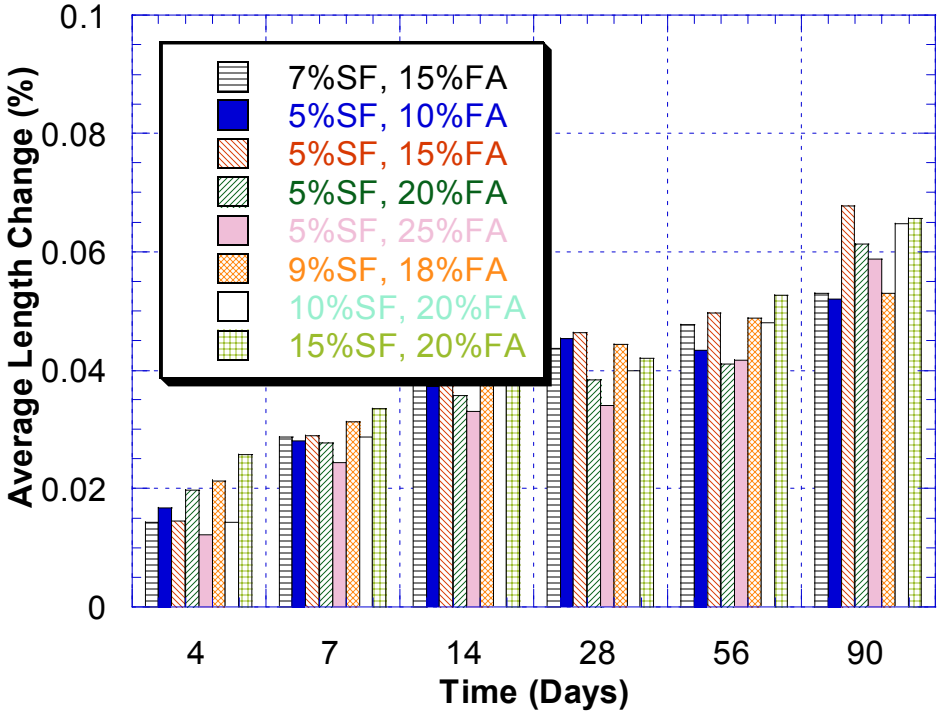

Figure 13. Drying shrinkage of HPC with w/b ratio of 0.29

Modulus of Elasticity

The modulus of elasticity was tested on selective mixes at different ages. The results were compared to ACI 318, as well as ACI 363, equation. ACI 363 equation is based on high strength concrete. Overall, it gives better correlation to the results obtained from the HPC mixes. Figure 14 shows a scatter plot of the modulus of elasticity obtained at different ages. The solid line represents the ACI 363 equation, and the dotted line represents ACI 318 equation.

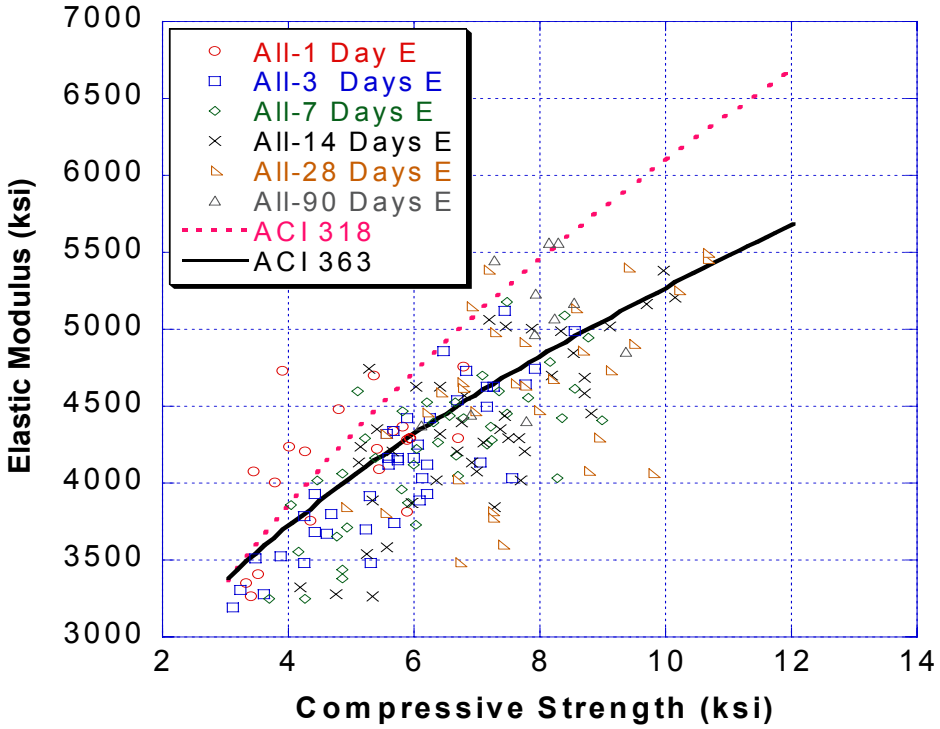

Figure 14. Scatter plot of the modulus of elasticity

Curing Methods

The effect of using four methods of curing on HPC is considered because of its effect on cracking and strength. The curing conditions consisted of 1) Moist curing; 2) Air-dry curing; 3) Burlap; and 4) Curing compound. Two similar batches of concrete containing 9 percent silica fume and 18 percent fly ash with w/b ratio of 0.39 were mixed. One mix is used for testing a total of 101 4-by-8-in cylinders cured by the four curing methods. All samples are divided into four groups. Group I is moist cured, group II is dry-cured, group III is cured using burlap, and group IV is cured using a curing compound.

Group III is further divided into four subgroups to simulate a more realistic curing procedure at the field. These subgroups include curing with burlap for 3, 7, 14, and 90 days.

Figure 15. Treatment of different curing methods on specimens


Figure 16. Method of applying burlap and curing compound on to specimens

Figure 17 shows when using any of the curing methods, the compressive strengths at 1 to 7 days are similar. However, at 28 days, the compressive strength using dry-cured (room temperature), curing compound, and burlap are about 12 percent less than those moist cured. At 56 days, the results are similar with a difference of about 10 percent.

Figure 18 shows a minimal 14-day curing duration is needed to ensure a compressive strength close to the specified 28-day compressive strength. A curing duration of only 3 and 7 days can result in reductions of about 5 to 10 percent.

In addition, the effect of curing on drying shrinkage was also investigated with the result presented in figure 19. Similarly, the dry cured and compound cured samples performed the worst in drying shrinkage. Specimens that were cured using wet burlap for 3 days also did not performed well. Specimens that were cured for 7 and 14 days using wet burlap performed satisfactory. The moist cured specimens performed the best.

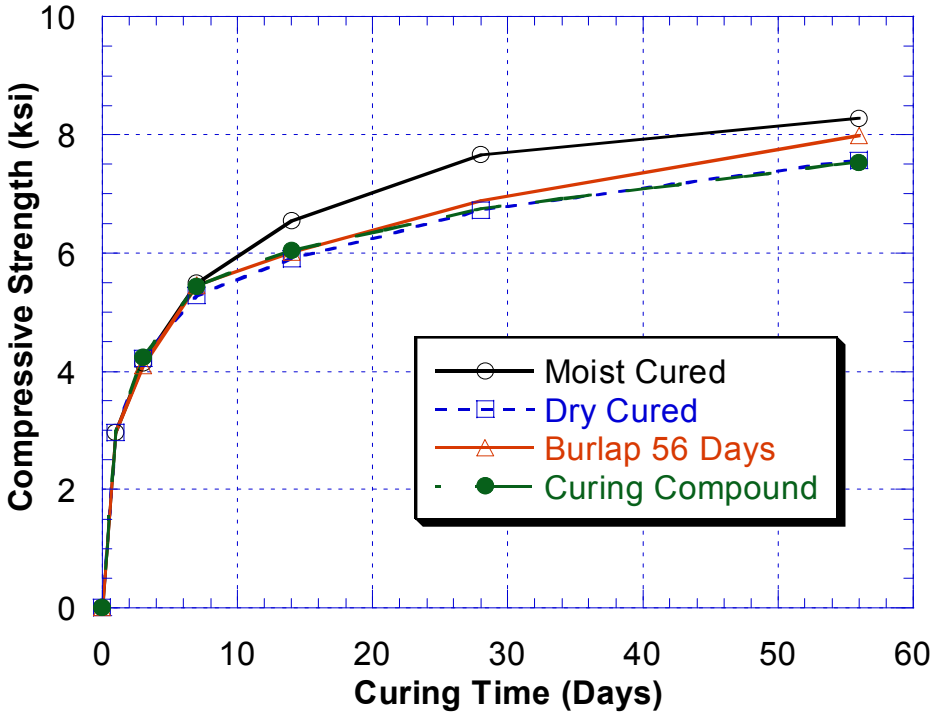

Figure 17. Compressive strength for various curing methods

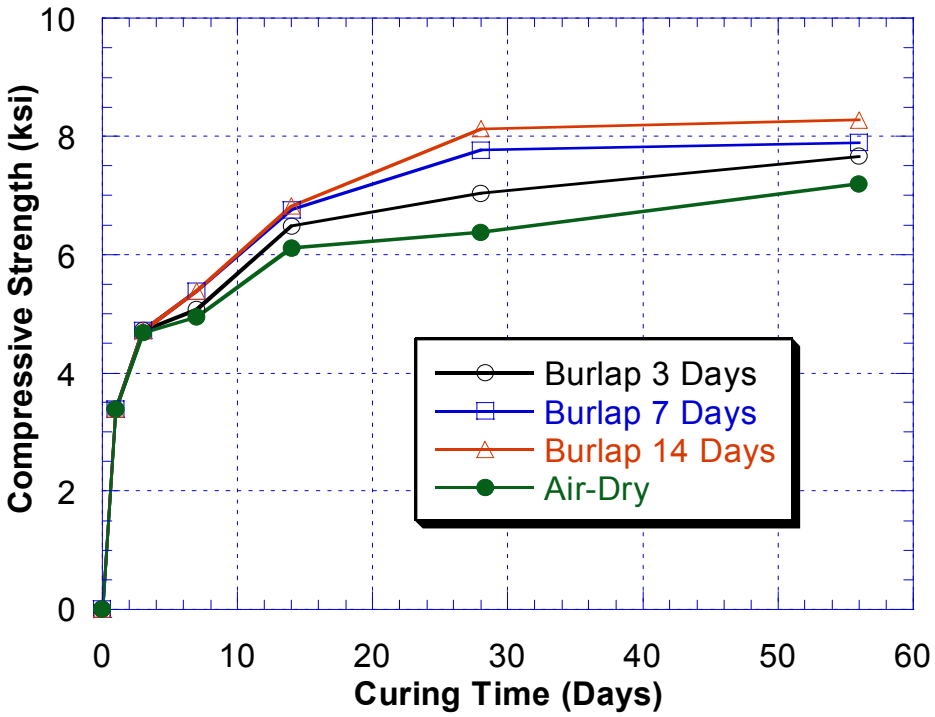

Figure 18. Compressive strength of different burlap curing durations

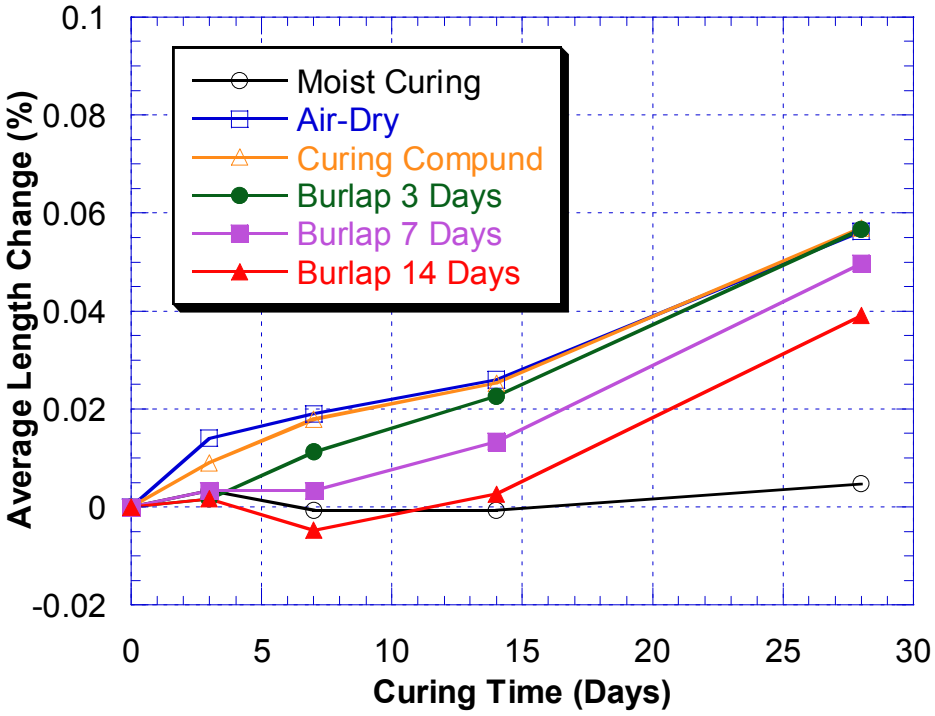

Figure 19. Effect of curing method on drying shrinkage

Phase II

Phase II was an extension of Phase I, where the selected mix designs were exposed to various durability tests. These tests include free-thaw, permeability, and scaling.

Freeze-Thaw Test (ASTM C666)

Three prisms, 3- by 5- by 15-in were made to test the freeze-thaw resistance of concrete. Each prism was tested after 14 days of moist curing. A sonometer, shown in figure 20, was used to determine the transverse resonance frequency of each test sample. The samples were subjected to freeze-thaw conditions using an apparatus shown in figure 21. The apparatus was controlled by computer software used to program 8 cycles per day. The samples were tested for transverse frequency every 5 days.

Figure 20. A sonometer

Figure 21. Freeze-thaw apparatus

Scaling Test (ASTM C672)

Three square slabs, each of a 12-in width and a 3-in height, were tested for their scaling resistance. Samples were also moist cured for 14 days inside the curing room and then left to dry in the environmental chamber for another 14 days. At the end of 28 days, each sample was covered with a thin film of a calcium-chloride and water solution, having a concentration such that each 100 ml of solution contains 4 grams of anhydrous calcium chloride. The specimens were then placed in a freezer (shown in figure 22) for a period of 16 to 18 hours. After that, the samples were removed and placed in the environmental chamber for a period of 6 to 8 hours. These cycles were repeated, and observations were made every 5 days. The test was continued for 50 cycles. A scaling sample is depicted in figure 23.

Figure 22. Laboratory freezer for scaling test

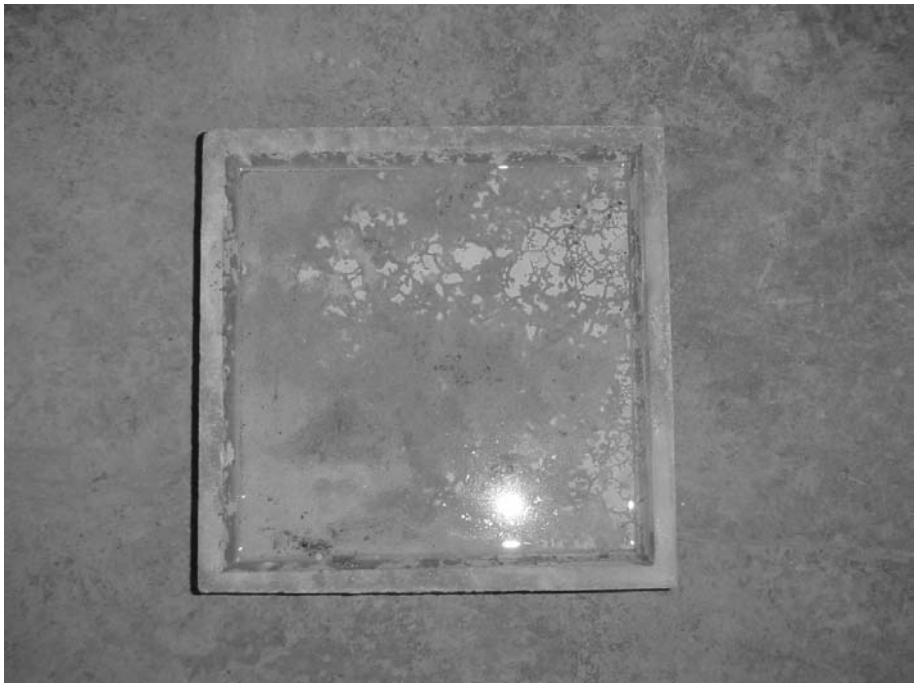
Figure 23. Scaling test sample

Chloride Permeability, (ASTM C1202-94)

The rapid chloride permeability tests were performed at NJDOT chemical laboratory. Four samples were tested for each mix at 28 (36 days in some cases), 56, and 90 days. First the four samples were cut into three lifts of 2-in slices using the water-cooled diamond saw or silicon-carbide saw. A belt sander was used to remove any burrs on the ends of the specimens. After the samples were cut, they were stored in the curing room until the test date. On the test date, the first lifts of each sample were allowed to dry for about 1 hour. After drying, the side surfaces of the specimens were coated with high strength epoxy. The specimens were then left for 24 hours to cure. When the coating was cured, about a gallon of water (depending on the size of the desiccators) had to be boiled and cooled. While doing that, the coated specimens were placed in the desiccators and vacuum for three hours. After three hours, the de-aerated water was drained into the vacuum from a separator funnel, and the vacuum was allowed to pump for 1 additional hour. Then the vacuum was turned off, allowing air to re-enter the desiccators, and the specimens were then soaked under water for 18 hours.

The specimens were removed from the water and towel dried. The cells were then coated on the sides with silicon material to prevent the chemical solutions from leaking. One side of the cells was filled with 3.0 percent NaCl solution (negative terminal) and the other (side) filled with 0.3 N NaOH solutions (positive terminal). The wires from the RCPT apparatus were connected with the cells. Then the power of the apparatus was turned on and set to 60 volts. The current was recorded every 30-minutes, for 6 hours. Table 7 shows the classification of chloride permeability. The calculation and of the total charges are performs as follows:

1) Plot current versus time and integrate the area underneath the graph to obtain the coulombs.
2) If the current is record every 30 min use the following equation:

$$Q = 900(I_0 + 2I_{30} + 2I_{60} + \ldots + 2I_{300} + 2I_{330} + I_{360}) \quad (3)$$

Where,

Q = total charges in coulombs

I_n = the current at n minutes

Table 7. Classification of chloride permeability

Charge Passed (Coulombs)	Chloride permeability
> 4000	High
2000 - 4000	Moderate
1000 - 2000	Low
100 - 1000	Very Low
< 100	Negligible

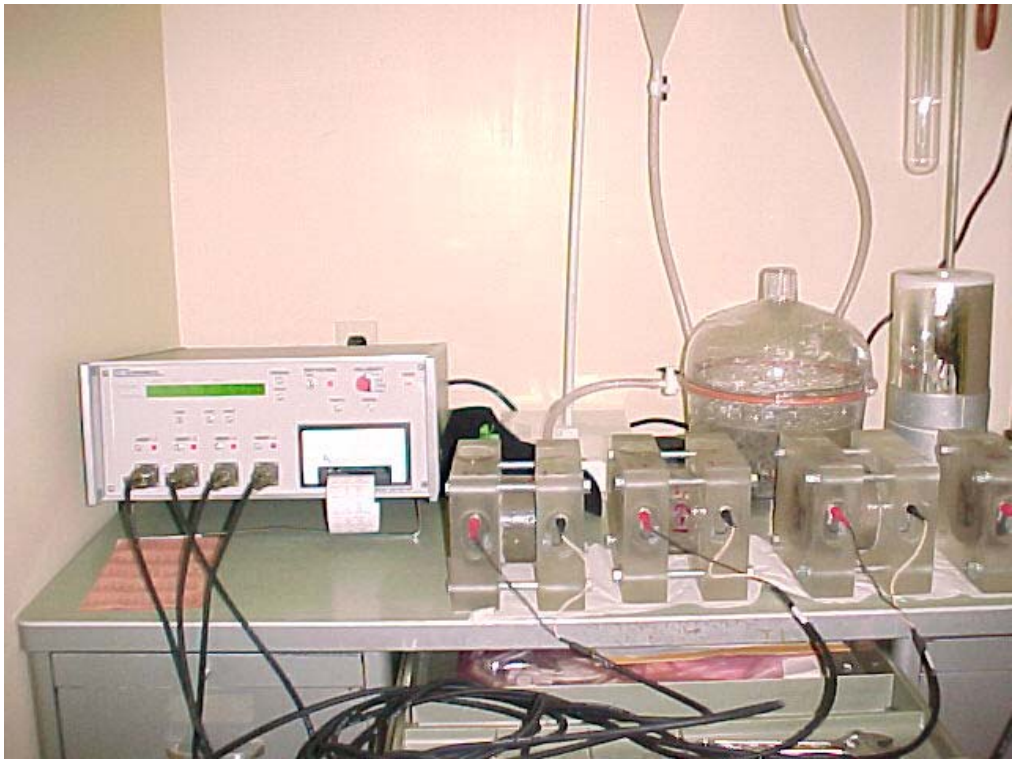

Figure 24. Rapid chloride permeability test equipment

Results and Discussion

Freeze-Thaw

All of the selected mixes have a durability factor greater than 85 percent, which meets the requirement for freeze-thaw durability as long as the air content in concrete is between 4 to 7 percent.

Scaling Test

The scaling test is very subjective because the rating scale is based on observation. However, none of the samples tested show a rating of 3 (moderate scaling) where coarse aggregate is visible.

Ponding Test

Ninety-day ponding tests were performed on some of the mixes. The NJDOT staff determined the total integral chlorides. The result is very promising especially with the chloride content ranging from 0.5 to 1.0 –in, at which level a tremendous decrease in chloride content is experienced.

Rapid Chloride Permeability

The results from the rapid chloride permeability test (RCPT) yield very low chloride permeability at 90 days for all the tested specimens. From the results, a direct correlation between the w/b ratio and the permeability of concrete could be established. Generally, concrete with low w/c ratio has lower chloride permeability, as shown in figure 25.

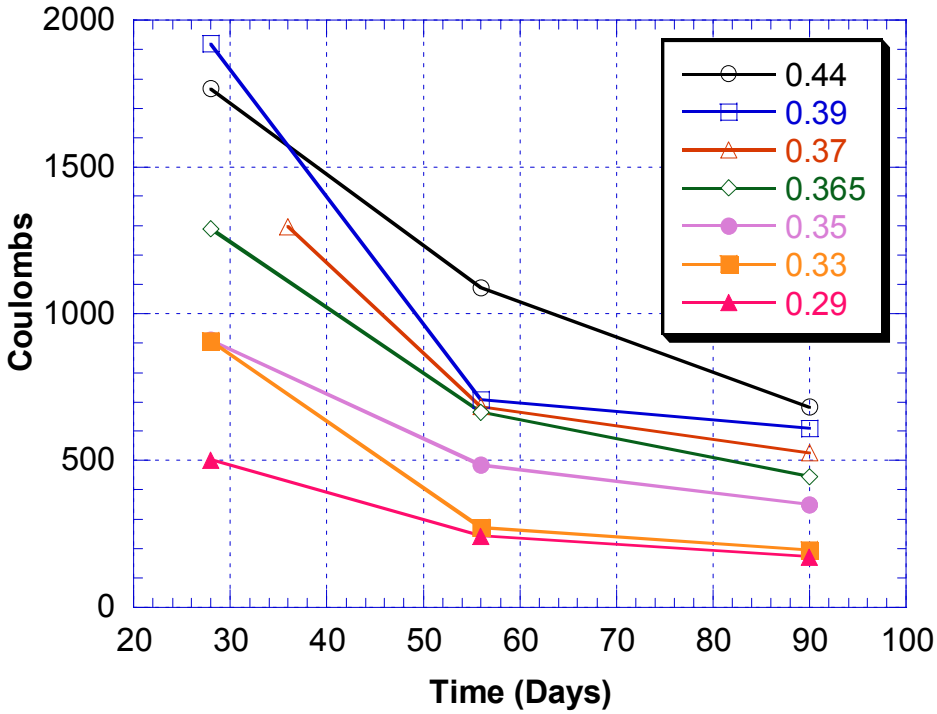

Figure 25. Effect of w/b ratio on RCPT

However, this is only true if the only variation between the mixtures is the w/b ratio; the pozzolanic effect has more influence on the chloride permeability. The concrete mixture with high volumes of pozzolanic materials decreases the permeability of concrete, as illustrated in figure 26. The RCPT results at 28 days are not a good indication of the permeability of concrete because the permeability readings vary dramatically whereas at 56 days the permeability readings begin to settle. Thus, the comparison is made at 56 days, as illustrated in figure 27. From the graph, as expected, the concrete mixture with 15 percent silica fume and 20 percent fly ash performs the best in RCPT because the mixture has the highest level of pozzolanic material replacement.

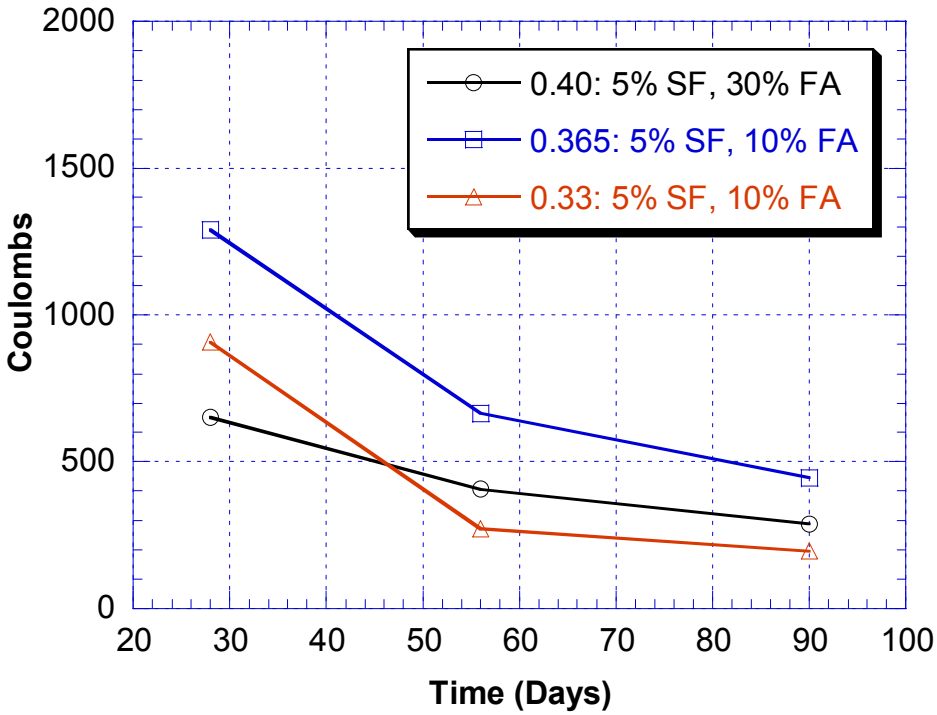

Figure 26. Effect of high volume of pozzolan on RCPT

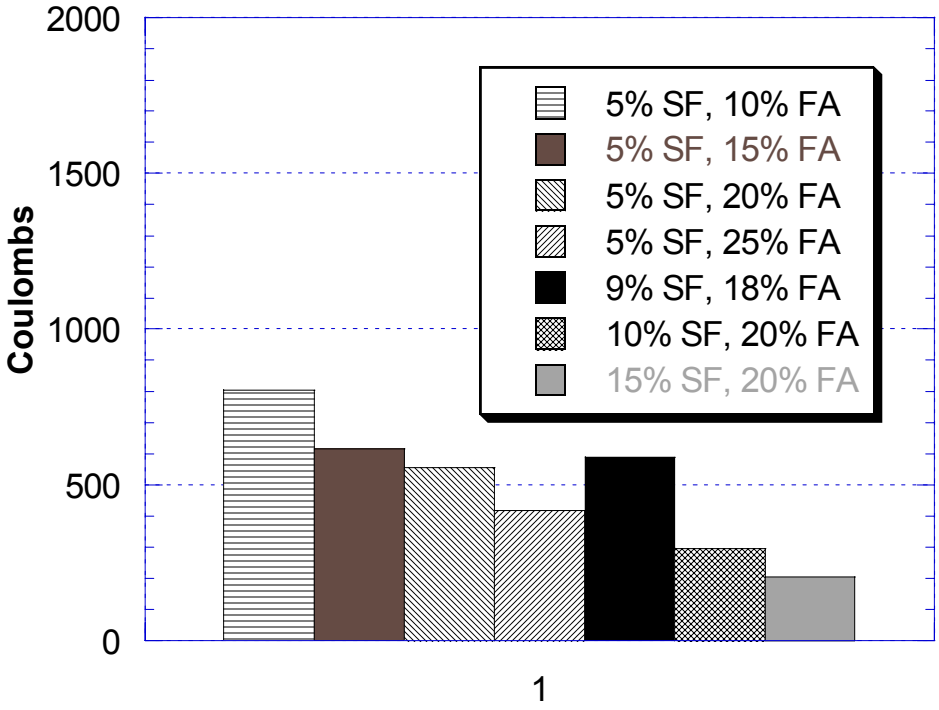

Figure 27. Effect of pozzolan on RCPT (w/b = 0.39)

The effects of individual pozzolanic material replacement were also observed. Figures 28 and 29 illustrate the effects of fly ash and silica fume on RCPT respectively. Both pozzolans have lower permeability than conventional concrete. The plots show silica fume significantly improves concrete permeability whereas 20 percent of fly ash is needed for the permeability to be classified as very low (less than 1000 coulombs).

Furthermore, as shown in figure 30, the RCPT results of these mixtures are compared with the mixtures containing both silica fume and fly ash. RCPT readings of the mixtures with both silica fume and fly ash, as expected, outperform the mixtures with either silica fume or fly ash.

The effect of RCPT on the size of aggregate is evaluated, as shown in figure 31. From the curve, a 27-percent increase in permeability is observed when using the larger size aggregate. The bigger voids in concrete with larger size aggregates contribute to this increase in permeability.

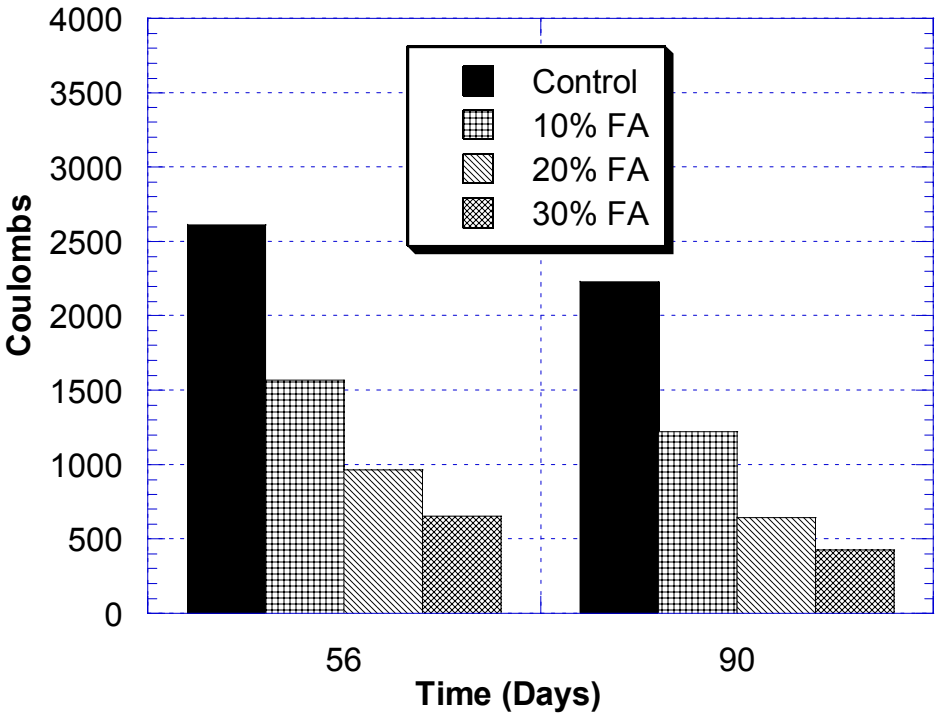

Figure 28. Effect of fly ash on RCPT (w/b = 0.39)

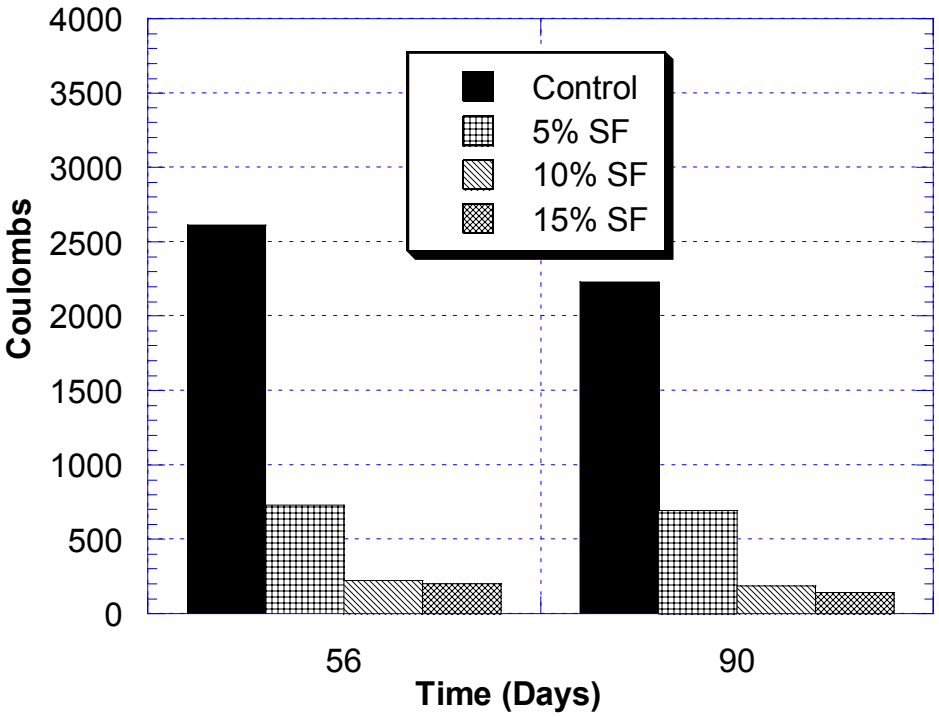

Figure 29. Effect of silica fume on RCPT (w/b = 0.39)

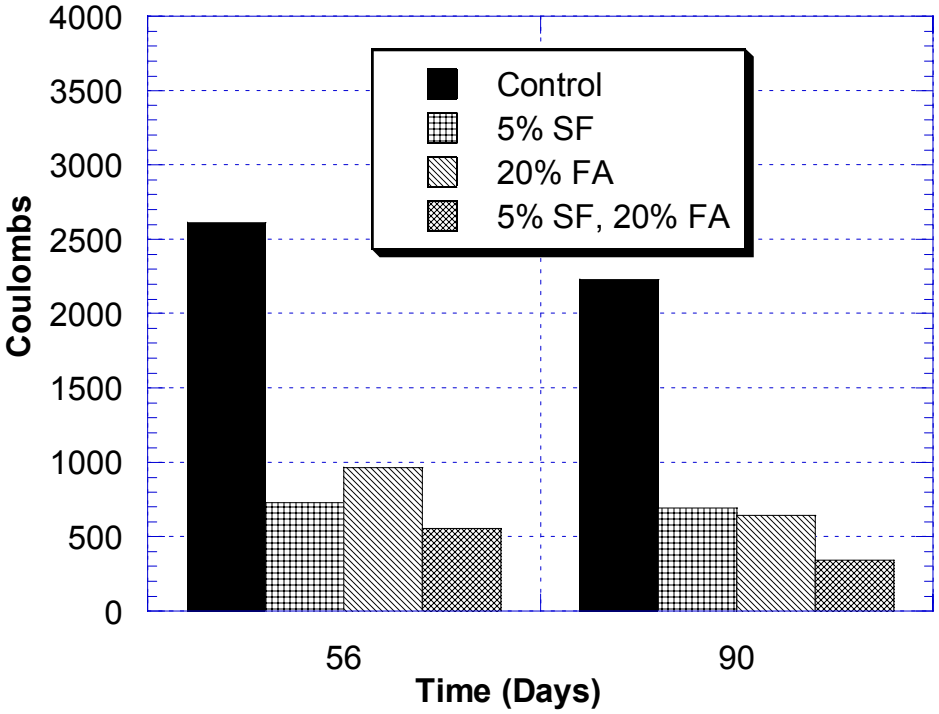

Figure 30. Effect of pozzolan on RCPT of HPC (w/b = 0.39)

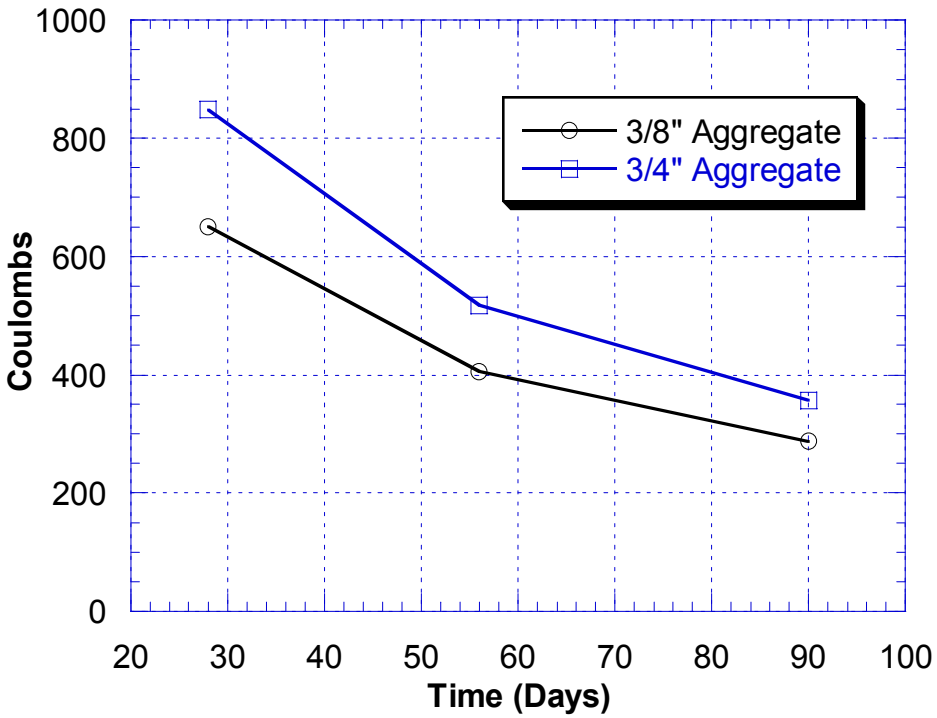

Figure 31. Effect of aggregate size on RCPT (w/b = 0.39)

Finally, as explained earlier the low strength concrete mixtures were developed, and their results are plotted on Figure 32a and b. From the graphs, mixtures with a combination of fly ash and silica fume at all w/b ratios have very low permeability at the 90-day test. Fly ash is more effective than silica fume, but this is probably attributed to the high amount of fly ash added. Also from the plots, HPC concrete could be developed using a high w/b ratio as long as a high amount of pozzolanic material exists. The coulombs could even be lower if more silica fume is added to the mix.

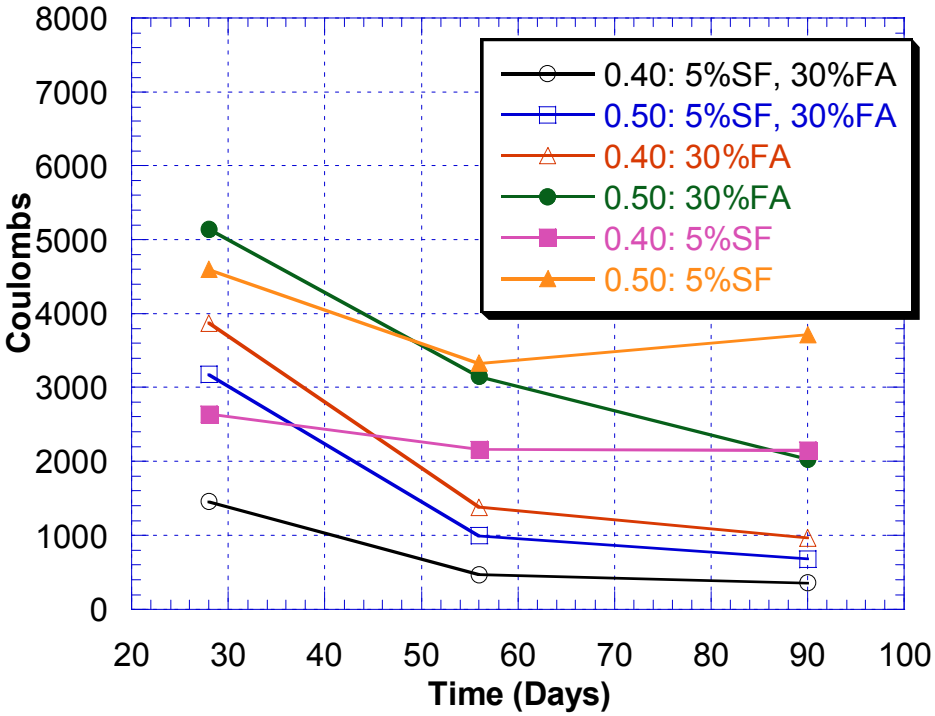

Figure 32a. Effect of low strength HPC on RCPT

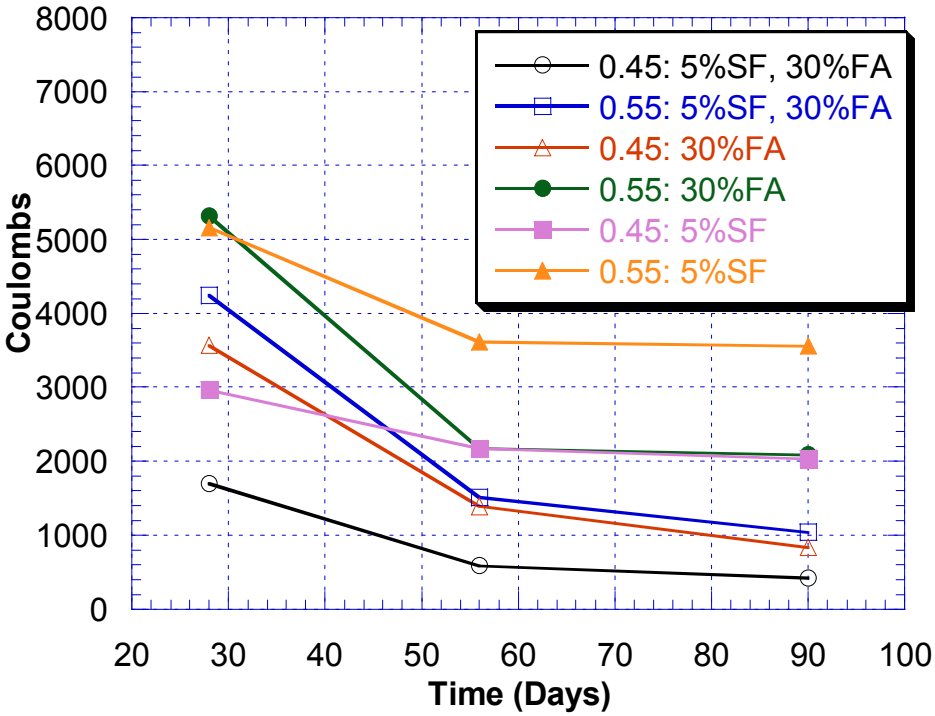

Figure 32b. Effect of low strength HPC on RCPT

Curing Methods

The effect of curing on RCPT was also investigated, and the results are shown in figure 33. From the plot, the same conclusion, as mentioned earlier, is deduced; the high water demand of the pozzolanic material makes curing a problem for the HPC mix. Therefore, the time in which the concrete is cured has to be increased from 7 to 14 days. As for the RCPT, the concrete that was cured with curing compound performs well compared with 14-day curing.

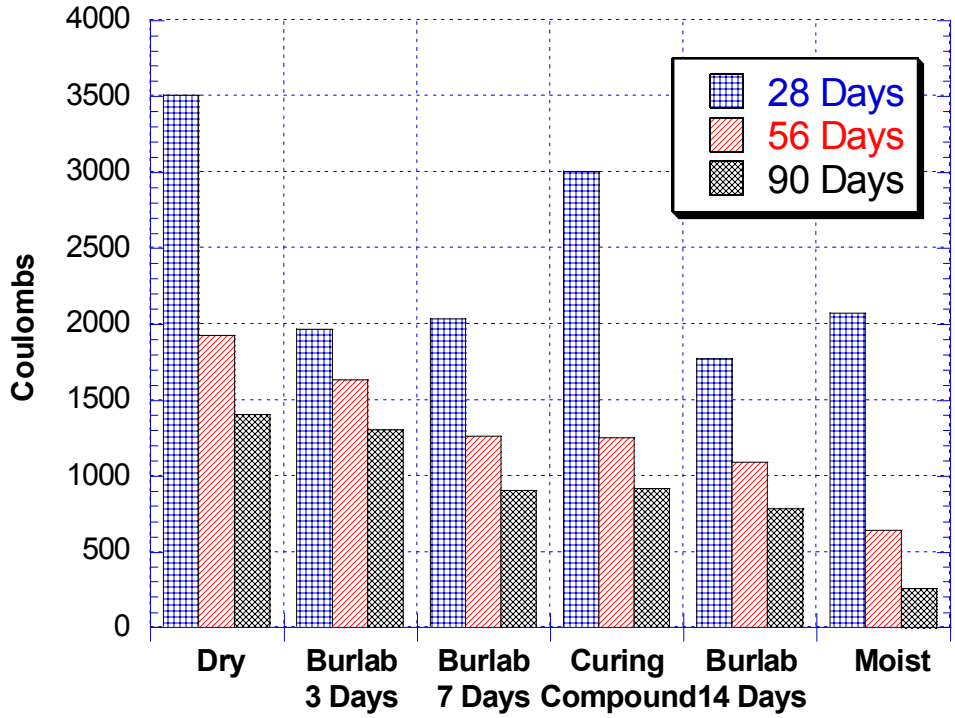

Figure 33. Effect of curing method on RCPT

Phase III

One of the problems with HPC is early-age shrinkage. Because HPC usually has low w/b ratio and higher water demand than regular concrete, early-age (autogenous) shrinkage, which is usually ignored for regular concrete, becomes more significant and can not be overlooked. In this phase, the effect of early-age shrinkage on HPC was investigated.

Mix Proportions

The mix proportion procedure is based on the same procedure as that followed in Phase I. Two w/b ratios, 0.29 and 0.35, were investigated. All mixes contained 10 percent silica fume. Mix L2 and L3 contained an addition of 20 percent fly ash and 20 percent slag respectively. Mix L1 is the same as mix L4 but using lightweight aggregate. Mix M1 and M2 are exactly the same, but mix M1 has a higher dose of superplasticizer. Mix M3 and M4 contain 20 percent fly ash and 20 percent slag respectively. Table 8 summarizes the mix proportions.

Table 8. Mix proportions for phase III

Mix	w/(c+p)	SF (%)	FA (%)	Slag (%)	SP (oz/100lb)	AEA (oz/100lb)
L1	0.29	10	0	0	22	2
L2	0.29	10	20	0	22	2
L3	0.29	10	0	20	22	2
L4	0.29	10	0	0	22	2
M1	0.35	10	0	0	20	2
M2	0.35	10	0	0	12	2
M3	0.35	10	20	0	12	2
M4	0.35	10	0	20	12	2

Figure 34. Autogenous shrinkage specimens

Autogenous Shrinkage

The concrete prisms tested for drying shrinkage were used to determine the autogenous shrinkage using the embedded Vibrating Wire Strain Gauge (VWSG) model VCE 4202 by Geokon. The main reason for its use was its sensitivity and low modulus of elasticity allowing the measurement of autogenous shrinkage. The VWSG data was collected immediately after placing the concrete in the molds using a data logger capable of recording data every 10 minutes. After one week, the VWSG was disconnected from the data logger, and a manual portable VWSG readout box was used to record data daily for 28 days. After that, the data was recorded on a weekly basis because the shrinkage rate became less drastic.

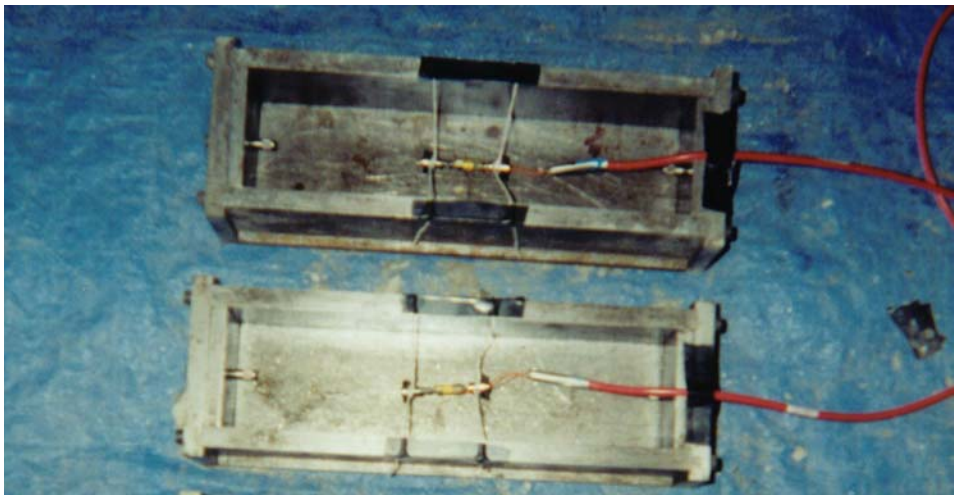

Figure 35. VWSG installation

Drying Shrinkage

Drying shrinkage was performed the same way as described in Phase I. However, the comparator readings were also compared to the embedded VWSG by taking the total strain minus the autogenous shrinkage strain (strain at 24 hours).

Results and Discussion

Fresh mix concrete and Compressive Strength

Both air content and slump of concrete were recorded for each mix. Table 9 summarizes the results. The compressive strength of the mixes is summarized in table 10. The results to those from Phase I; the strength decreases if the concrete is improperly cured. Note that for the burlap-cured specimens, the wet burlap was removed at 28 days.

Table 9. Mix proportioning and fresh concrete properties

Mix	w/(c+p)	SF (%)	FA (%)	Slag (%)	SP (oz/cwt)	AEA (oz/cwt)	Air Content (%)	Slump (in)
L1	0.29	10	0	0	22	2	2.50	2.50
L2	0.29	10	20	0	22	2	6.75	8.00
L3	0.29	10	0	20	22	2	2.25	1.25
L4	0.29	10	0	0	22	2	1.75	3.50
M1	0.35	10	0	0	20	2	7.75	7.75
M2	0.35	10	0	0	12	2	4.00	4.00
M3	0.35	10	20	0	12	2	6.50	7.00
M4	0.35	10	0	20	12	2	2.00	4.50

Table 10 Compressive strength results of phase III mixes

Mix	**Curing Method**	**Day 1 (psi)**	**Day 3 (psi)**	**Day 7 (psi)**	**Day 14 (psi)**	**Day 28 (psi)**
L1	B	5929	7441	8993	9967	10191
	C	5372	7779	8555	8813	9793
	D	5949	7262	8276	8714	9112
L2	B	3899	5889	6784	7441	8674
	C	4019	6207	6705	6923	7401
	D	3780	5592	5989	7103	7242
L3	B	6784	8555	8396	9709	9400
	C	5809	7918	8356	8714	8917
	D	6704	7560	7480	7501	8757
L4	B	3344	5493	5175	5569	5610
	C	3463	4777	5255	5291	5569
	D	3284	4936	5056	5131	5414
M1	B	5451	6068	6565	6687	8194
	C	4358	5990	6665	7006	7240
	D	3446	6129	6028	5573	6722
M2	B	5889	6824	7481	8197	8712
	C	5670	6466	7222	7679	7757
	D	5412	6685	7242	7699	8592
M3	B	3522	4418	4936	5414	6550
	C	3402	4617	4856	5254	5569
	D	3343	4418	4856	5334	5675
M4	B	4795	6210	7085	7882	9255
	C	5889	6090	7165	7762	7399
	D	4258	5573	6050	7285	7849

Drying Shrinkage

Figure 36 shows the effects of curing methods on the drying shrinkage of concrete measured with a length comparator. Here, moist cured samples outperform the dry samples. Figure 37 shows the effect of the pozzolan on the drying shrinkage for dry-cured samples. The mixture containing silica fume with fly ash has the least shrinkage value when compared with other mixtures. Figure 38 shows the effect of the aggregate type on drying shrinkage. Lightweight aggregate shrinks less in comparison with normal aggregate. The reason for this is the high absorption rate of lightweight aggregate, which causes the internal curing. The absorbed water in the lightweight aggregate is released to the binding material; thus, less shrinkage is observed. Figure 39 shows the effect of superplasticizer on the drying shrinkage of concrete. The mix with a higher dosage of superplasticizer shrinks more than the mix with a lower dosage. It should be noted that all the drying shrinkage results from the length comparator were in agreement with the results obtained from the vibrating wire strain gauges in all cases.

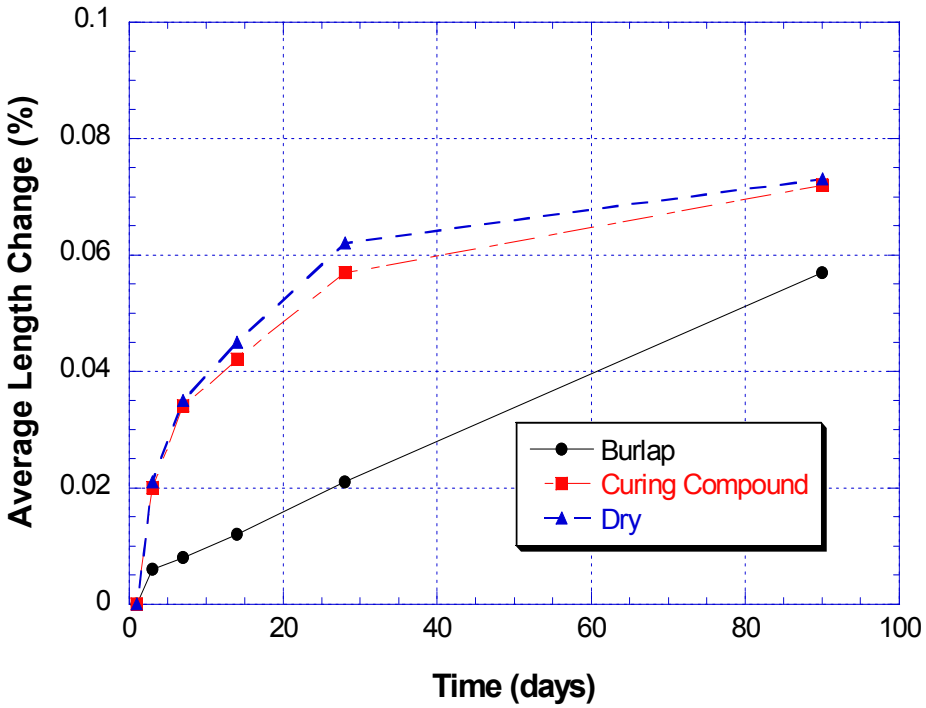

Figure 36. Effect of curing method on drying shrinkage

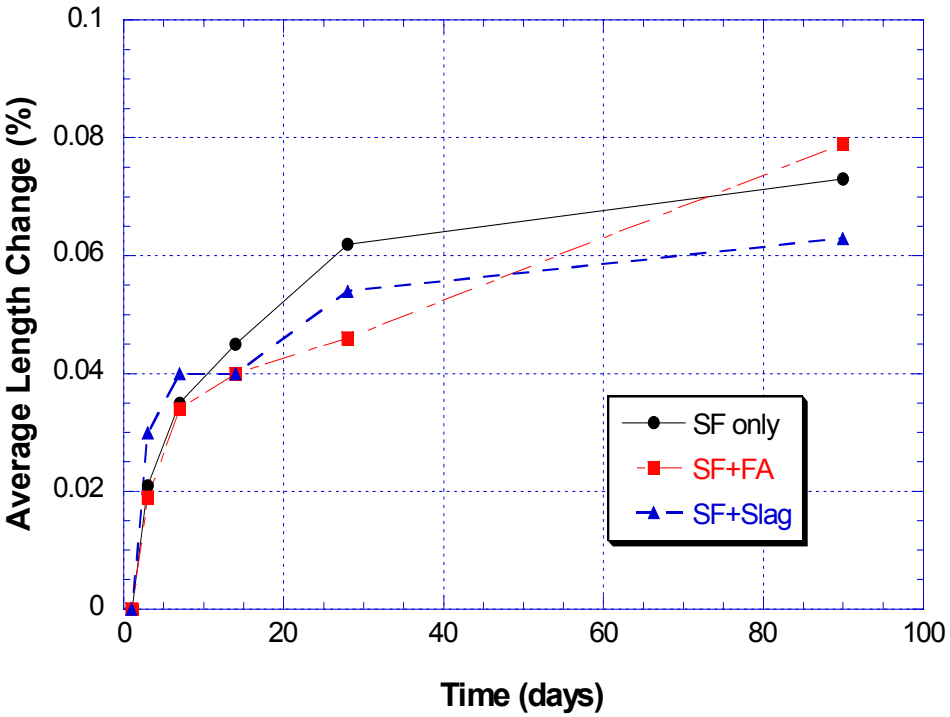

Figure 37. Effect of pozzolan on drying shrinkage

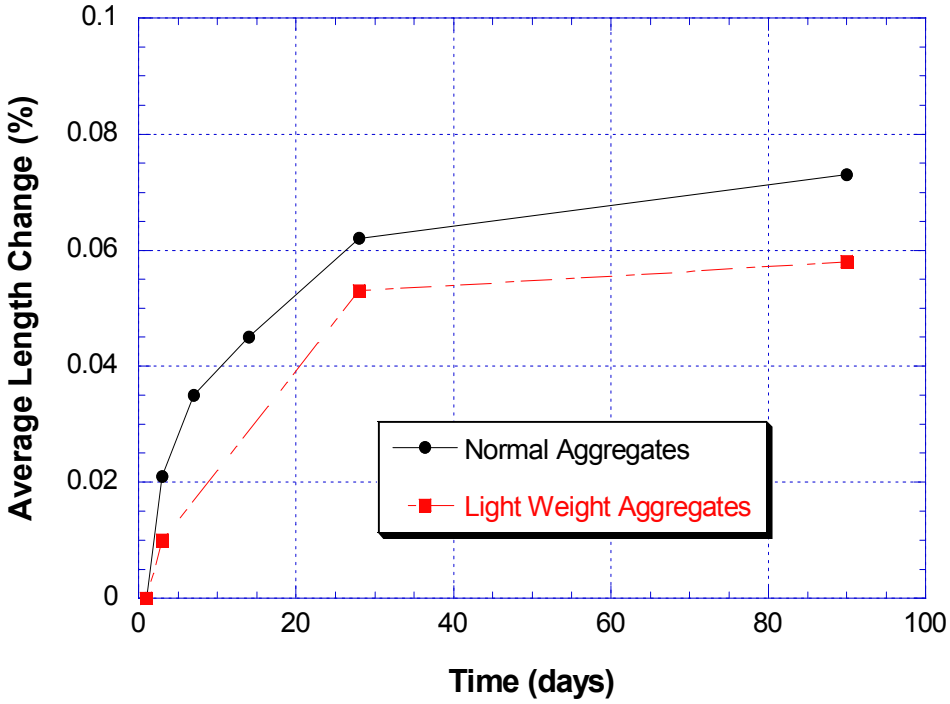

Figure 38. Effect of type of aggregate on drying shrinkage

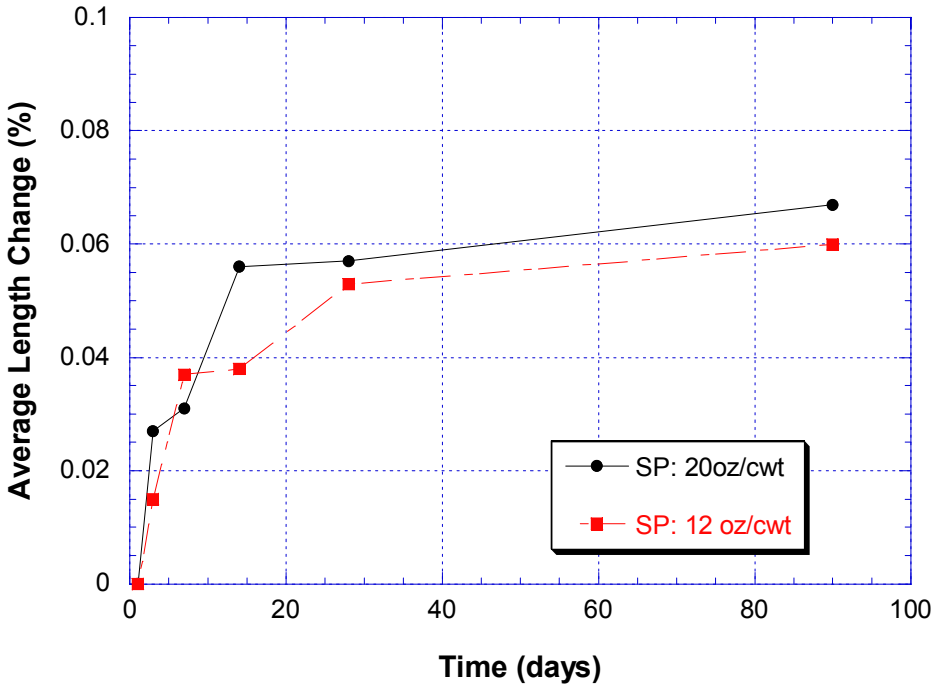

Figure 39. Effect of superplasticizer on drying shrinkage

Autogenous Shrinkage

Figure 40a shows the effects of the curing method on autogenous shrinkage of concrete in the first 48 hours. For all the w/b ratios, pozzolan contents, aggregate types, and amounts of superplasticizer, it was observed that moist burlap curing helped reduce the shrinkage. Burlap cured samples for all the mixes outperformed in shrinkage followed by samples cured with a curing compound. Dry-cured samples experienced the worst shrinkage, the reason being the hydration process demanded a lot of water, which was not supplied in the dry cured condition.

Figure 41 depicts the effect of pozzolans on the autogenous shrinkage of concrete within the first 48 hours of its placement. The mix containing fly ash shows the least autogenous shrinkage. After all, fly ash slows down the rate of the hydration process. Mixtures containing only silica fume or silica fume with slag have higher shrinkage. Figure 42 illustrates the effect of lightweight aggregate on the autogenous shrinkage of concrete in the first 48 hours for the dry-cured samples. Likewise, the lightweight aggregate helps reduce autogenous shrinkage.

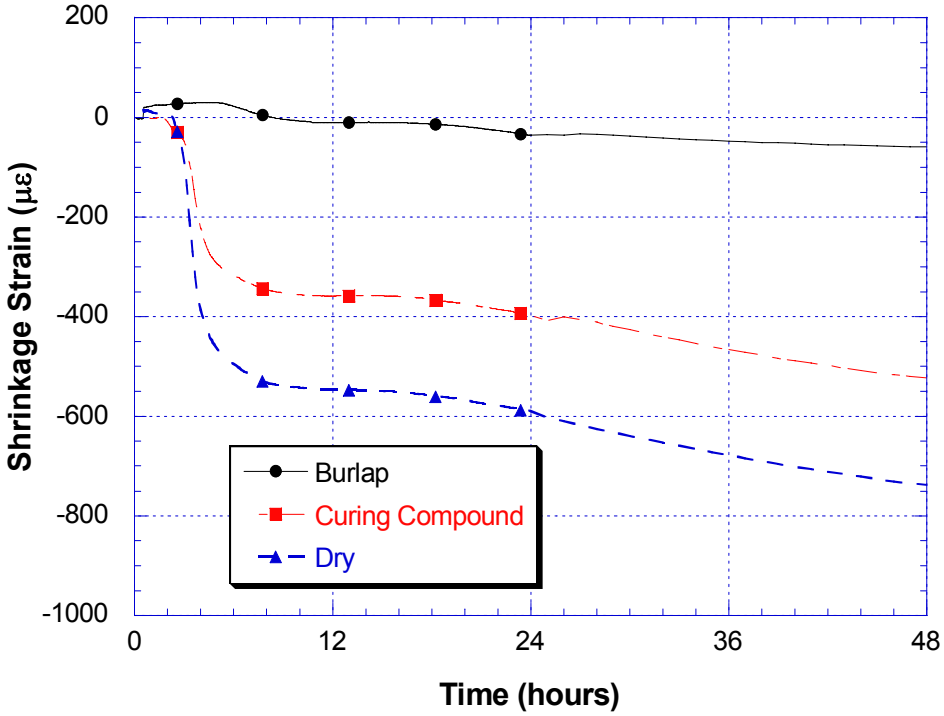

Figure 40a. Effect of curing methods on autogenous shrinkage

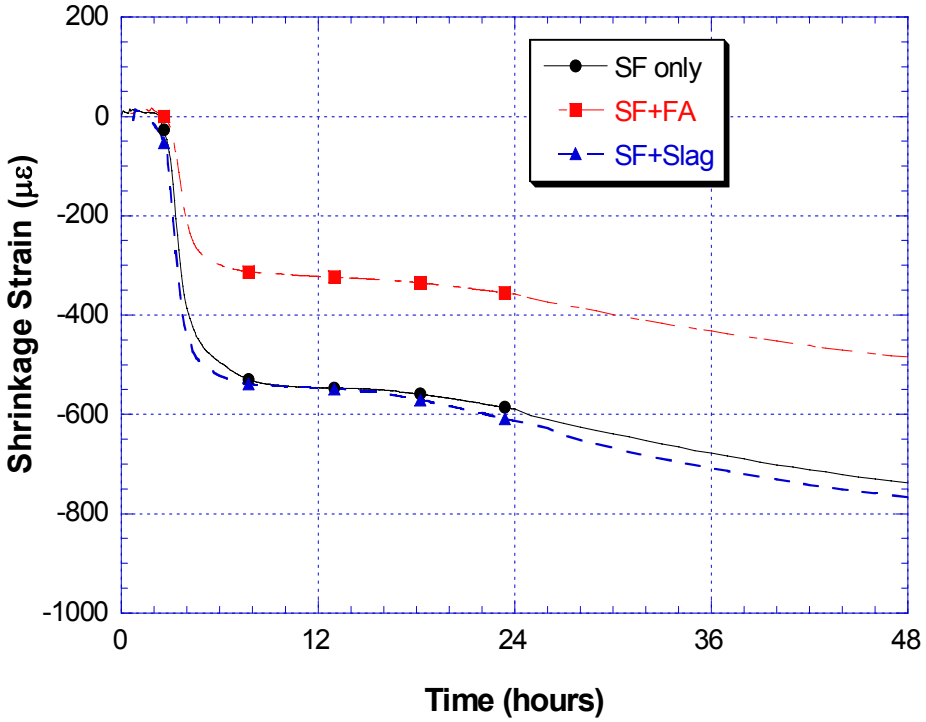

Figure 40b. Effect of pozzolans on autogenous shrinkage

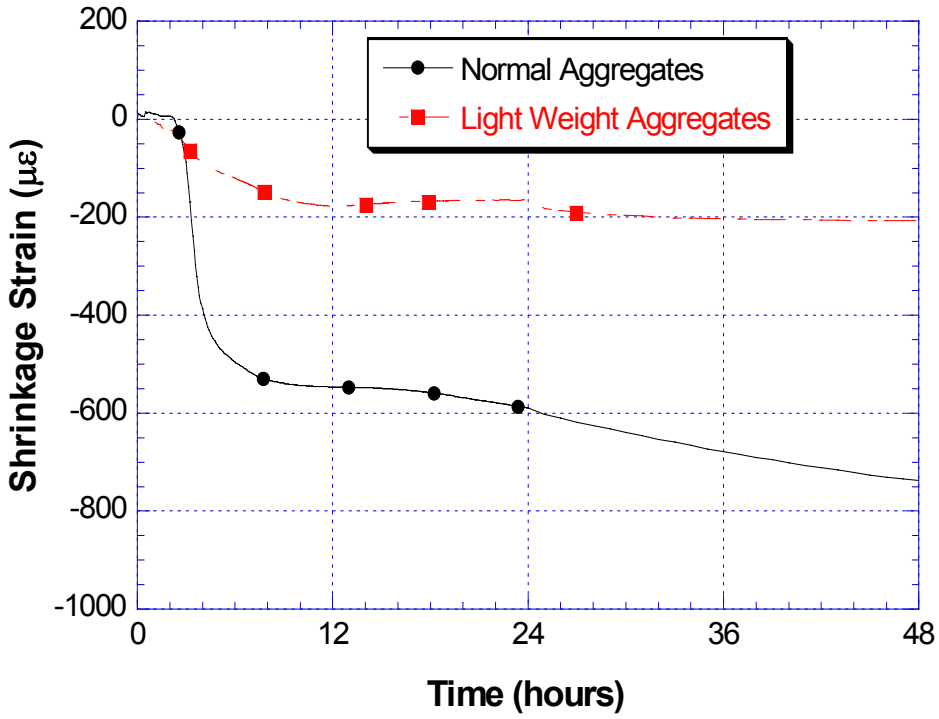

Figure 41. Effect of type of aggregate on autogenous shrinkage

An attempt was also made to measure the temperature of the samples during the hydration process with the help of a vibrating wire strain gauge. Figure 42 displays the temperatures of the samples in the first 48 hours for different curing conditions. Evidently, the temperature at the peak of the hydration process is highest for the moist cured samples even though they are cured with burlap immediately after placing. This phenomenon occurs because moist cured samples use all the water for the hydration process; any hydration is associated with the liberation of heat during the chemical reaction. For the samples cured by means other than moist curing, the water is not enough for a complete hydration reaction, and thus, liberation of heat is very low. Figure 43 shows the temperature variation for moist burlap cured samples for different types of pozzolan; the mix containing only silica fume has a higher temperature than the mix containing silica fume with fly ash. This occurs because fly ash is less reactive to water and does not help in the hydration process. Thus, the liberated heat was lower than in other mixtures.

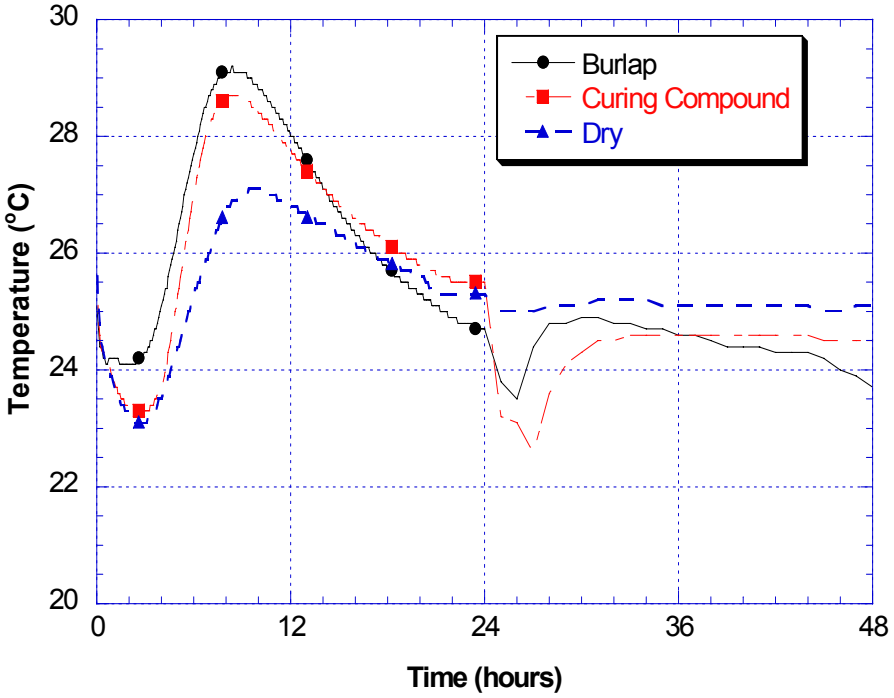

Figure 42. Effect of curing method on the internal temperature of concrete

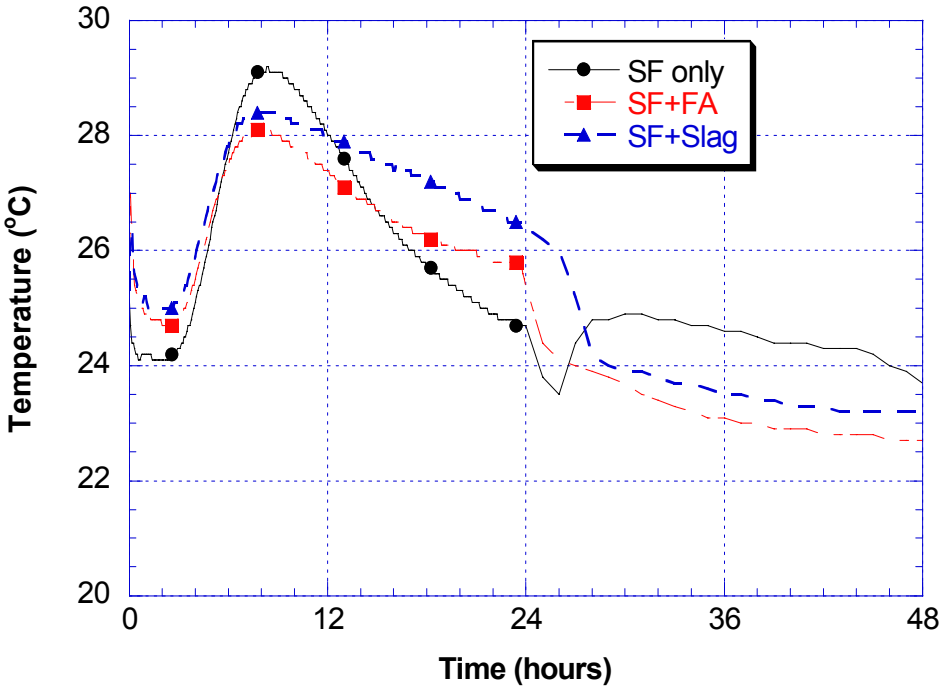

Figure 43. Effect of pozzolan on the internal temperature of concrete

Phase IV

The implementation of HPC is not only limited to bridge decks but also bridge girders. Today, concrete bridges are designed and constructed using prestressed concrete girders. One of the key elements in designing prestressed concrete is to determine the partial losses of prestressing. These losses are usually assumed, but because the constituents of HPC differ from regular concrete, these losses must be examined for HPC. One of the important prestressing losses is the creep of concrete. Phase IV investigates the compressive creep of HPC.

Mix Design

There are a total of eleven mixes that were used in this study. The first three mixes, shown in table 11, are based on the optimum HPC mix developed in phase I. They all have the same percentage of silica fume (5 percent) and fly ash (10 percent) and they have a compressive strength of 8, 10, and 12 ksi, respectively. The other two mixes represent different combinations of pozzolanic materials. Table 12 shows the remaining six mixes used for determining the effect of one type of pozzolan on creep, where the first three contain silica fume only and the remaining three contain fly ash only.

Creep Chamber

The environmental chamber, used for creep and shrinkage measurements, is a 24- by 16- by 8-ft walk-in chamber made of insulated aluminum walls. The temperature and humidity of the room is controlled by a digital control unit located outside the room next to the entrance. The digital control unit acquires the temperature and humidity readout from an environmental sensor inside the room. This sensor is positioned so the overall temperature and humidity is at the set point. The range of temperature and humidity at which the chamber could be set are 39- to 104-degrees Fahrenheit and 30- to 80-percent respectively. Inside the room, the temperature is adjusted through the heaters and freezer units that occupied one side of the wall. The unit is shielded with aluminum sheet with blowers attached to it so that the air can be circulated. The room is also equipped with a dryer and a humidifier located on the same wall and on top of the chamber, respectively.

A total of 18 creep loading rigs are in the chamber. Each rig is designed for testing three 6- by 12-in creep specimens. The rig is build up of two 20- by 20- by 2.5-in plates, two 15- by 15- by 2.5-in plates, five double coiled springs, and four 1-in diameter high strength threaded rods. The two 20- by 20- by 2.5-in plates are used for sandwiching the five double-coiled springs so that one plate, the specimen platform, is free to move and the other is fixed; when the specimens are loaded the springs will be compressed and maintain the applied load.

The two 15- by 15- by 2.5in plates are used as a top cover plate and a jacking stand. The five double-coiled springs are designed for a 200-kip load or 7-ksi for 6- by 12-in cylinders. Assuming that the applied load is 30 percent of the ultimate load, the rig is capable of loading concrete with a 23-ksi compressive strength. The load is monitored by a 200-kip load cell located between the specimens and the bottom platform. Figure 45a shows the actual creep rig and figure 45b shows a schematic drawing of the creep rig design.

Table 11. Creep mix design for mixes containing fly ash and silica fume

Raw Materials	Mix Identification				
	C5SF10FA	G5SF10FA	H5SF10FA	H5SF20FA	H10SF20FA
Portland Cement Type I (Lb/yd3)	664	777	988	872	813
Class F Fly Ash (Lb/yd3)	78	149	116	232	232
Silica Fume (Lb/yd3)	39	70	58	58	116
3/8-in Crushed Stone (Lb/yd3)	---	---	1722	1722	1722
3/4-in Crushed Stone (Lb/yd3)	1871	1871	---	---	---
Sand (Lb/yd3)	1191	1015	933	933	933
Water (Lb/yd3)	289	289	314	314	314
W/B	0.37	0.29	0.27	0.27	0.27
Superplasticizer (oz/cwt)	13	20	18	16	30
AEA (oz/cwt)	1.5	1.5	2.2	2.2	2.2
Slump (in)	3	4	3	5.5	2
Air Content (%)	5	3.5	1	2	0.5
28 days Compressive Strength (ksi)	8	10	13	12	12
56 days Compressive Strength (ksi)	9	11	N/A	N/A	N/A
28 days Shrinkage (%)	0.04	0.05	0.04	0.045	N/A
RCP @ 56 days	800	300	<300	<300	<300

Table 12. Creep mix design for mixes containing either fly ash or silica fume

Raw Materials	Mix Identification					
	H5SF	H10SF	H15SF	H10FA	H20FA	H30FA
Portland Cement Type I (Lb/yd3)	1104	1046	988	1046	930	813
Class F Fly Ash (Lb/yd3)	---	---	---	116	232	349
Silica Fume (Lb/yd3)	58	116	174	---	---	---
3/8-in Crushed Stone (Lb/yd3)	1722	1722	1722	1722	1722	1722
Sand (Lb/yd3)	933	933	933	933	933	933
Water (Lb/yd3)	314	314	314	314	314	314
W/B	0.27	0.27	0.27	0.27	0.27	0.27
Superplasticizer (oz/cwt)	18	20	22	14	9	10
AEA (oz/cwt)	2.2	2.2	2.2	2.2	2.2	2.2
Slump (in)	6	6	4.5	6	3.75	6.5
Air Content (%)	2	1	1	2	2.5	1
28 days Compressive Strength (ksi)	10	12	12	12	11	10
56 days Compressive Strength (ksi)	12	13	13	13	N/A	11
28 days Shrinkage (%)	0.06	N/A	N/A	0.054	N/A	0.046
RCP @ 56 days	<300	<300	<300	<300	<300	<300

Figure 44. Environmental chamber

Figure 45a. Creep rig

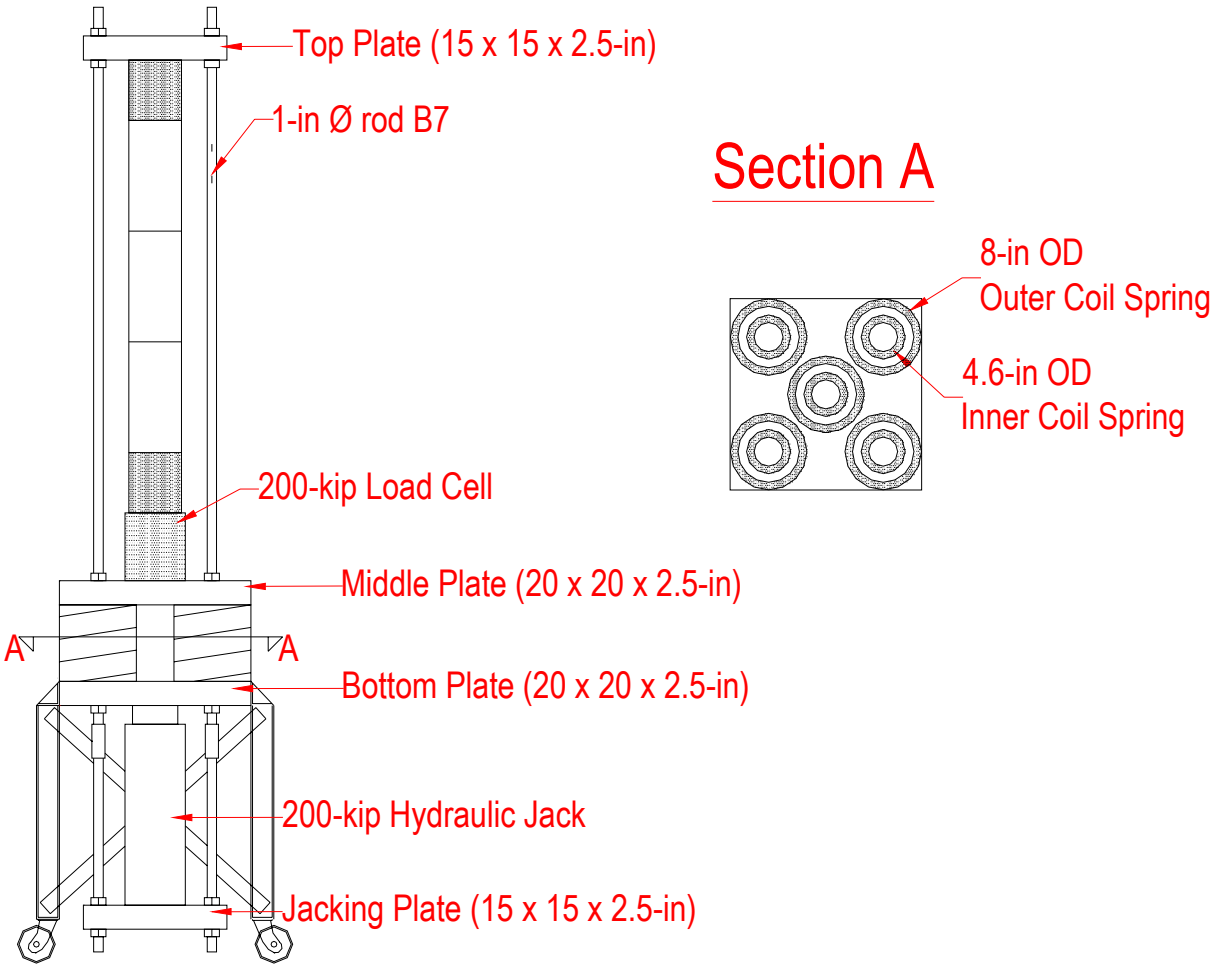

Figure 45b. Creep rig design

The creep and shrinkage strains are measured by vibrating wire strain gauges (VWSGs). Two types are used; one is an embedded gauge, and the other is an external gauge designed by Rutgers University. The embedded gauges, shown in figure 46, are used mainly in shrinkage specimens, and they are capable of measuring both autogenous and drying shrinkage. Furthermore, a conventional stud was also embedded at each end of the specimens so that the drying shrinkage strain from the gauges could be compared to measured strain using a length comparator.

External gauges are used for the creep specimens. The creep specimens are instrumented with external gauges using preinstalled threaded bolts; about a 1/2-in of the bolts are exposed so that the external gauges may be attached using lock nuts.

On each specimen, three external gauges are installed at 120 degrees to minimize the eccentric loading effects. The average strain of the three external gauges is used to calculate the total strain. The VWSGs are used because they provide long-term durability and accuracy. They are also unaffected by the change in resistance in the attached cable, and they are also temperature compensated. In addition to the three loaded creep specimens, external VWSGs are also installed on control or unloaded specimens to measure the strain caused by drying shrinkage. Figure 47 shows the external gauges on creep specimens.

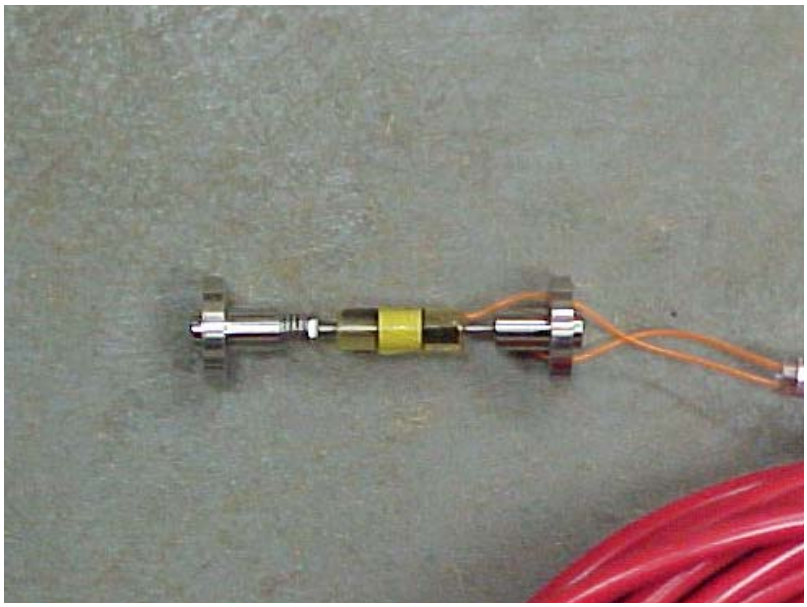

Figure 46. Embedded VWSG

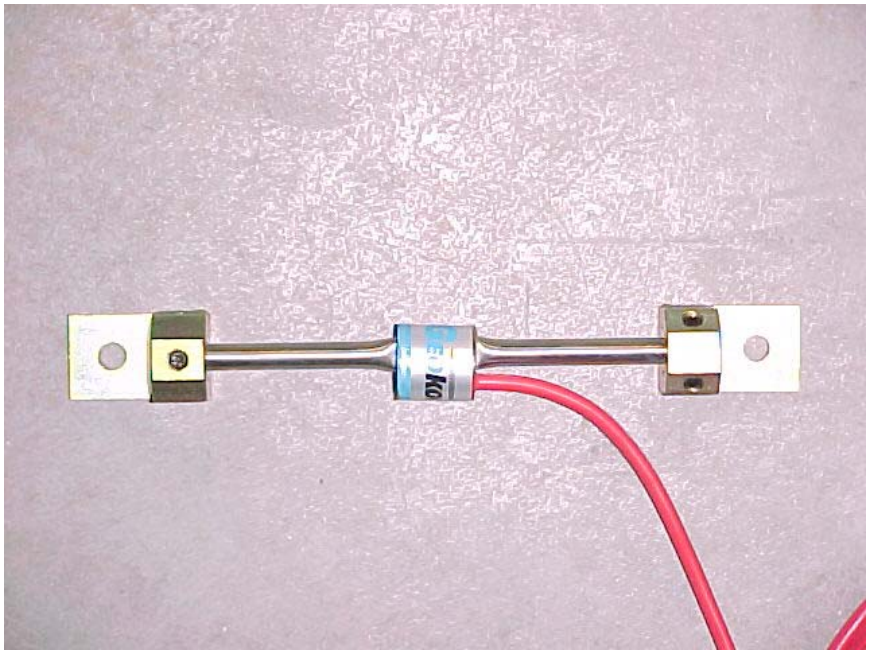

Figure 47. External VWSG

Because of the data-intensive nature of the project, two 96-channel data loggers are used to collect the data. The data loggers automatically collect strain and load data at 10-minute increments. The data can then be exported to Excel or any other program for processing. The data loggers are located next the chamber control unit shown in figure 48.

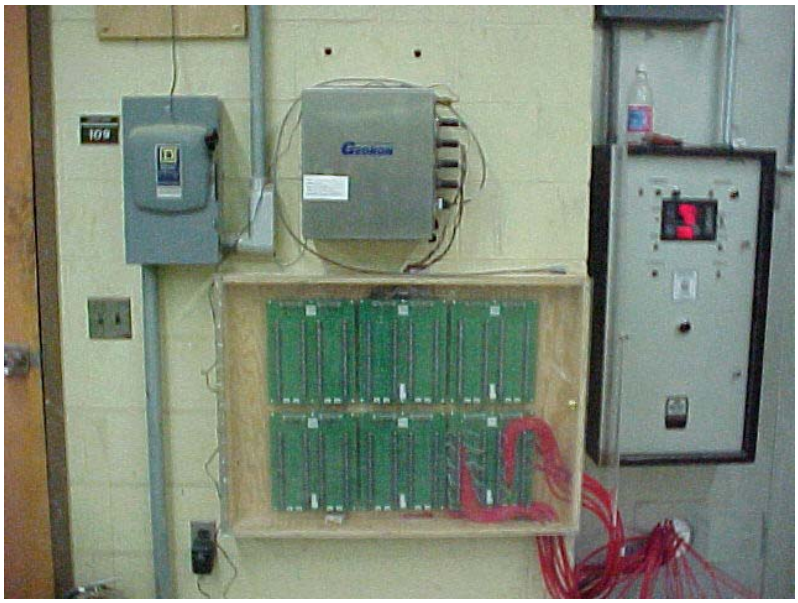

Figure 48. Data logger

Sample Preparations

Eight 6- by 12-in cylinders are made in order to perform creep testing. Five of the cylinders have embedded bolts, which are used for attaching the external VWSG's. Two cylinders are used for determining the compressive strength on the loading day. The last cylinder is cut in half and placed on top and bottom of the three loaded cylinders. These half cylinders eliminated local failure on the test specimens. The loaded specimens as well as the two half cylinders are covered with capping compound before loading. The capping compound is used to ensure smooth and flat contact surface between each cylinders.

Loading

During the loading day, the specimens are removed from the curing room. Three of the 6- by 12-in cylinders with bolts are used as loaded creep specimens. They are covered with sulfur capping to make a smooth surface before being loaded. Another two cylinders with bolts are used as control specimens. Another two without bolts are loaded in a compression machine to determine the ultimate compressive strength of concrete at the age of loading; thirty-five percent of the ultimate compressive strength is the constant load that should be applied to the specimens while loading.

In addition, a third sample without bolts is cut to obtain two 6- by 5-in concrete specimens. The five specimens with bolts are instrumented with external VWSG's. After fixing the sensors to the five specimens, the three capped specimens are inserted into the creep rig. The two small 6- by 5in small specimens are also capped and assembled inside the rig at the top and bottom of the three other creep specimens. Because of the data-intensive nature of the project, two 96-channel data loggers are used to collect the data. The data loggers automatically collect strain and load data every ten-minutes.

Figure 49. Loaded creep rigs

Results and Discussion

There are three main investigations performed in this project. These investigations consisted of 1) the effect of w/b ratio, 2) the effect of cement type, and 3) the effect of pozzolanic materials on compressive creep. In order to determine these effects, the specific creeps were calculated and used for comparison since dividing the creep strain by the applied load normalizes the specific creep. The creep results are plotted in figures 50 to 54. Figure 50 shows the effect of w/b ratio on the specific creep. The mix with higher w/b ratio has higher specific creep. Figure 51 illustrates the effect of cement type on the specific creep. From the figure, there are no significant effects on the cement type on specific creep. The effects of pozzolanic materials are divided into three groups, 1) effect of different percentage of silica fume, 2) different percentage fly ash, and 3) the effects of a combination of silica fume and fly ash on creep. These effects are plotted in figure 52 to 54. From the figures, an addition of silica fume lowers the specific creep whereas fly ash increases the specific creep. However, the specific creep of fly ash concrete could be lower by adding silica fume (and vice versa).

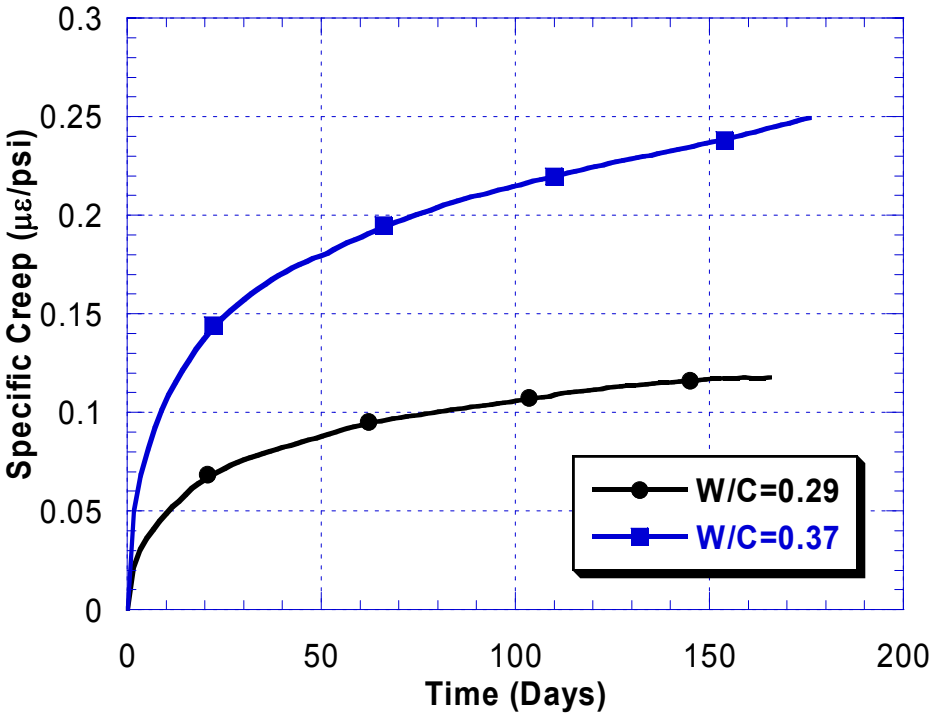

Figure 50. Effect of w/b ratio on specific creep

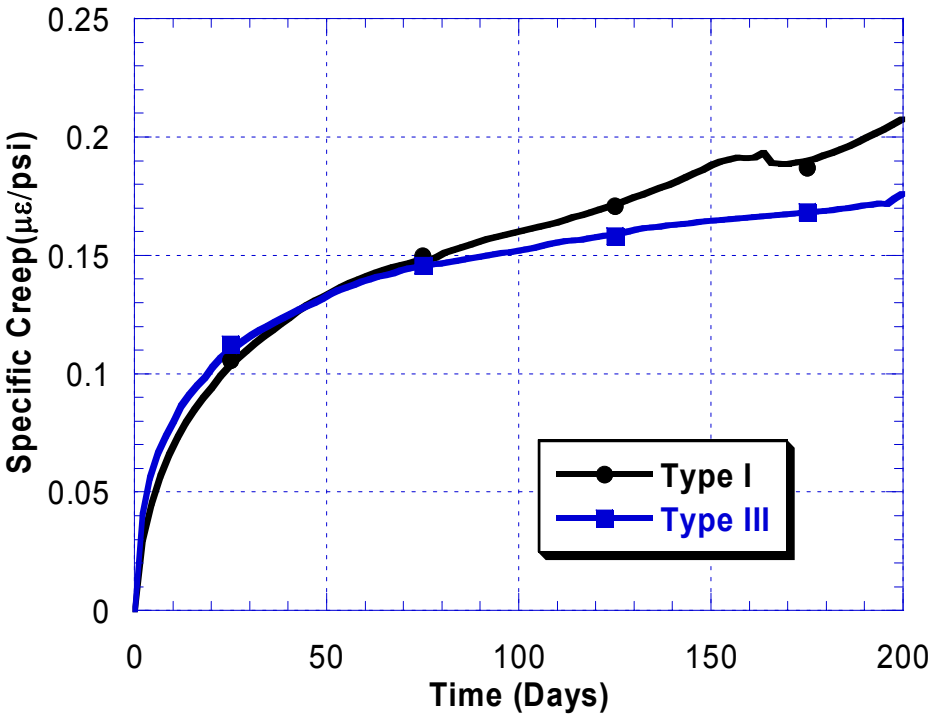

Figure 51. Effect of cement type on specific creep

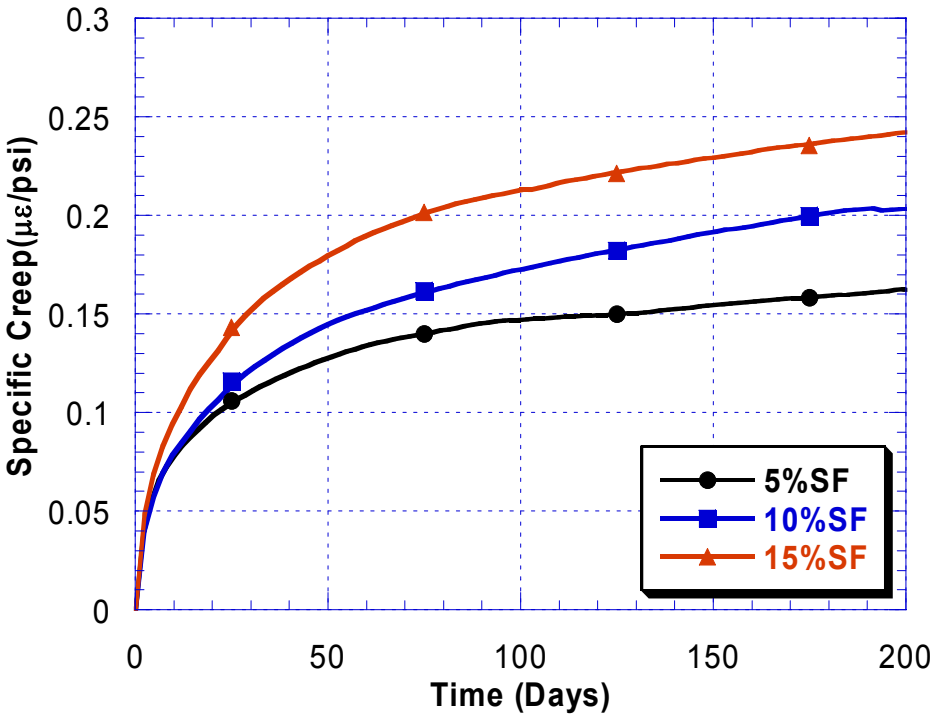

Figure 52. Effect of silica fume on specific creep

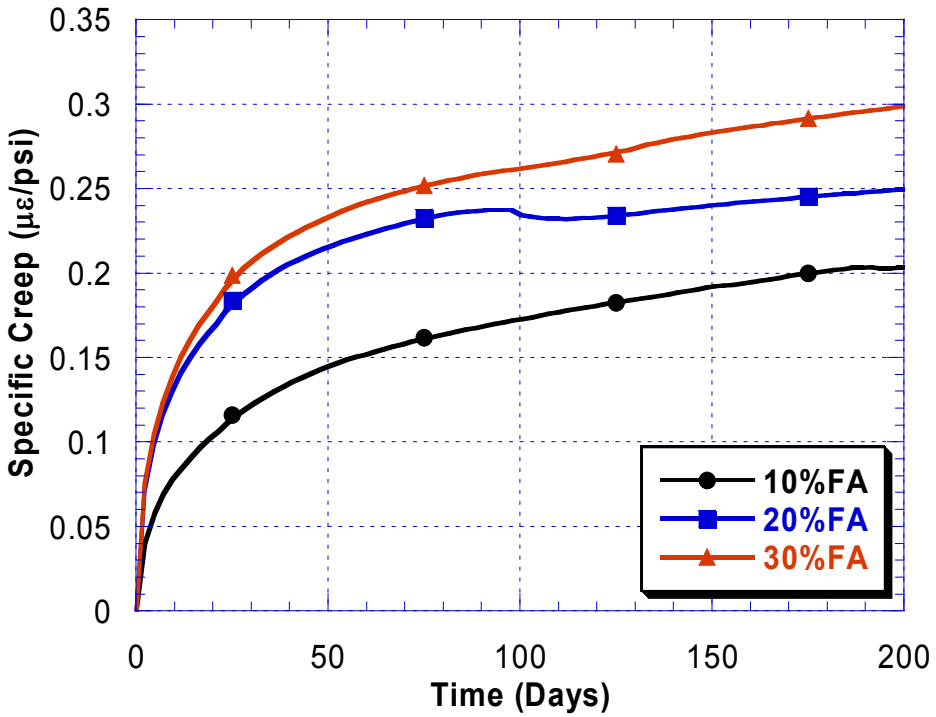

Figure 53. Effect of fly ash on specific creep

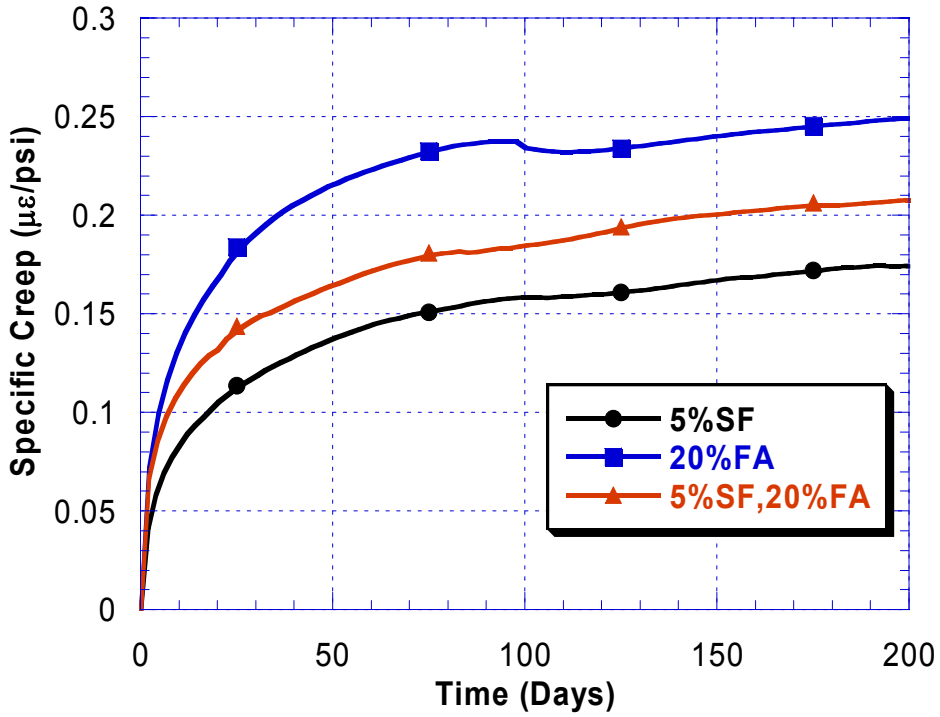

Figure 54a. Effect of combination of silica fume and fly ash on specific creep

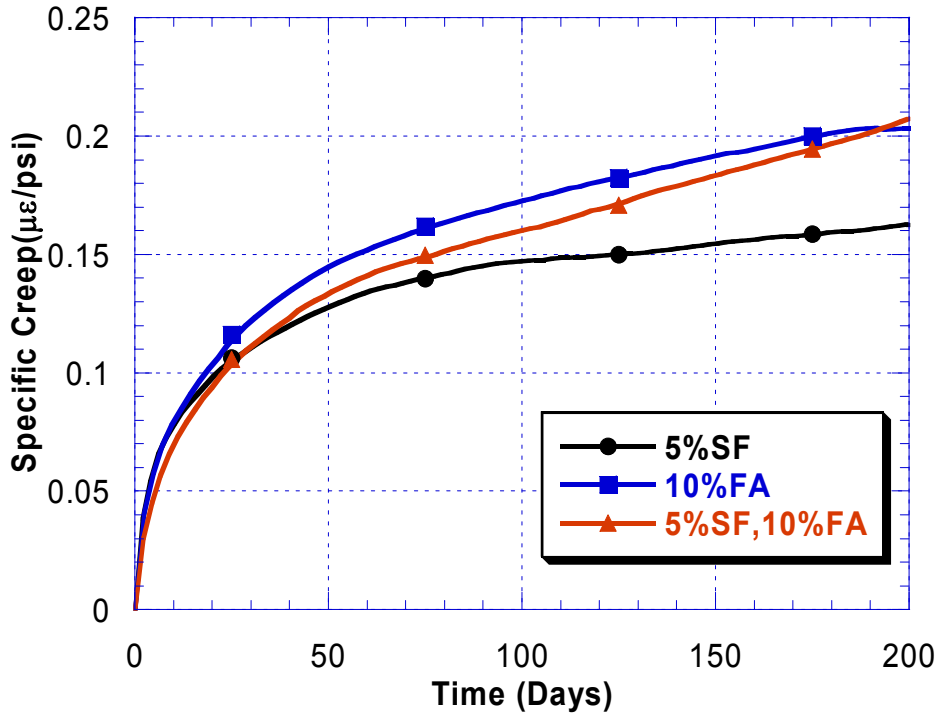

Figure 54b. Effect of combination of silica fume and fly ash on specific creep

CONCLUSIONS AND RECOMMENDATIONS

The following conclusions and recommendation were drawn from this project:

1) The presence of silica fume increases the early strength of concrete. The optimum range of silica fume is between 5 to 10 percent. Adding more silica fume could improve durability and strength but it is not economical. Moreover, the mix has very low workability, which requires more superplasticizer.
2) Fly ash increases the workability of concrete and therefore helps reduce the use of superplasticizer. However, adding more fly ash reduces the early-age compressive strength of HPC. The optimum range for adding fly ash is between 10 to 20 percent. Adding more fly ash than the optimum range will not be beneficial since there is a 20 percent strength reduction in both the early-age and later age of concrete.
3) Combining silica fume and fly ash enhances the durability and mechanical properties of HPC. In fact, it is highly recommended that a minimum of 5 percent silica fume be added to fly ash concrete to improve its durability. Moreover, the ductility of concrete increases when comparing to ACI recommendation.
4) Curing method plays major role in HPC. Both mechanical and durability properties are greatly influence by the method curing. Early-age cracking could occur if HPC is not properly cured. It is highly recommended that HPC be cured immediately or within 3 hours after the HPC is placed to avoid early-age cracking. This could be done, by either placing wet burlap or fog curing follows by wet burlap when the concrete is finished. The most effective curing method is moist curing. However, since this is not practical, it is recommended that HPC be cured for a minimum of 14 days using wet burlap. The use of curing compound is not effective in providing good curing method since the compound only seals the water from escaping whereas the HPC demands more water during the hydration process.
5) For a very low w/b ratio, fly ash could improve the shrinkage performance. However, the compressive strength will be reduced, and an optimization between early age shrinkage and strength is needed in the case of high strength concrete.
6) Lightweight aggregate reduces the autogenous shrinkage because of its ability to internally cure or in other word self-curing the concrete. However, the mechanical and durability properties of concrete will be affected.
7) Mixes need to be designed for the optimum amount of superplasticizer because higher doses of superplasticizer increase shrinkage and reduce strength.
8) All the HPC mixes are found to have a large relative dynamic modulus after 300 cycles. Thus, a durability factor of 90 percent can be easily achieved providing that there is sufficient air content in the HPC. In addition scaling of concrete is not a problem in HPC. All HPC mixes have a visual rating of 2 or lower.
9) Silica fume reduces the compressive creep of concrete, whereas fly ash increases the creep of concrete. Nevertheless, adding silica fume in fly ash concrete could reduce the compressive creep.

APPENDIX

Table 13. Compressive strength (w/b = 0.44)

W/B	SF	FA	Compressive Strength					
0.44	(%)	(%)	1 day	3 days	7 days	14 days	28 days	56 days
A1	7%	15%	1759	3223	4337	4894	6287	6525
			1870	3302	4377	5133	6247	6844
			1767	3342	4257	4735	6088	6486
			1799	**3289**	**4324**	**4921**	**6207**	**6618**
A2	5%	10%	1974	3621	4854	5411	6525	7162
			1989	3700	4814	5491	6008	7082
			2029	3621	4735	5332	6127	6923
			1997	**3647**	**4801**	**5411**	**6220**	**7056**
A3	5%	15%	1464	3422	4536	5292	6127	7122
			1480	3414	4655	5173	6207	7003
			1504	3342	4695	5173	6127	7242
			1483	**3393**	**4629**	**5213**	**6154**	**7122**
A4	5%	20%	1472	3223	4257	5013	6247	6605
			1671	3226	4218	5212	6048	6685
			1504	3143	4456	5419	6287	6724
			1549	**3197**	**4310**	**5215**	**6194**	**6671**
A5	5%	25%	1830	3159	3860	4456	5570	6247
			1830	3104	3955	4735	5849	6247
			1870	3159	4019	4735	5491	6127
			1843	**3141**	**3945**	**4642**	**5637**	**6207**
A6	9%	18%	1950	3183	4138	5212	6048	6287
			1790	3239	4218	5093	5730	6804
			2069	3231	4178	5013	6366	6804
			1936	**3218**	**4178**	**5106**	**6048**	**6632**
A7	10%	20%	1552	3104	4536	5252	6287	7082
			1512	3024	4337	5093	6207	6883
			1432	3223	4297	5371	6565	6724
			1499	**3117**	**4390**	**5239**	**6353**	**6896**
A8	15%	20%	1870	3143	4218	5610	6685	7122
			1989	3064	4297	5570	6406	6804
			1711	3183	4377	5531	6446	6844
			1857	**3130**	**4297**	**5570**	**6512**	**6923**

Table 14. Compressive strength (w/b = 0.39)

W/B	SF	FA	Compressive strength (psi)					
0.39	(%)	(%)	1 day	3 days	7 days	14 days	28 days	56 days
B1	7%	15%	1997	3740	4854	5809	6963	8037
			1989	3581	4894	5968	6923	7837
			2069	3621	4854	5849	6565	8117
			2018	**3647**	**4867**	**5875**	**6817**	**7997**
B2	5%	10%	3143	4417	5371	5968	6764	7162
			3104	4098	5570	5730	6844	7480
			3064	4019	5292	5809	6764	7719
			3104	**4178**	**5411**	**5836**	**6791**	**7454**
B3	5%	15%	2706	4058	5133	6048	6764	7759
			2145	4098	5053	5929	6804	7716
			2188	3820	5093	6008	6605	7918
			2346	**3992**	**5093**	**5995**	**6724**	**7798**
B4	5%	20%	2228	3143	3979	5173	5650	6963
			2149	3223	4019	5212	5889	7242
			2308	3382	4138	5013	5849	6724
			2228	**3249**	**4045**	**5133**	**5796**	**6976**
B5	5%	25%	2149	4138	4854	5929	7083	8276
			2570	4218	4615	5690	6923	7790
			2379	3979	4894	5451	6963	7759
			2366	**4112**	**4788**	**5690**	**6990**	**7942**
B6	9%	18%	2546	4138	5252	6446	7560	8356
			2913	3860	5650	6605	7401	8037
			2801	4058	5252	6167	7520	8196
			2753	**4019**	**5385**	**6406**	**7494**	**8196**
B7	10%	20%	2507	3899	5411	6366	7003	7998
			2602	3740	5053	6048	7162	7679
			2753	3907	5332	5929	7122	7639
			2621	**3849**	**5265**	**6114**	**7096**	**7772**

Table 15. Compressive strength (w/b = 0.37)

W/B	SF	FA	Compressive strength (psi)						
0.37	(%)	(%)	1 day	3 days	7 days	14 days	28 days	56 days	90 days
C1	7%	15%	3318	4576	5332	5730	7361	8117	8754
			3350	4615	5451	6446	7202	8356	8833
			3334	4536	5371	6287	7520	8271	
			3334	**4576**	**5385**	**6154**	**7361**	**8248**	**8794**
C2	5%	10%	3422	5252	5968	7162	8475	9390	10342
			3478	5093	6207	6923	8594	9430	9549
			3446	5173	6127	7003	8356	9191	9151
			3449	**5173**	**6101**	**7029**	**8475**	**9337**	**9681**
C3	5%	15%	3287	4615	5570	6645	7719	8600	8913
			3127	4894	5849	6724	7679	8555	9072
			3207	4735	5730	6685	7679	8754	8992
			3207	**4748**	**5716**	**6685**	**7692**	**8636**	**8992**
C4	5%	20%	3159	4281	5491	6366	7480	8793	9231
			3167	4337	5332	6127	7480	8236	8594
				4615	5252	6207	7082	8754	8276
			3163	**4411**	**5358**	**6233**	**7347**	**8594**	**8700**
C5	5%	25%	2586	3661	4615	5570	6207	7560	8594
			2403	3724	4456	5730	6127	7878	7958
			2515	3708	4576	5690	6088	7719	7799
			2501	**3698**	**4549**	**5663**	**6141**	**7719**	**8117**
C6	9%	18%	2825	4058	5093	5968	6605	8117	8077
			2885	4019	4814	6048	6963	7639	7998
			2889	4098	4934	6008	6645	7759	8037
			2866	**4058**	**4947**	**6008**	**6738**	**7838**	**8037**
C7	10%	20%	3183	3740	5013	5929	6844	7281	8395
			2913	3820	4894	6048	6746	8114	8117
			3008	3836	4934	6008	6923	7679	8356
			3035	**3799**	**4947**	**5995**	**6838**	**7691**	**8289**
C8	15%	20%	2865	3907	4894	6207	7082	7958	8515
			2801	3883	5173	6048	7043	7998	8117
			2793	3860	5013	6167	7242	8037	8276
			2820	**3883**	**5027**	**6141**	**7122**	**7998**	**8303**

Table 16. Compressive strength (w/b = 0.35)

W/B	SF	FA	Compressive strength (psi)					
0.35	(%)	(%)	1 day	3 days	7 days	14 days	28 days	56 days
B1N	7%	15%	4615	6446	7958	8992	9748	10027
			4138	6287	8117	8674	9708	10027
			4615	6446	8037	8634	9748	10305
			4456	**6393**	**8037**	**8767**	**9735**	**10120**
B2N	5%	10%	5411	6565	7639	8356	9629	10345
			5371	6486	7958	8594	9788	10305
			5371	6844	7719	8515	10027	10300
			5384	**6632**	**7772**	**8488**	**9815**	**10325**
B3N	5%	15%	4854	6525	7639	8674	8674	9629
			4456	6008	7560	8754	9748	9788
			4576	6127	7679	8714	9311	9629
			4629	**6220**	**7626**	**8714**	**9244**	**9682**
B5N	5%	25%	3661	4735	5849	6446	6963	7878
			3263	4735	5690	6605	7003	7799
			3661	4456	5650	6525	6963	7888
			3528	**4642**	**5730**	**6525**	**6976**	**7839**
B6N	9%	18%	4019	5491	6923	7838	8515	9669
			4138	5411	6804	7799	8741	9669
			4019	5610	6764	7958	8754	9666
			4059	**5504**	**6830**	**7865**	**8670**	**9669**
B8N	15%	20%	3581	5013	6366	7639	8236	9311
			3382	4854	6048	7639	8196	9151
			3581	4814	6127	7600	8157	9191
			3515	**4894**	**6180**	**7626**	**8196**	**9218**

Table 17. Compressive strength (w/b = 0.33)

W/B	SF	FA	Compressive strength (psi)						
0.33	(%)	(%)	1 day	3 days	7 days	14 days	28 days	56 days	90 days
D1	7%	15%	5411	6883	8037	8992	10000	10902	10425
			5292	6844	8157	8793	10345	10425	10504
			5332		8077	8833	10186	10265	10600
			5345	**6864**	**8090**	**8873**	**10177**	**10531**	**10510**
D2	5%	10%	4814	6486	7639	8515	9151	10504	9947
			4655	5849	7480	7759	9748	10067	9788
			4735	6287	7520	8435	9470	10345	9828
			4735	**6207**	**7546**	**8236**	**9456**	**10305**	**9854**
D3	5%	15%	6127	7043	8037	8594	9430	10902	10743
			6127	6764	8196	8913	10027	10942	11141
			6167	6923	8077	8754	9788	10027	10902
			6140	**6910**	**8103**	**8754**	**9748**	**10624**	**10929**
D4	5%	20%	5252	6366	7242	8117	8674	10265	10822
			5570	6247	7679	8674	8515	10504	10902
			5400	6287	7401	8356	8754	10385	10854
			5411	**6300**	**7441**	**8382**	**8648**	**10385**	**10859**
D5	5%	25%	4938	5610	6645	7401	8992	8674	9430
			4615	5531	6605	7162	8754	9390	9470
			4735	5570	6565	7242	8276	10106	9500
			4763	**5570**	**6605**	**7268**	**8674**	**9390**	**9467**
D6	9%	18%	4178	5531	6247	7034	8754	9788	10027
			4218	5332	6326	7639	8435	9350	9470
			4098	5411	6406	7440	8515	9191	10027
			4165	**5425**	**6326**	**7371**	**8568**	**9443**	**9841**
D7	10%	20%	3581	5411	6406	7401	8793	9708	10504
			3549	5334	6645	7799	8674	10027	9868
			3573	5371	6525	7560	8913	9947	10663
			3568	**5372**	**6525**	**7587**	**8793**	**9894**	**10345**
D8	15%	20%	4854	6207	6844	7958	8674	8754	9788
			4934	5889	6605	8077	8714	9032	9868
			4894	6008	6724	7998	8833	9629	9800
			4894	**6035**	**6724**	**8011**	**8740**	**9138**	**9819**

Table 18. Compressive strength (w/b = 0.29)

W/B	SF	FA	Compressive strength (psi)						
0.29	(%)	(%)	1 day	3 days	7 days	14 days	28 days	56 days	90 days
G1	7%	15%	5690	6844	8196	9311	10265	11579	12016
			5929	6883	8435	9032	10823	11300	11777
			5809	6804	8395	9112	10823	11419	11539
			5809	**6844**	**8342**	**9152**	**10637**	**11433**	**11777**
G2	5%	10%	6127	7639	9231	9788	10106	11976	12414
			6366	7560	8833	9510	10265	11698	11857
			6247	7600	8913	9669	9947	11738	12414
			6247	**7600**	**8992**	**9656**	**10106**	**11804**	**12228**
G3	5%	15%	5650	7480	8594	9311	10902	11101	12414
			5491	7321	8754	9430	9151	11220	12374
			5531	7361	8674	9390	9669	11141	11817
			5557	**7387**	**8674**	**9377**	**9907**	**11154**	**12202**
G4	5%	20%	5809	6406	8117	8316	9708	11141	10902
			5411	6724	7639	8754	9788	10743	11220
			5650	6605	7878	8594	10027	10902	11000
			5623	**6578**	**7878**	**8555**	**9841**	**10929**	**11041**
G5	5%	25%	5013	6048	6923	8236	9072	11061	10226
			4934	6207	7043	8395	9151	10920	10186
			4974	6127	7162	8276	9271	10743	10200
			4974	**6127**	**7043**	**8302**	**9165**	**10908**	**10204**
G6	9%	18%	6008	7242	7998	8594	9907	10345	11976
			5720	7321	8196	9231	10027	11141	11618
			5889	7162	8117	8873	10504	9868	11300
			5872	**7242**	**8104**	**8899**	**10146**	**10451**	**11631**
G7	10%	20%	5411	6605	7679	8754	9311	11220	11200
			5292	6600	7719	8515	10027	10584	11000
			5371	6700	7639	8634	9470	10862	11000
			5358	**6635**	**7679**	**8634**	**9603**	**10889**	**11067**
G8	15%	20%	4775	5889	7321	8674	8833	9708	9708
			4735	5890	7162	8714	9788	9231	10186
			4814	5900	7242	8634	9072	9390	10000
			4775	**5893**	**7242**	**8674**	**9231**	**9443**	**9965**

Table 19. Compressive strength (w/b = 0.40)

W/B	SF	FA	Compressive strength (psi)						
0.40	(%)	(%)	1 day	3 days	7 days	14 days	28 days	56 days	90 days
FA30	5%	30%	2745	4019	4695	5491	6048	7321	7700
			2785	3716	4576	5730	6287	7560	7719
			2761	3883	4615	5531	6844	7520	7560
			2764	**3873**	**4629**	**5584**	**6393**	**7467**	**7660**
FA35	5%	35%	2204	3263	3820	4775	6048	6844	7110
			2300	3143	3907	5173	5809	6565	7200
			2252	3167	3875	4934	5849	6844	7122
			2252	**3191**	**3867**	**4961**	**5902**	**6751**	**7144**

Table 20. Compressive strength (w/b = 0.365)

W/B	SF	FA	Compressive strength (psi)						
0.365	(%)	(%)	1 day	3 days	7 days	14 days	28 days	56 days	90 days
F1	7%	15%	3462	4894	5889	6565	8356	8276	8833
			3621	4775	5650	6287	7799	8196	9311
			3597	4615	5769	6366	6605	8992	8674
			3560	**4761**	**5769**	**6406**	**7587**	**8488**	**8939**
F6	9%	18%	2984	4536	5491	6326	8356	7799	8992
			3143	4297	5411	6645	7639	9151	8674
			3056	4337	5451	6486	8000	7958	9311
			3061	**4390**	**5451**	**6486**	**7998**	**8303**	**8992**

Table 21. Compressive strength (w/b = 0.30)

W/B	SF	FA	Compressive strength (psi)						
0.30	(%)	(%)	1 day	3 days	7 days	14 days	28 days	56 days	90 days
E1	7%	15%	5173	6008	8037	8833	10663	10504	11200
			5411	6366	7719	9151	9350	10902	11220
			5332	6207	7838	8992	10464	10703	11181
			5305	**6194**	**7865**	**8992**	**10159**	**10703**	**11201**
E2	5%	10%	5292	6923	7958	8594	9470	9868	11300
			5173	6685	7918	9072	9589	10464	10743
			5252	6844	7878	8276	9191	10027	10663
			5239	**6817**	**7918**	**8647**	**9417**	**10120**	**10902**

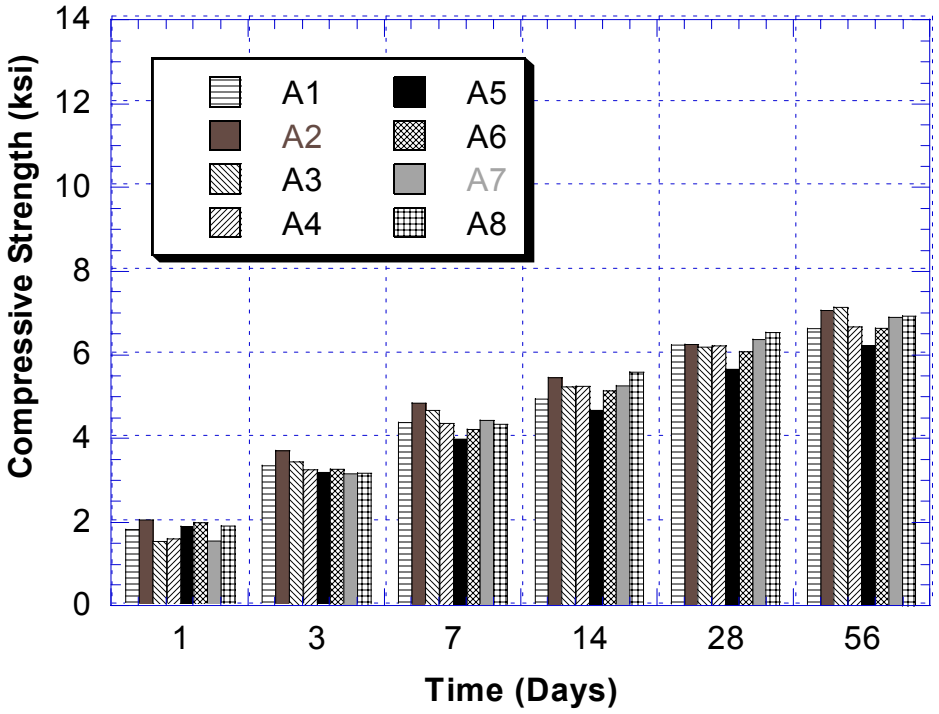

Figure 55. Compressive strength (w/b = 0.44)

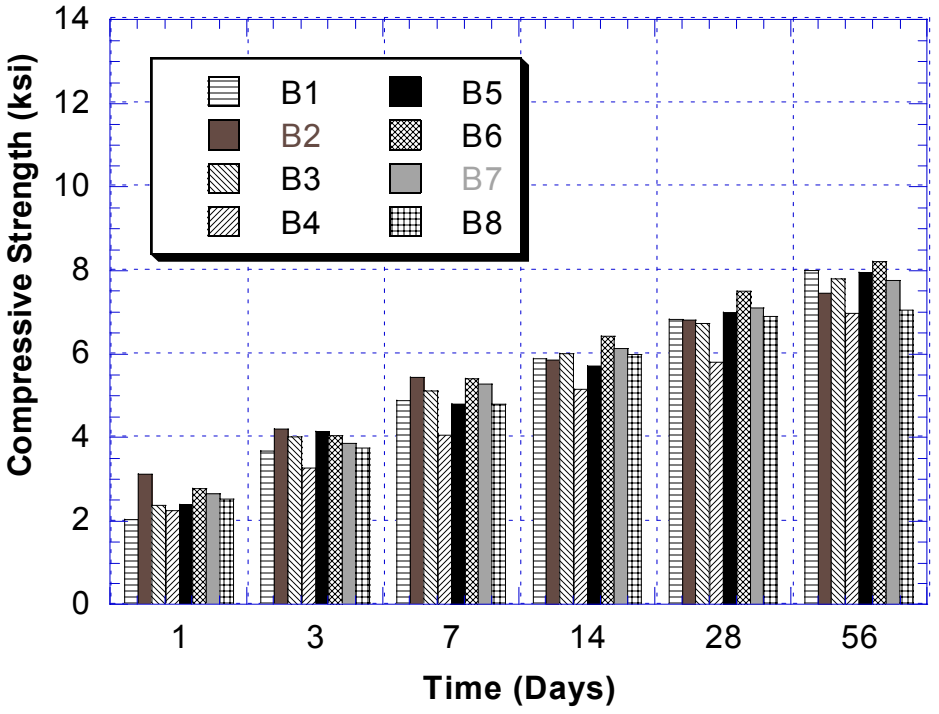

Figure 56. Compressive strength (w/b = 0.39)

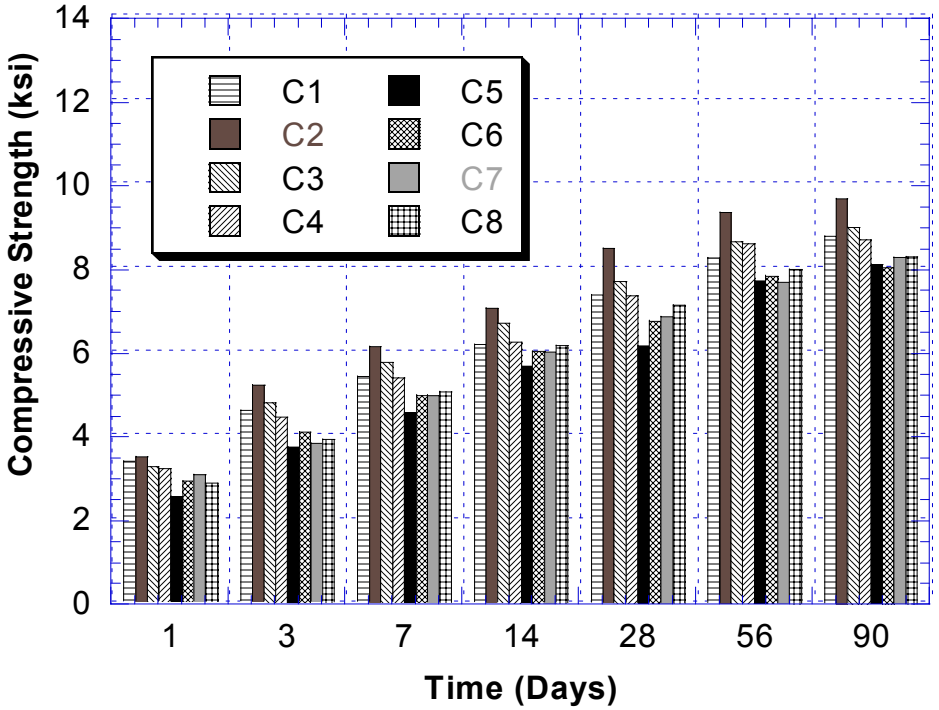

Figure 57. Compressive strength (w/b = 0.37)

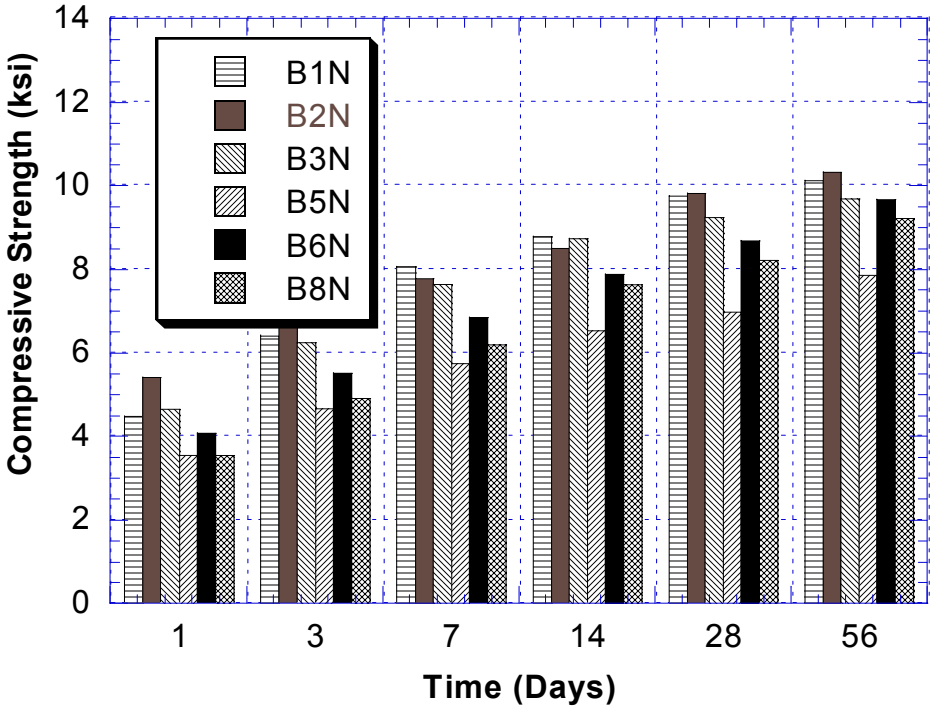

Figure 58. Compressive strength (w/b = 0.35)

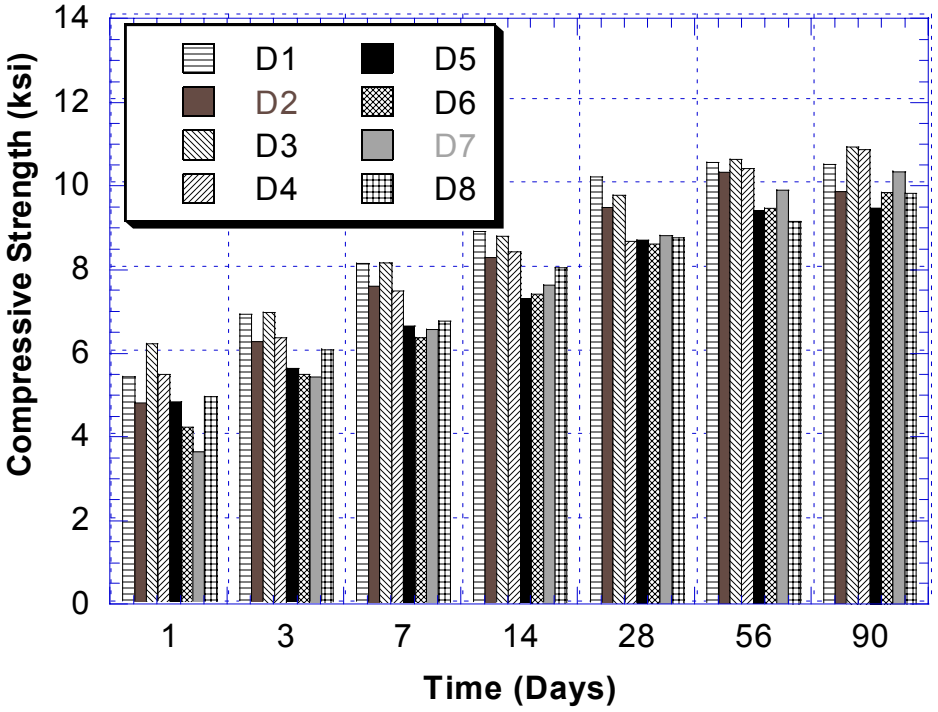

Figure 59. Compressive strength (w/b = 0.33)

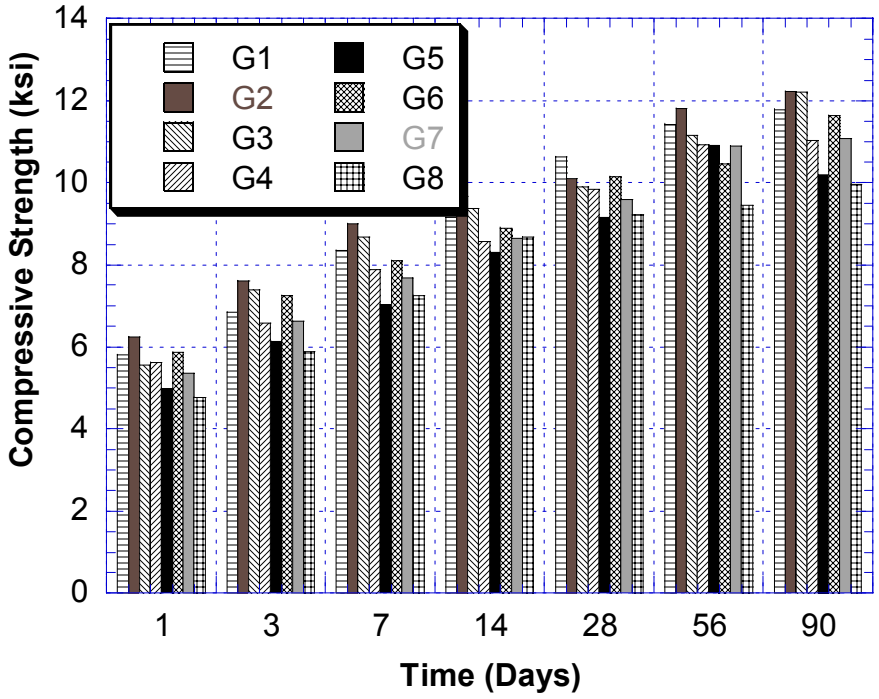

Figure 60. Compressive strength (w/b = 0.29)

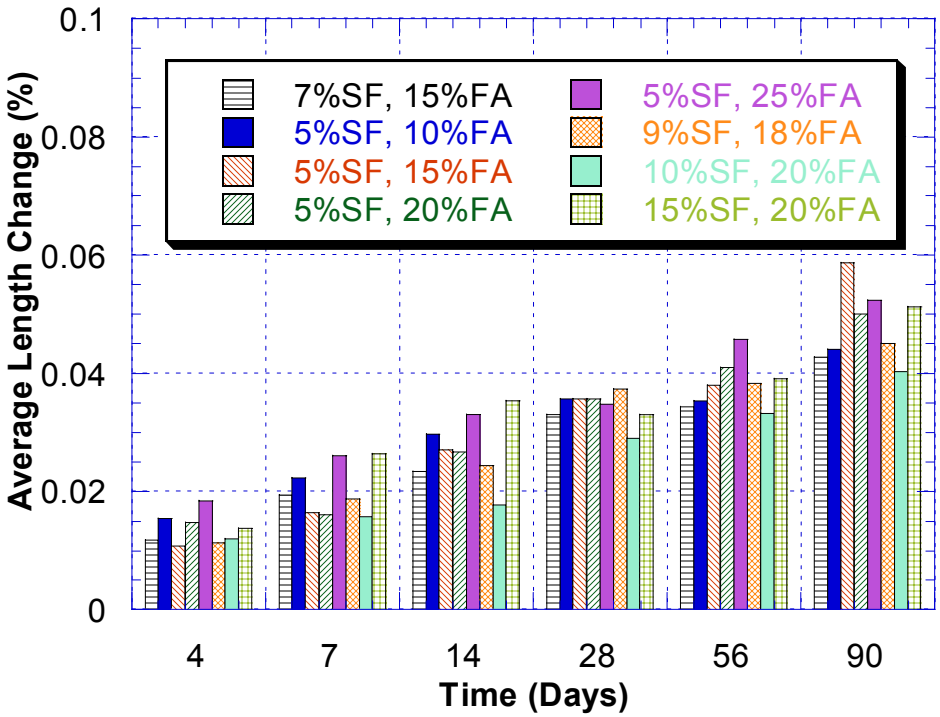

Figure 61. Drying shrinkage (w/b = 0.37)

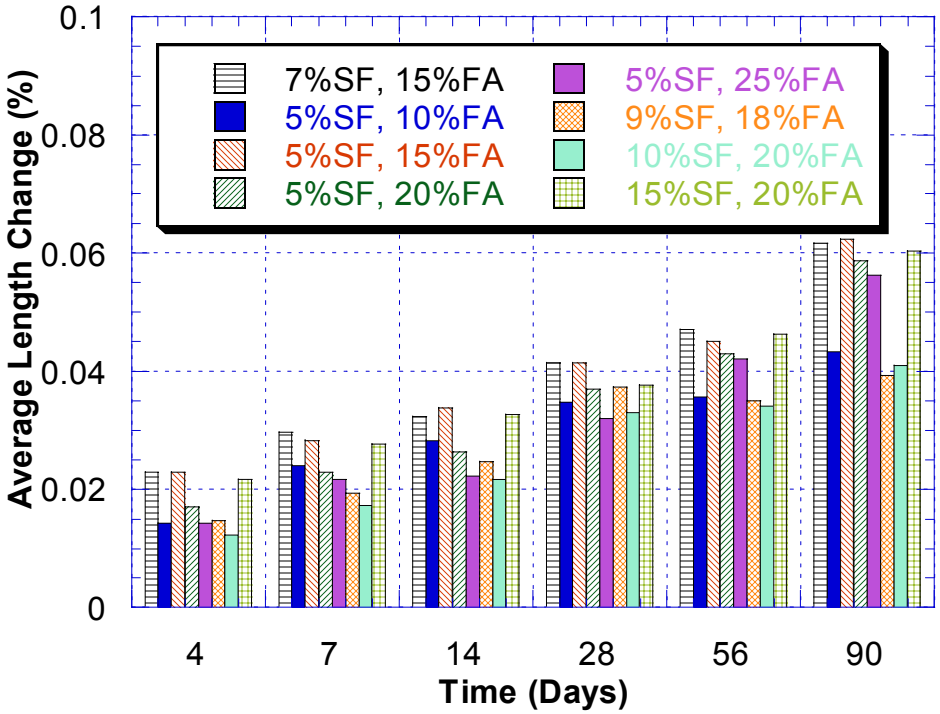

Figure 62. Drying shrinkage (w/b = 0.33)

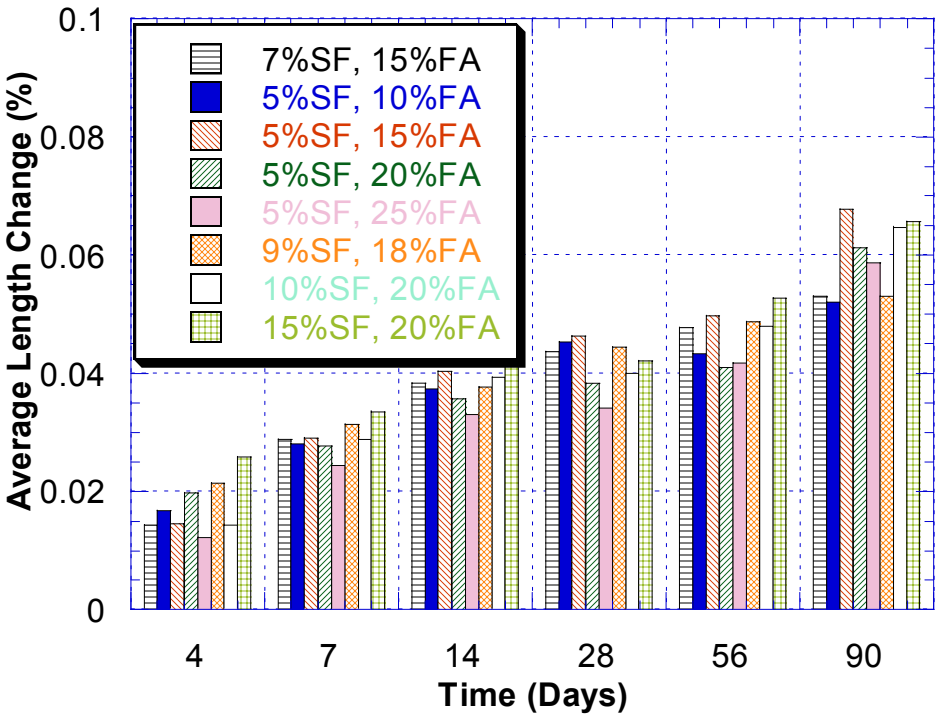

Figure 63. Drying shrinkage (w/b = 029)

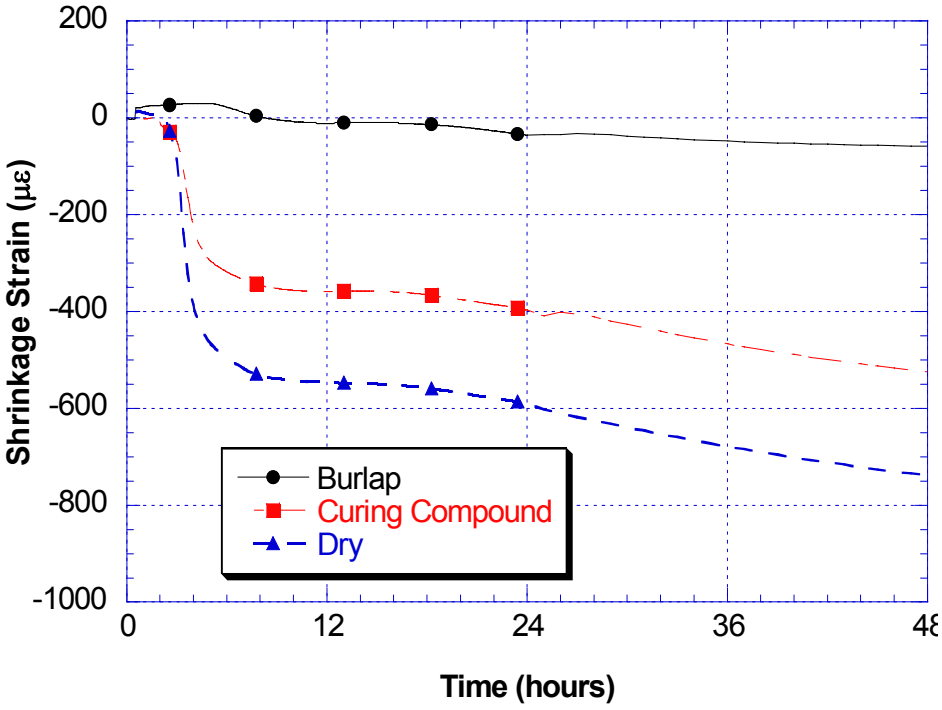

Figure 64. Effect of curing on autogenous shrinkage of mix L1

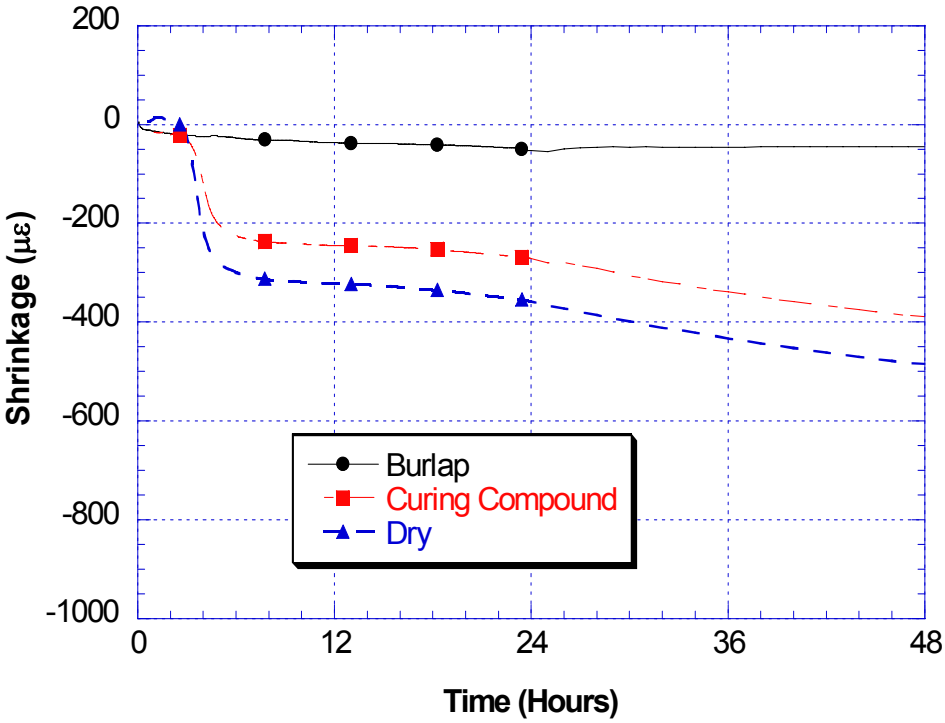

Figure 65. Effect of curing on autogenous shrinkage of mix L2

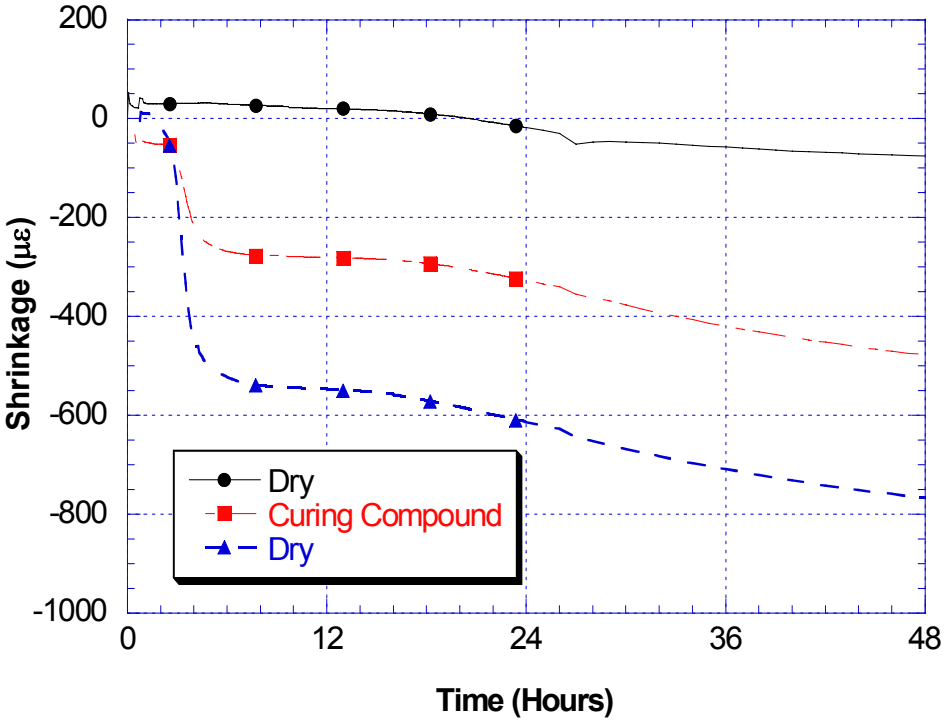

Figure 66. Effect of curing on autogenous shrinkage of mix L3

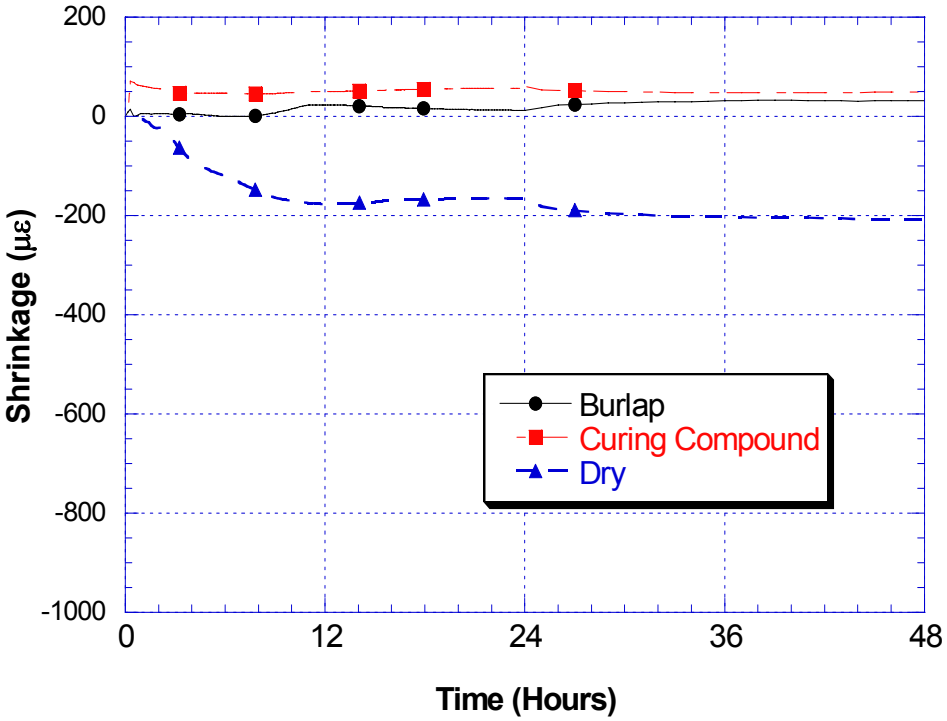

Figure 67. Effect of curing on autogenous shrinkage of mix L4

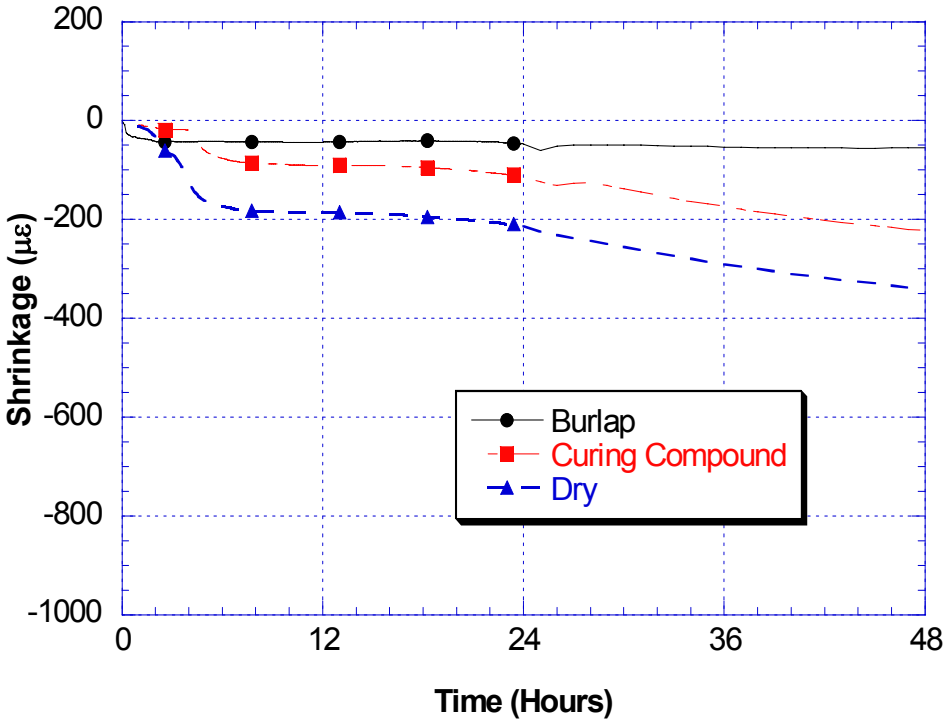

Figure 68. Effect of curing on autogenous shrinkage of mix M1

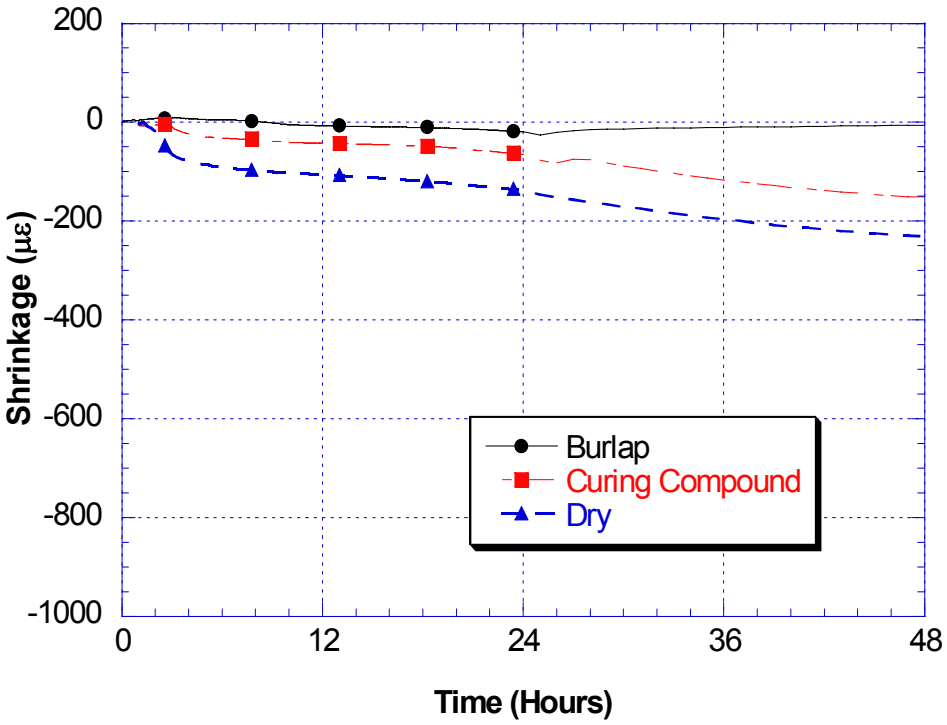

Figure 69. Effect of curing on autogenous shrinkage of mix M2

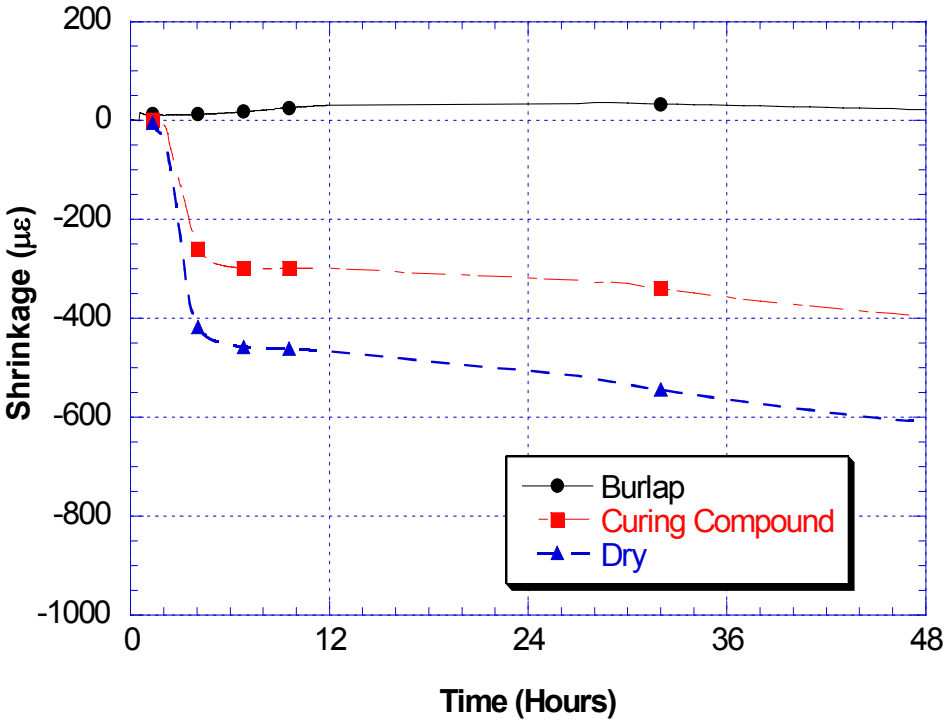

Figure 70. Effect of curing on autogenous shrinkage of mix M3

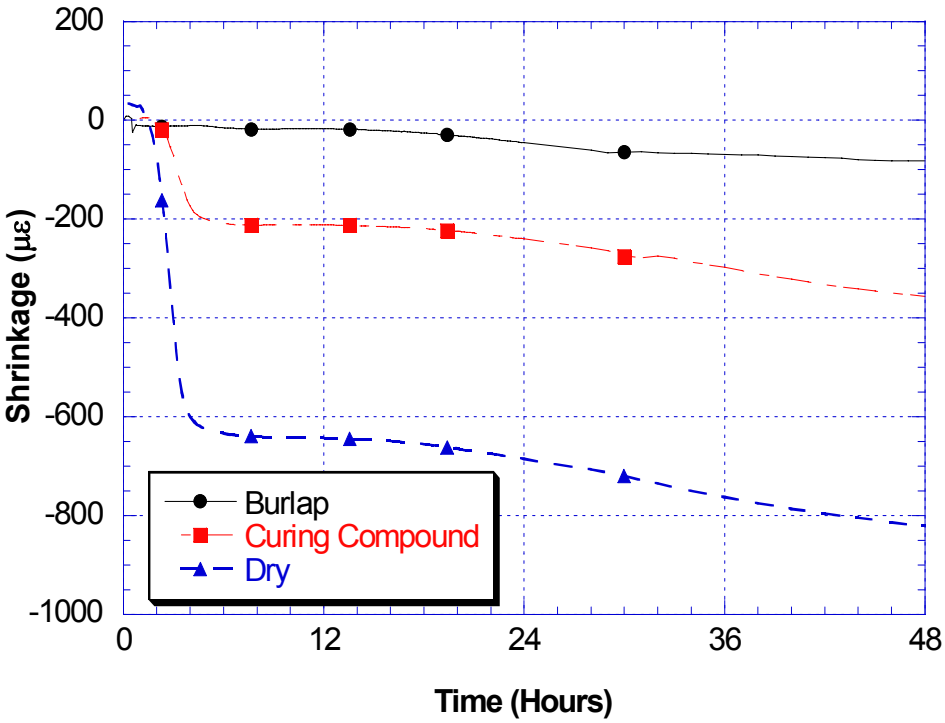

Figure 71. Effect of curing on autogenous shrinkage of mix M4

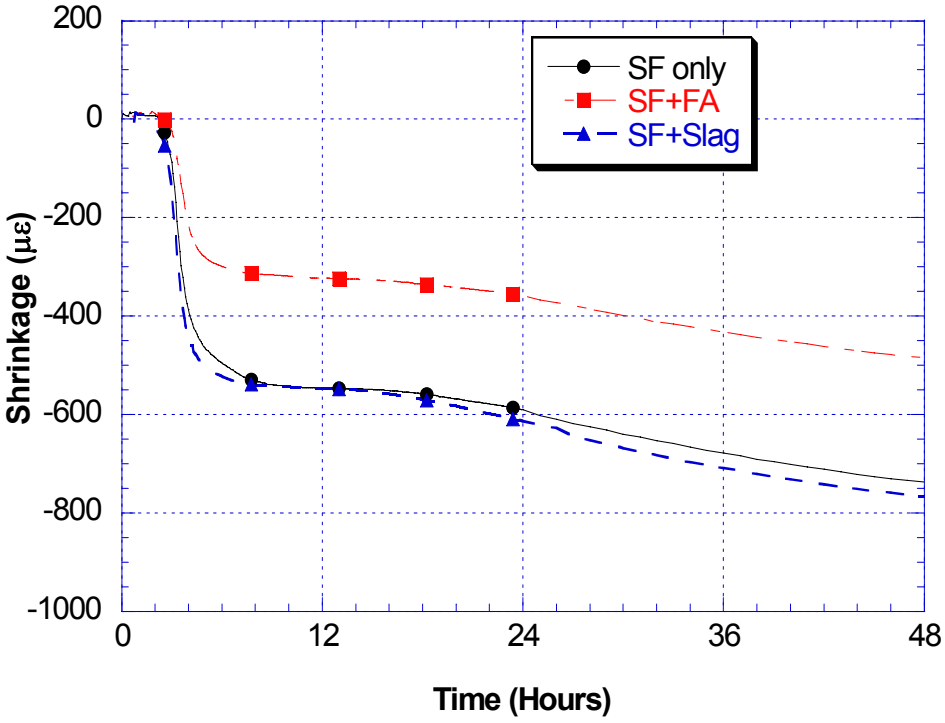

Figure 72. Effect of pozzolans on mix of w/b ratio 0.29 with dry curing

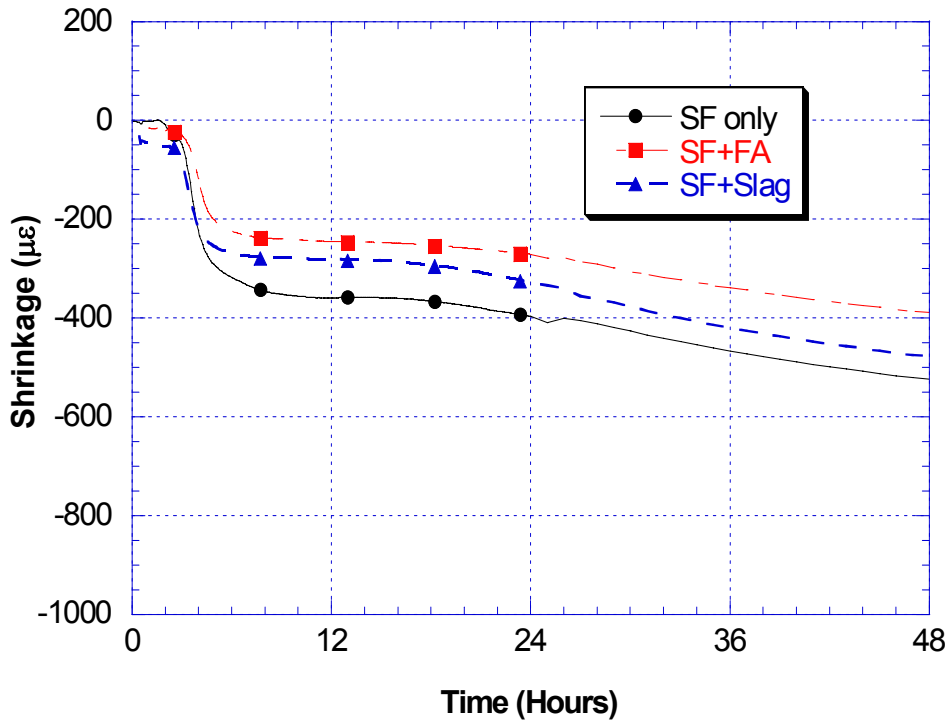

Figure 73. Effect of pozzolans on mix of w/b ratio 0.29 with Curing Compound

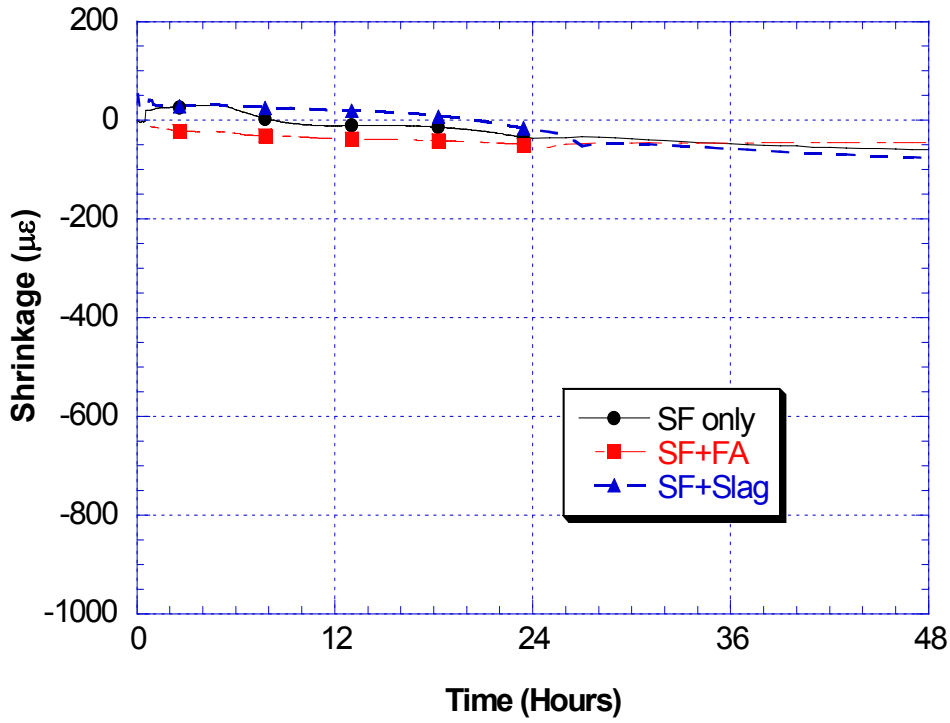

Figure 74. Effect of pozzolans on mix of w/b ratio 0.29 with burlap curing

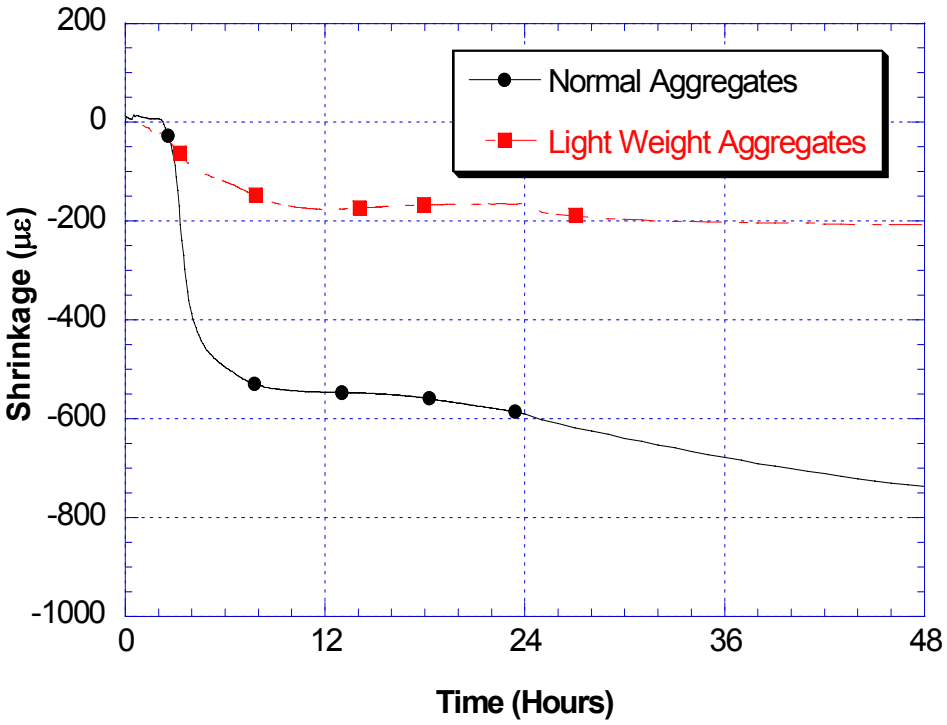

Figure 75. Effect of aggregates on autogenous shrinkage with dry curing

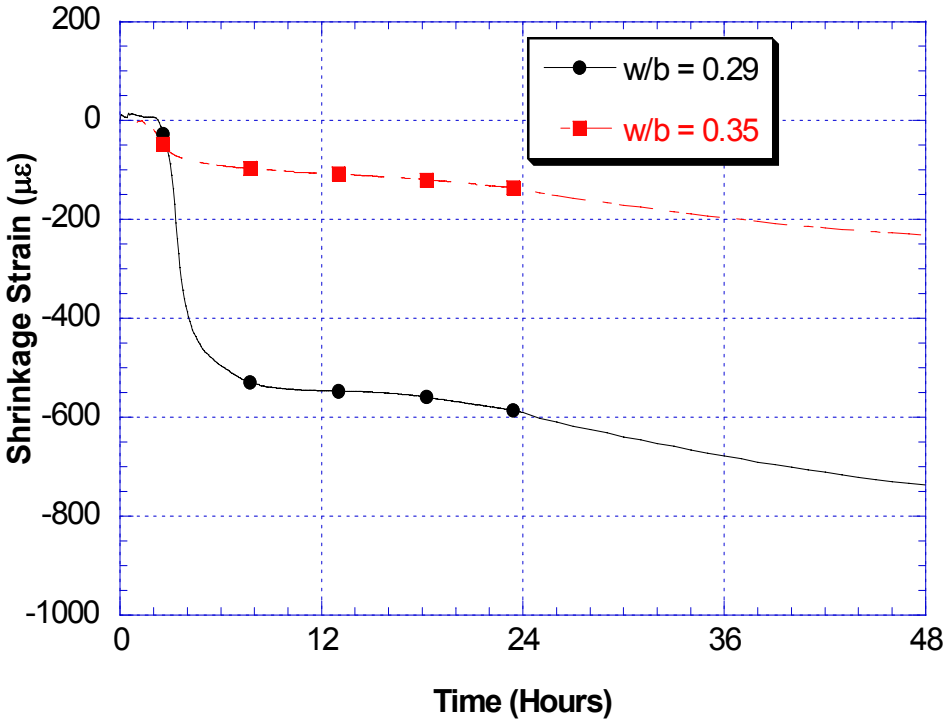

Figure 76. Effect of w/b on autogenous shrinkage with dry curing

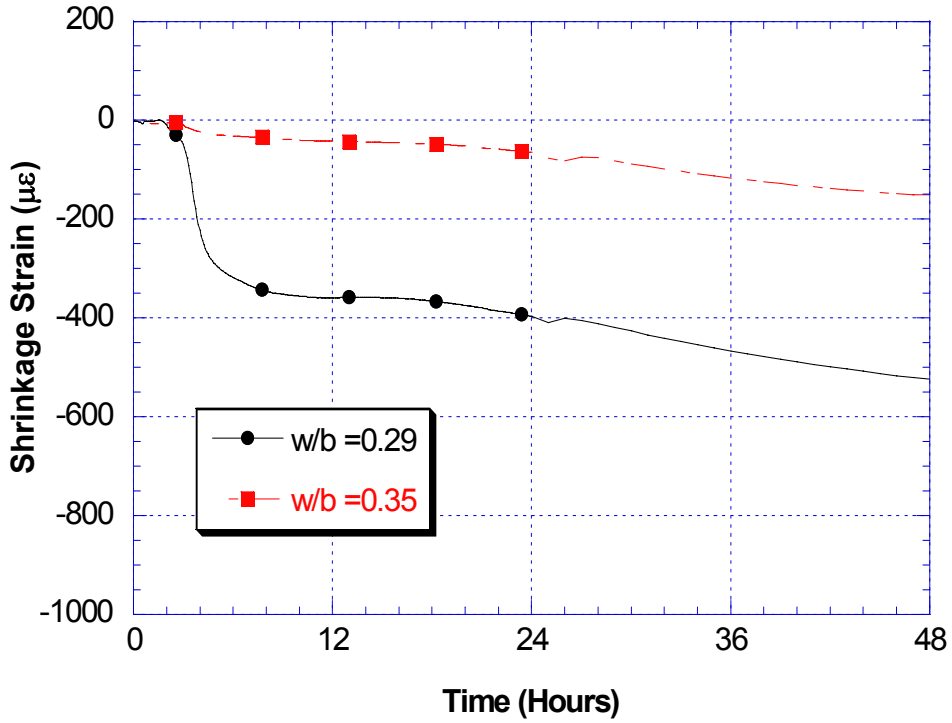

Figure 77. Effect of w/b on autogenous shrinkage with curing compound

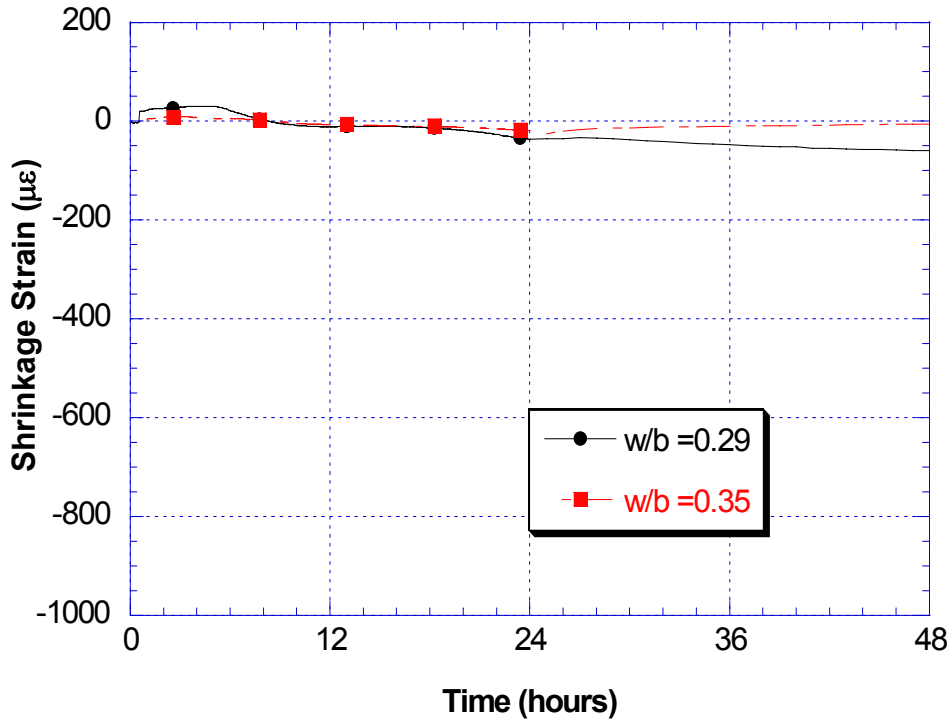

Figure 78. Effect of w/b on autogenous shrinkage with burlap curing

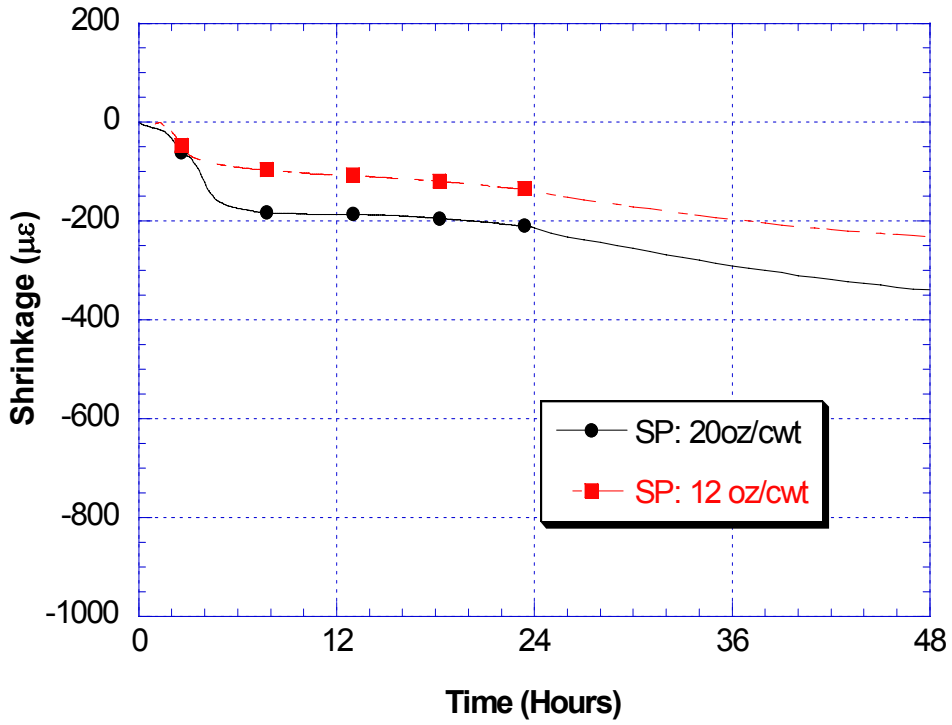

Figure 79. Effect of amount of superplasticizer on the autogenous shrinkage with dry curing

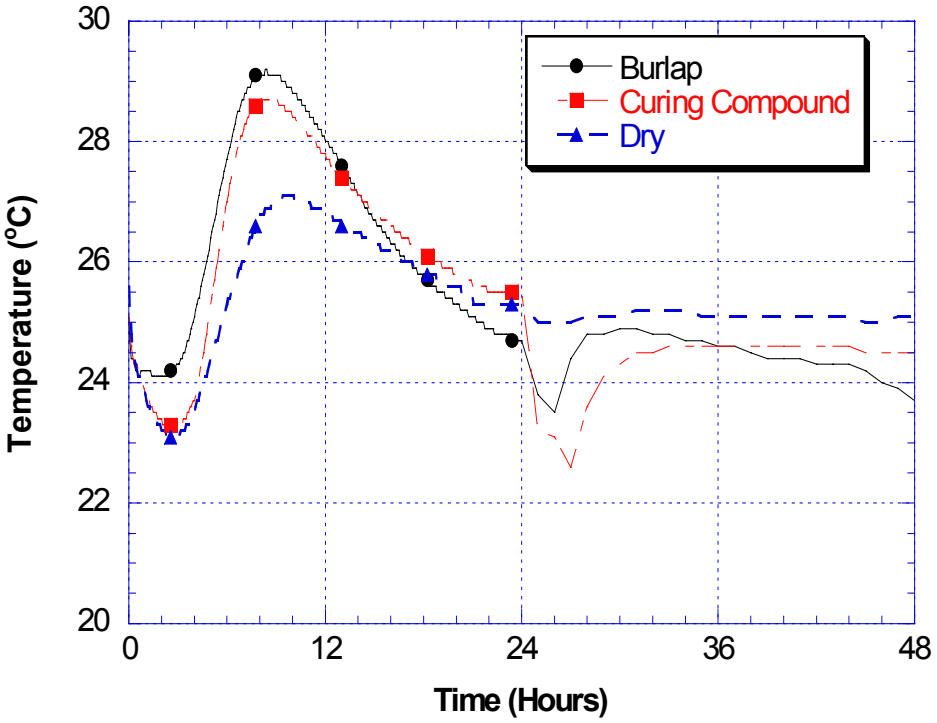

Figure 80. Temperature variations inside the sample of mix L1

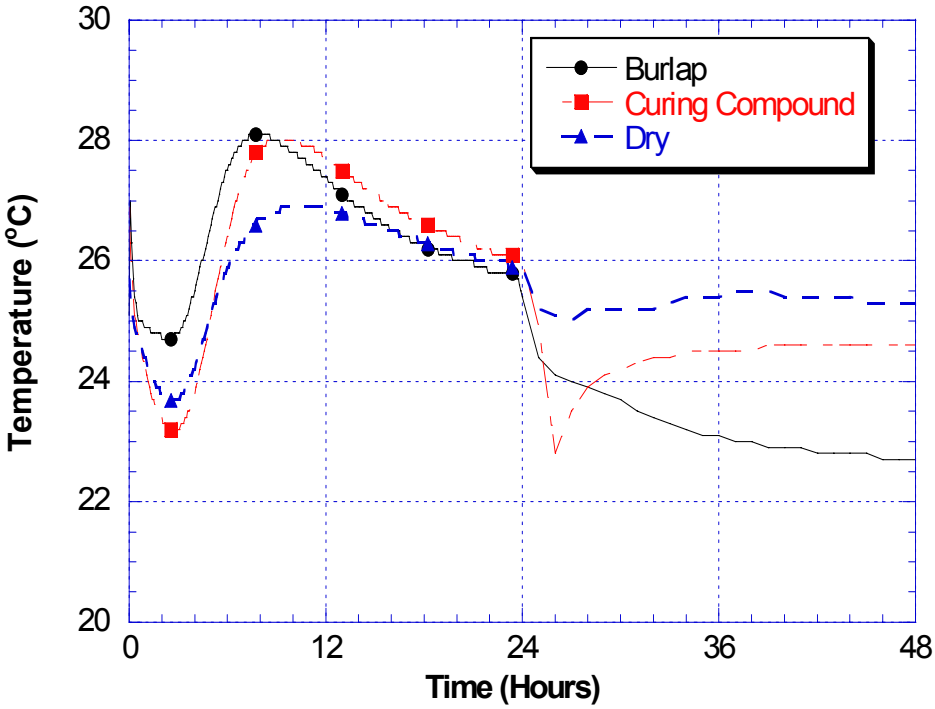

Figure 81. Temperature variations inside the sample of mix L2

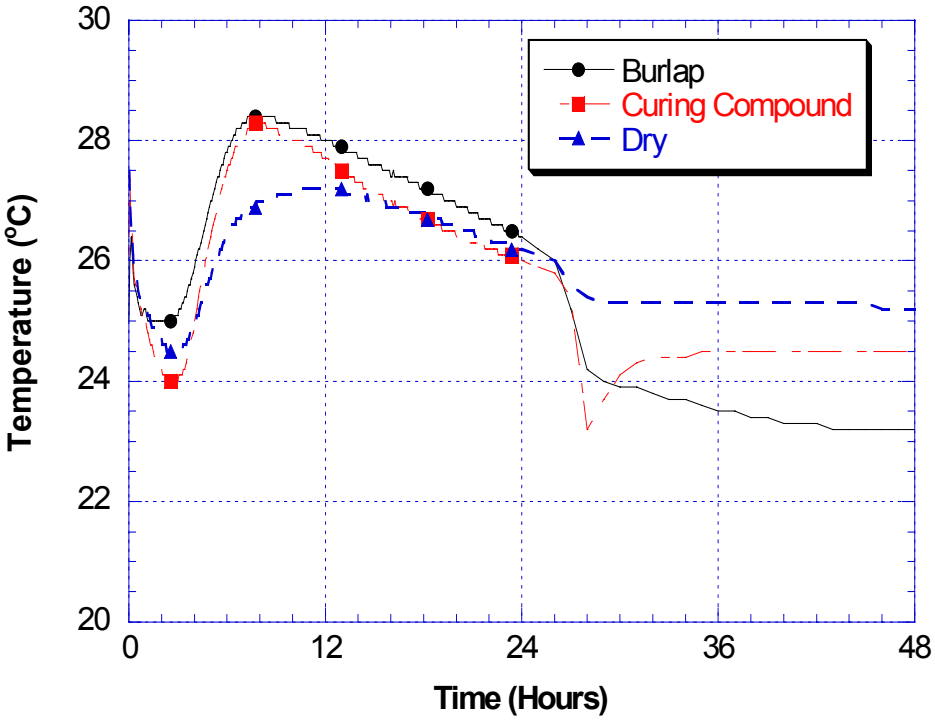

Figure 82. Temperature variations inside the sample of mix L3

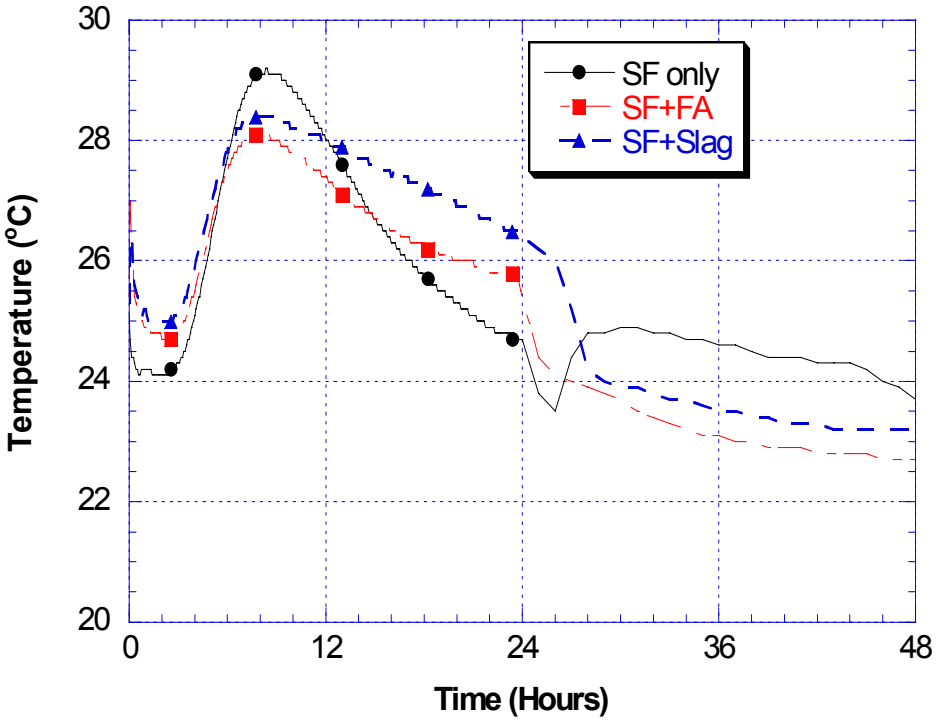

Figure 83. Temperature variation inside the samples with different pozzolans and with burlap curing

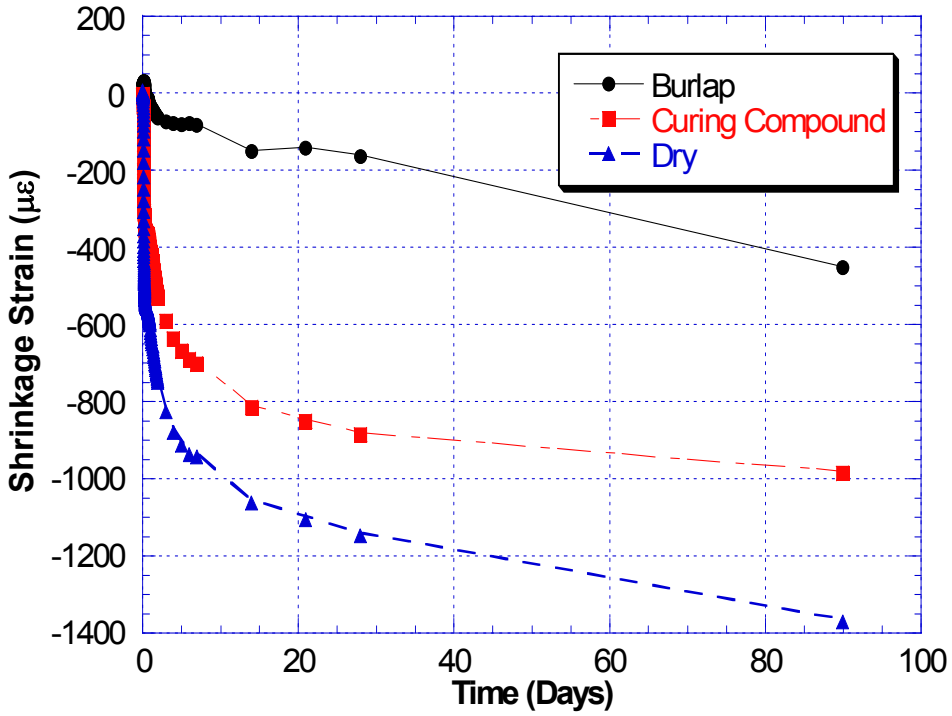

Figure 84. Effect of curing on long-term shrinkage of mix L1

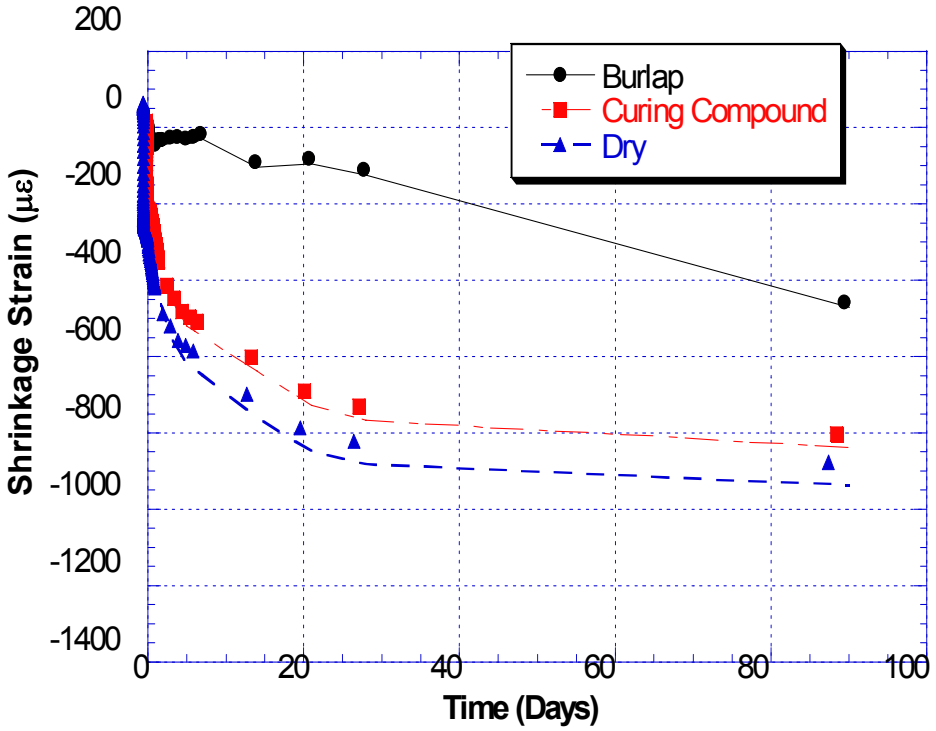

Figure 85. Effect of curing on long-term shrinkage of mix L2

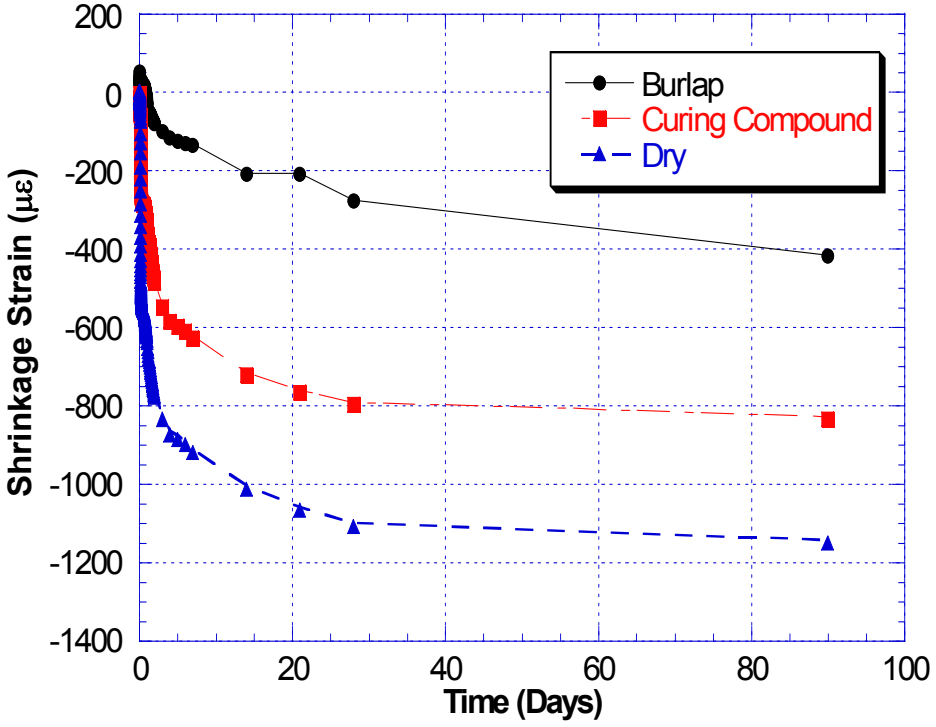

Figure 86. Effect of curing on long-term shrinkage of mix L3

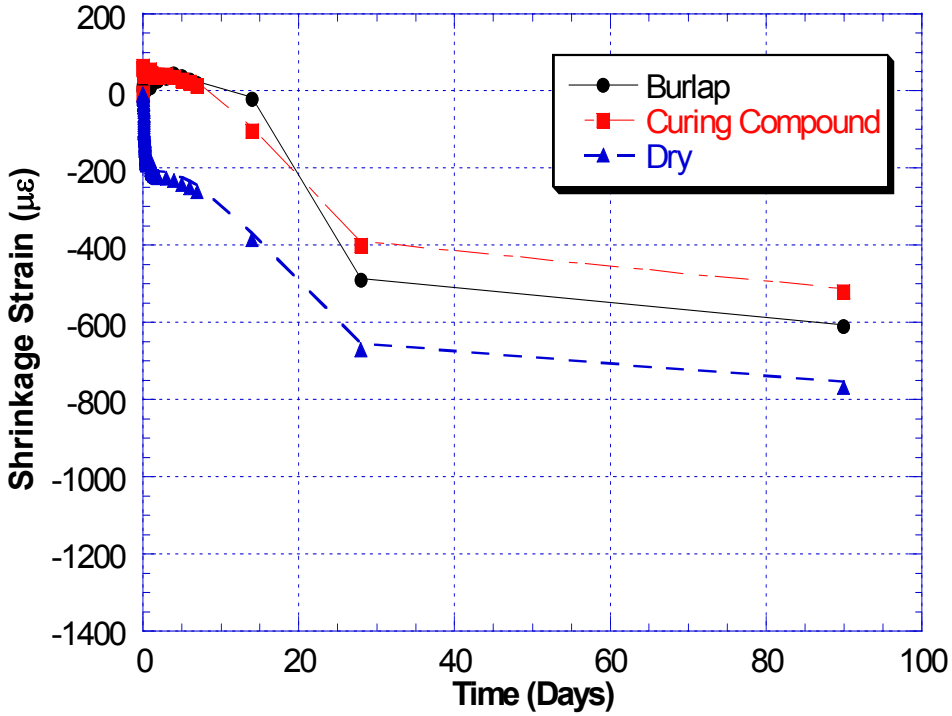

Figure 87. Effect of curing on long-term shrinkage of mix L4

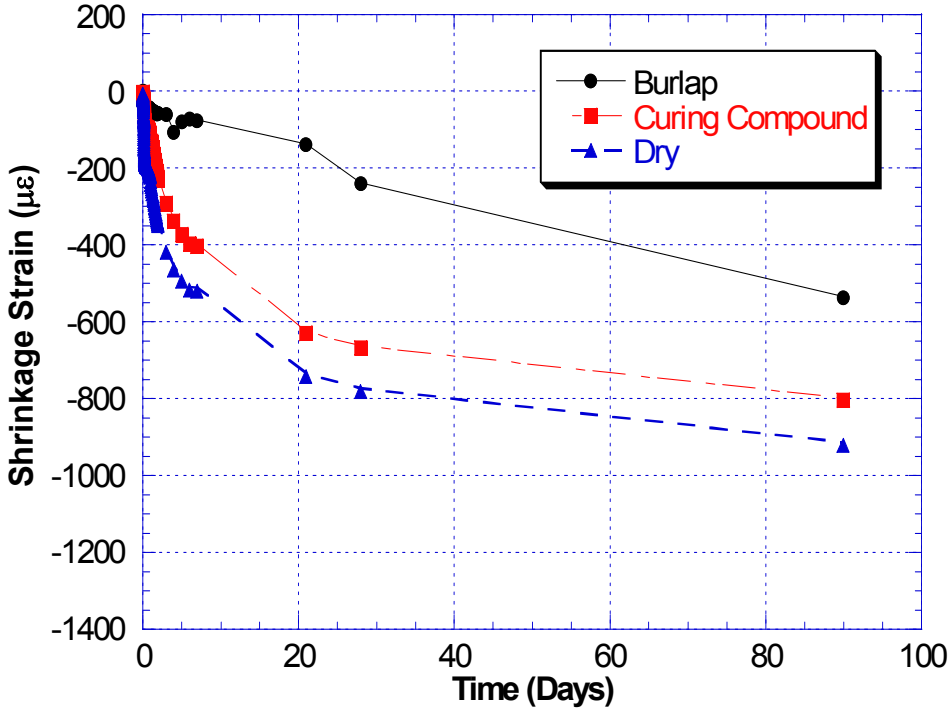

Figure 88. Effect of curing on long-term shrinkage of mix M1

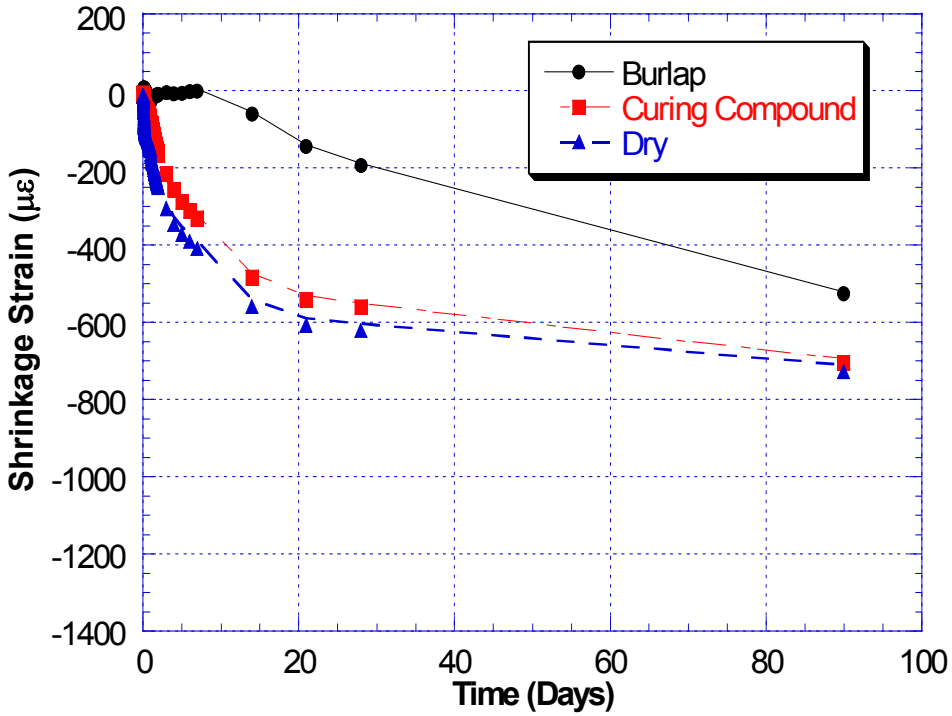

Figure 89. Effect of curing on long-term shrinkage of mix M2

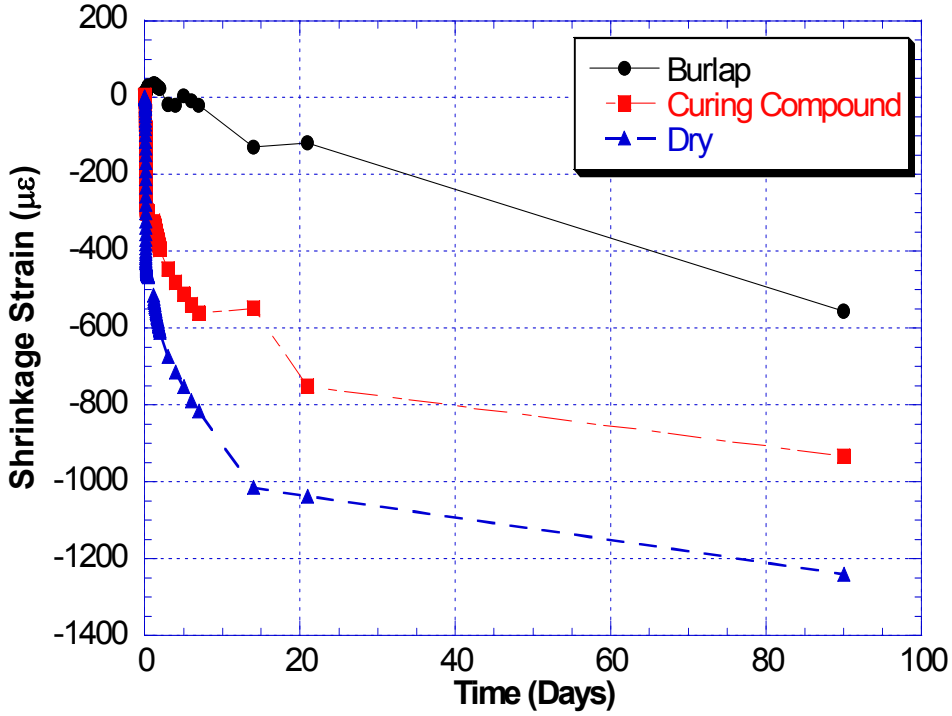

Figure 90. Effect of curing on long-term shrinkage of mix M3

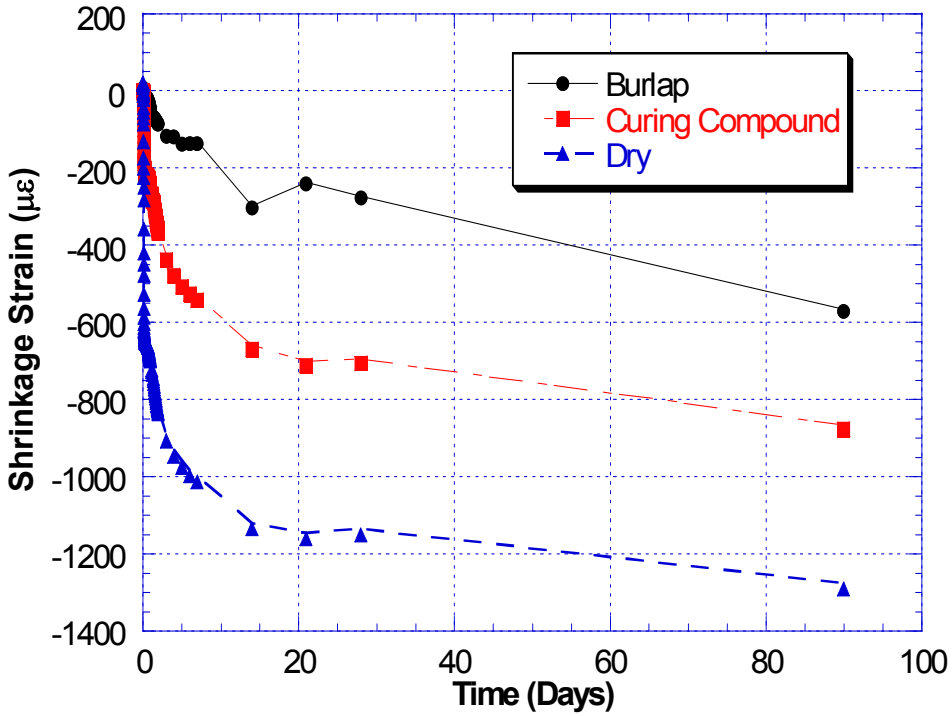

Figure 91. Effect of curing on long-term shrinkage of mix M4

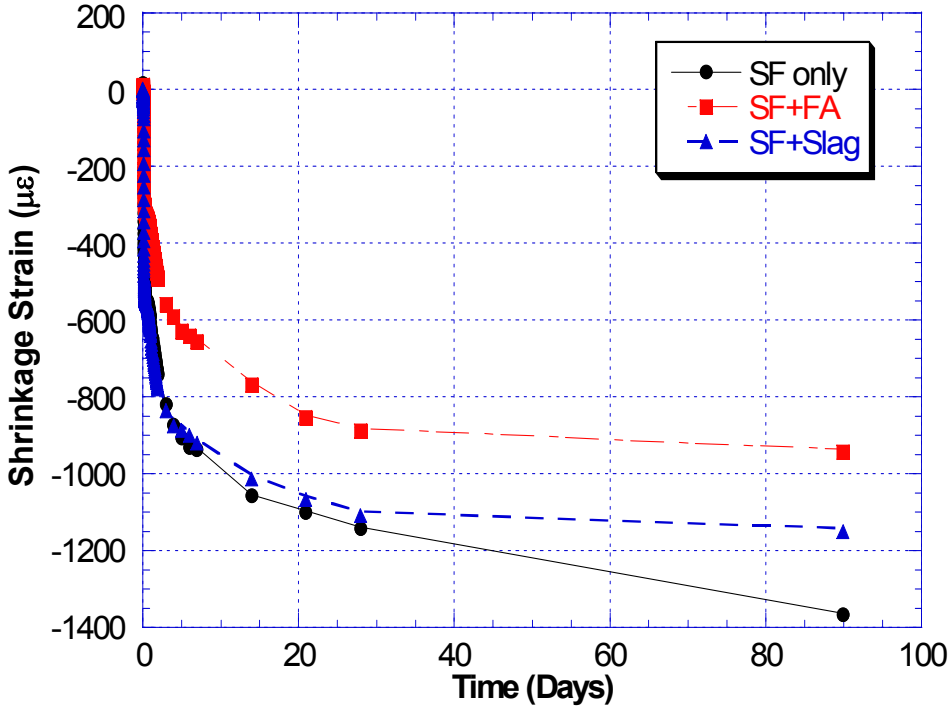

Figure 92. Effect of pozzolans on long-term shrinkage with dry curing

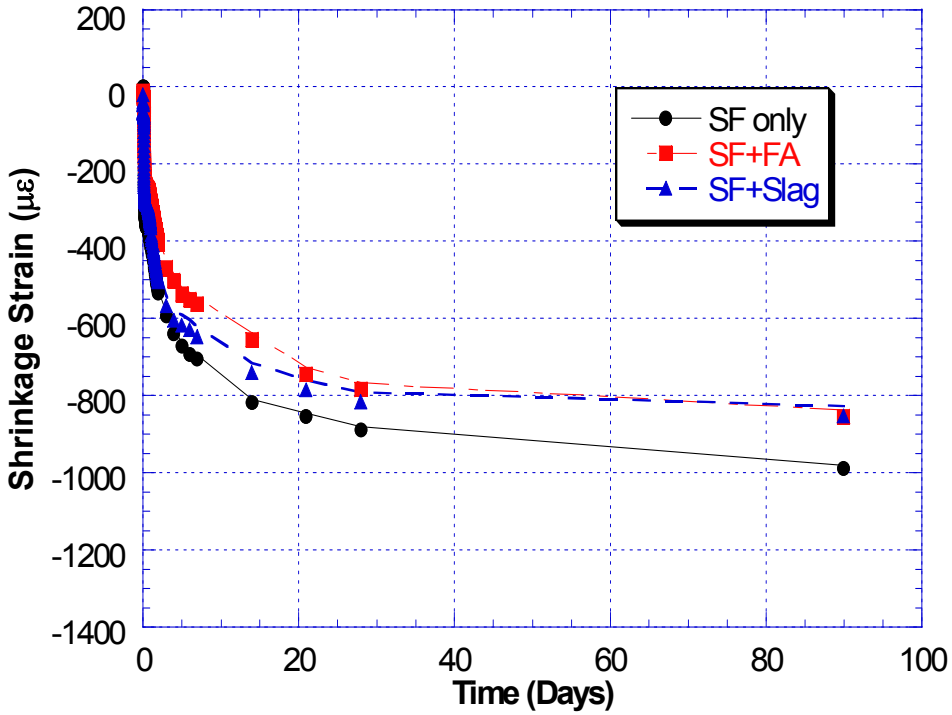

Figure 93. Effect of pozzolans on long-term shrinkage when with curing compound

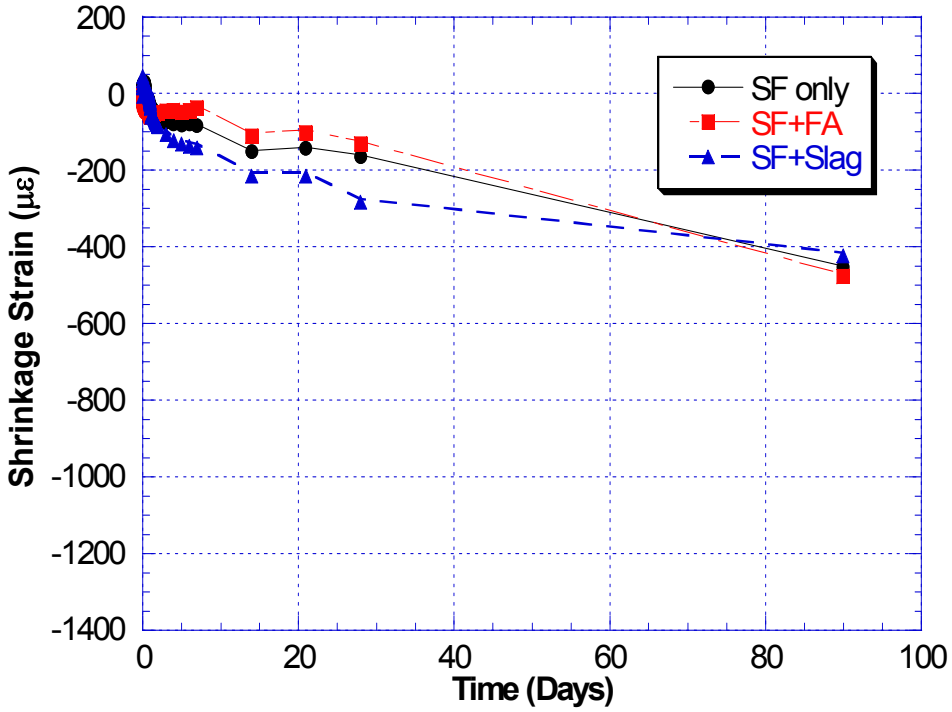

Figure 94. Effect of pozzolans on long-term shrinkage with burlap curing

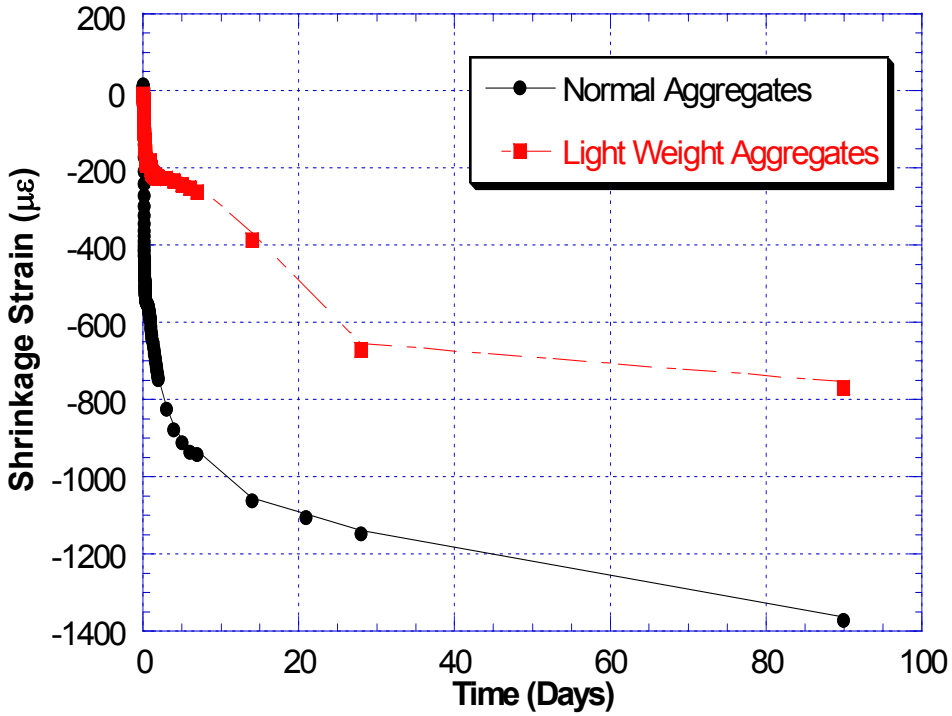

Figure 95. Effect of aggregates on long-term shrinkage with dry curing

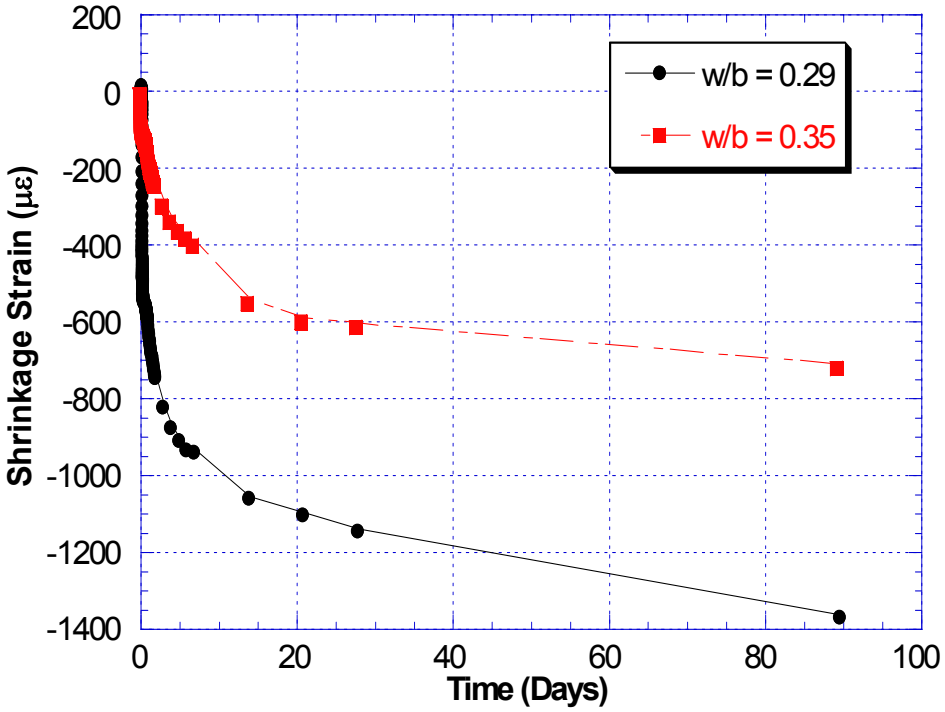

Figure 96. Effect of w/b on long-term shrinkage with dry curing

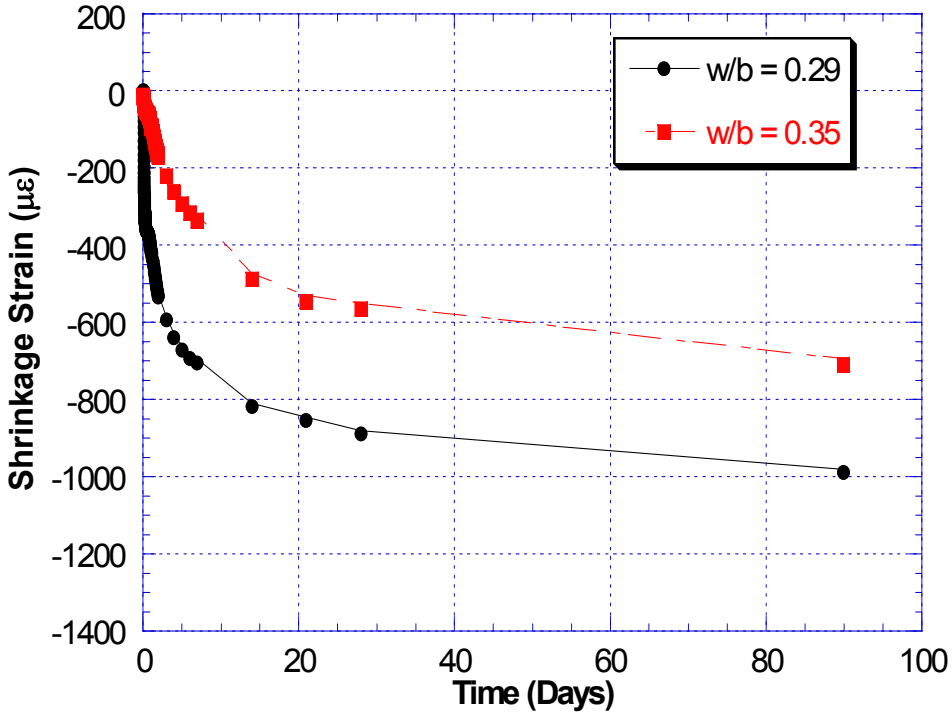

Figure 97. Effect of w/b on long-term shrinkage with curing compound

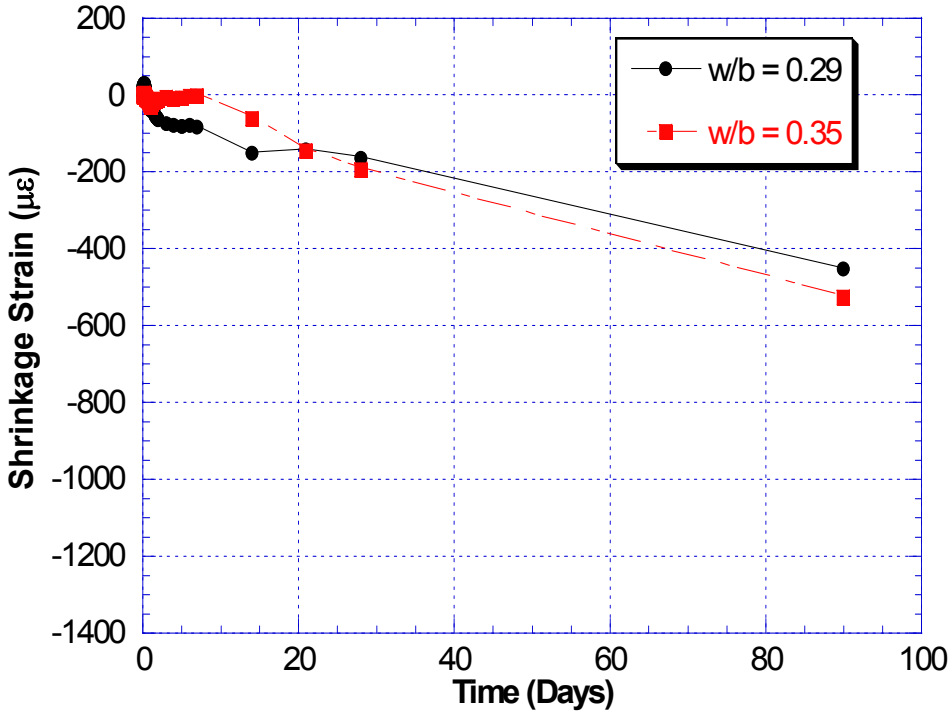

Figure 98. Effect of w/b on long-term shrinkage with burlap curing

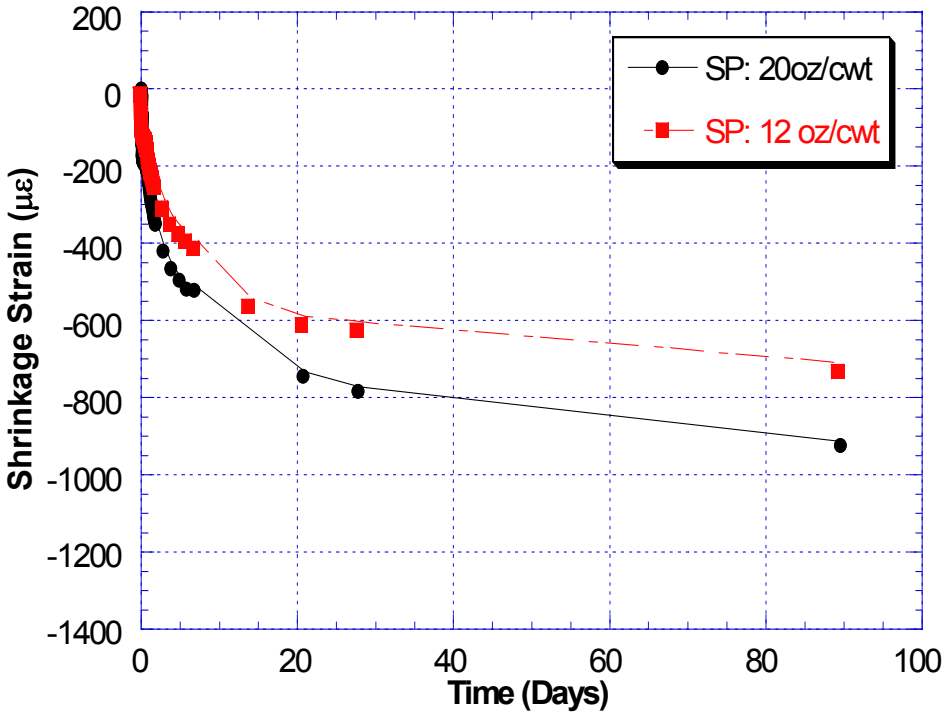

Figure 99. Effect of amount of superplasticizer on long-term shrinkage with dry curing

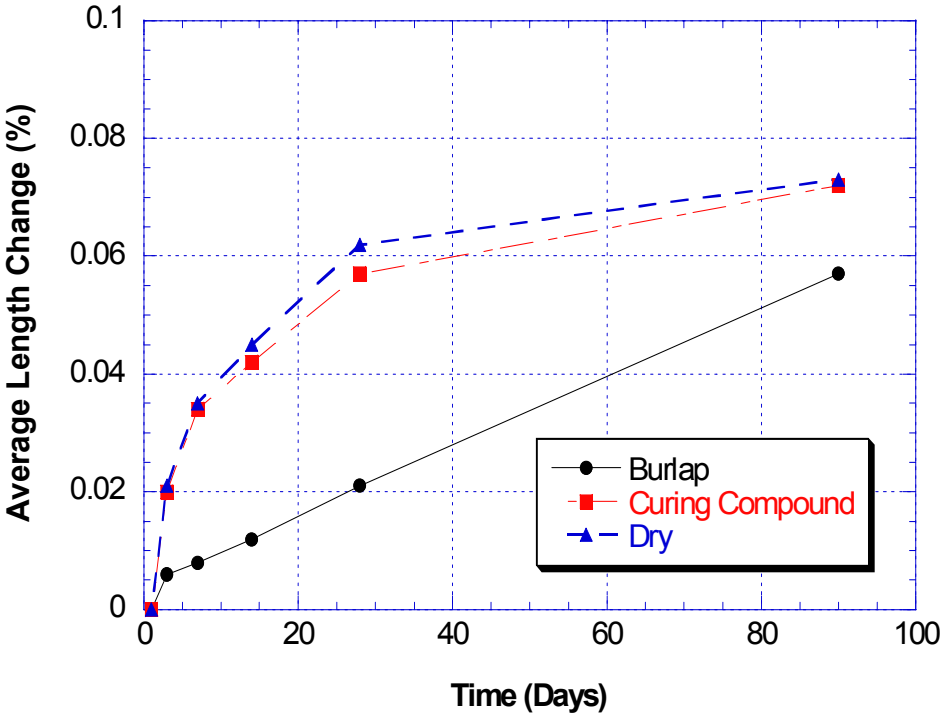

Figure 100. Effect of curing methods on drying shrinkage of mix L1

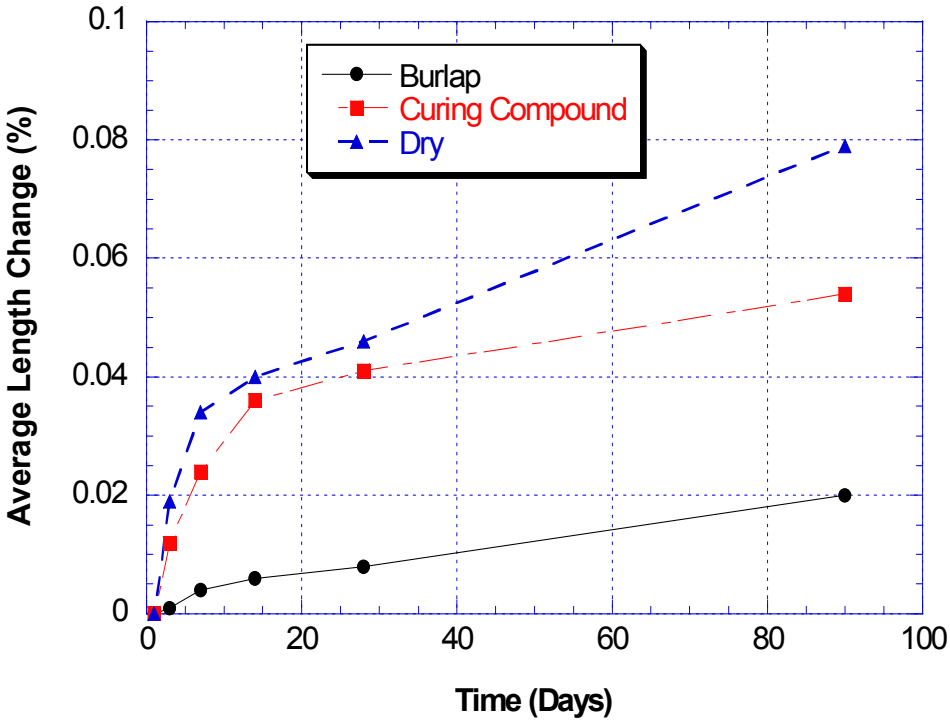

Figure 101. Effect of curing methods on drying shrinkage of mix L2

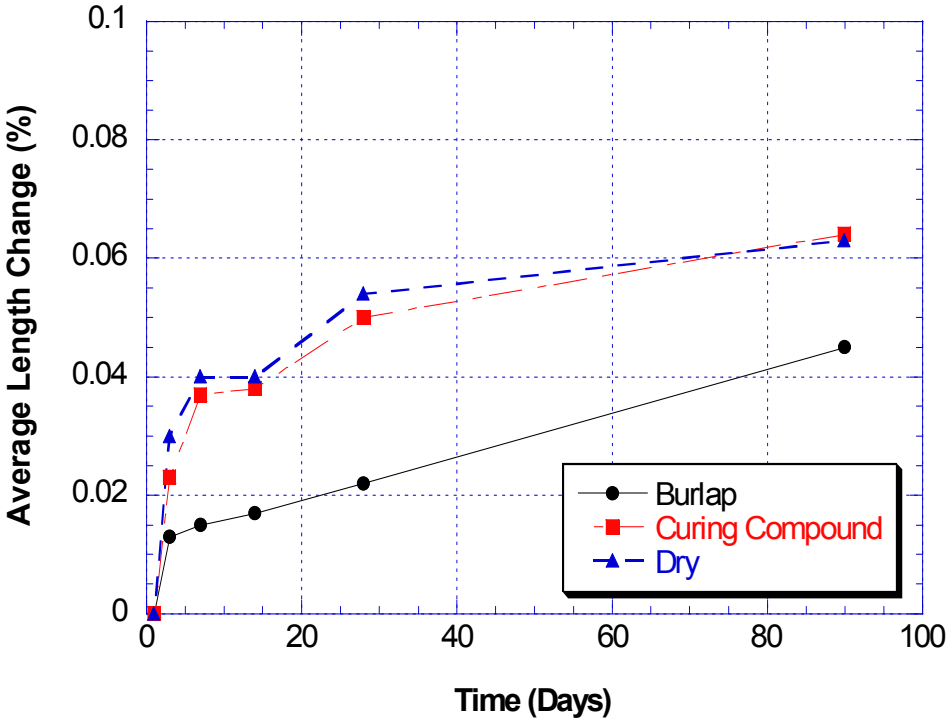

Figure 102. Effect of curing methods on drying shrinkage of mix L3

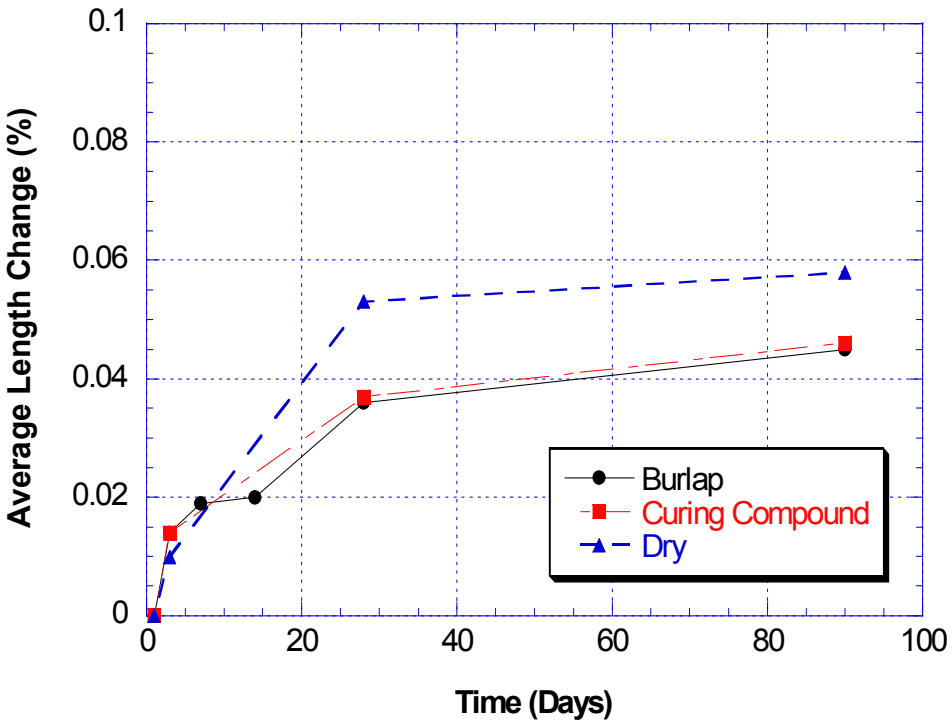

Figure 103. Effect of curing methods on drying shrinkage of mix L4

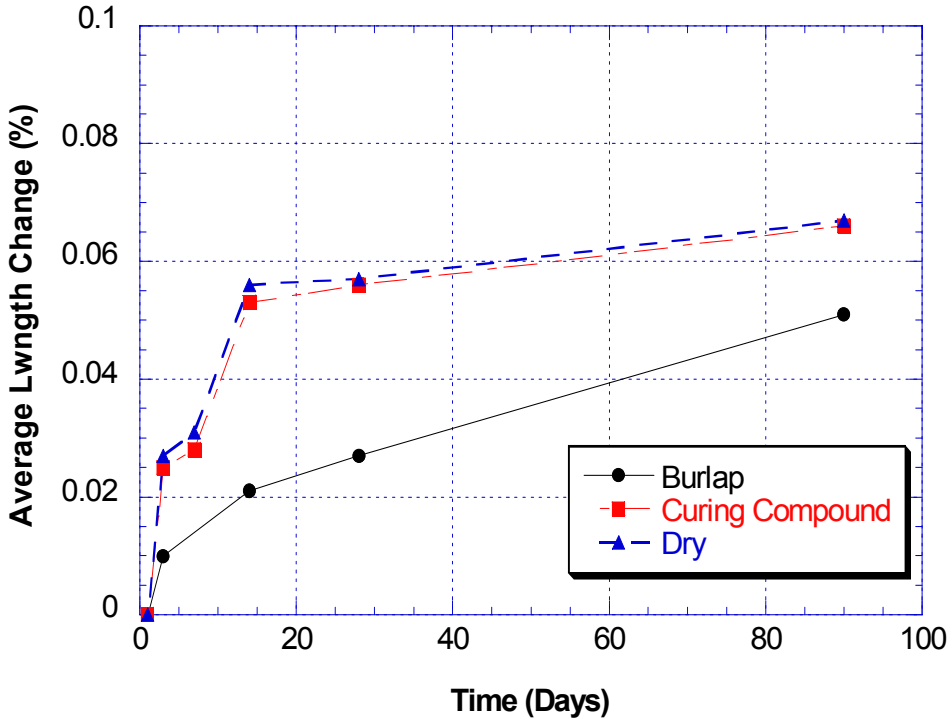

Figure 104. Effect of curing methods on drying shrinkage of mix M1

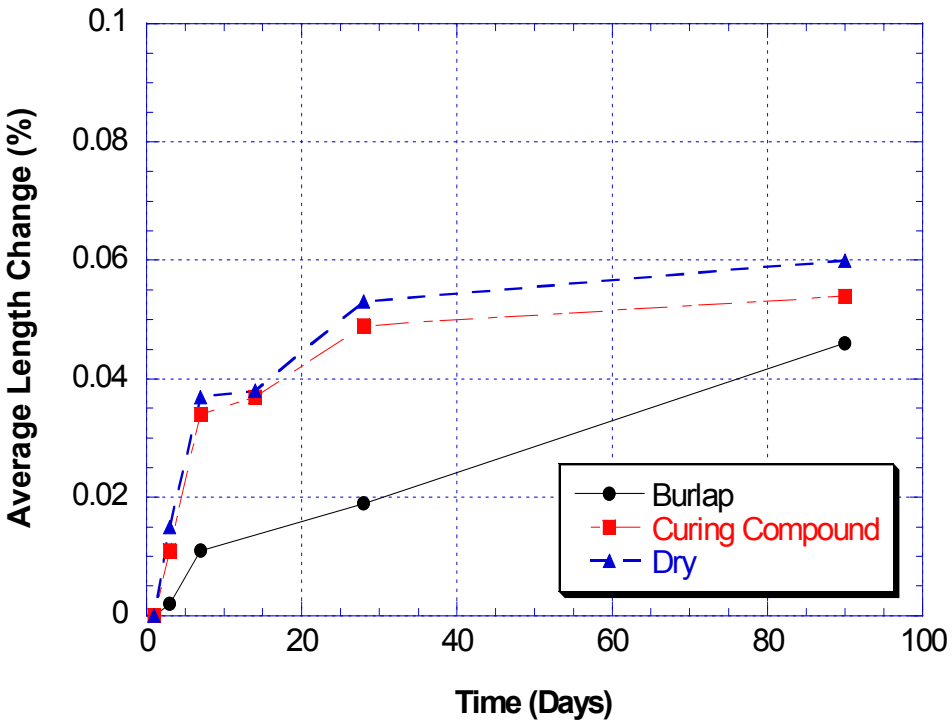

Figure 105. Effect of curing methods on drying shrinkage of mix M2

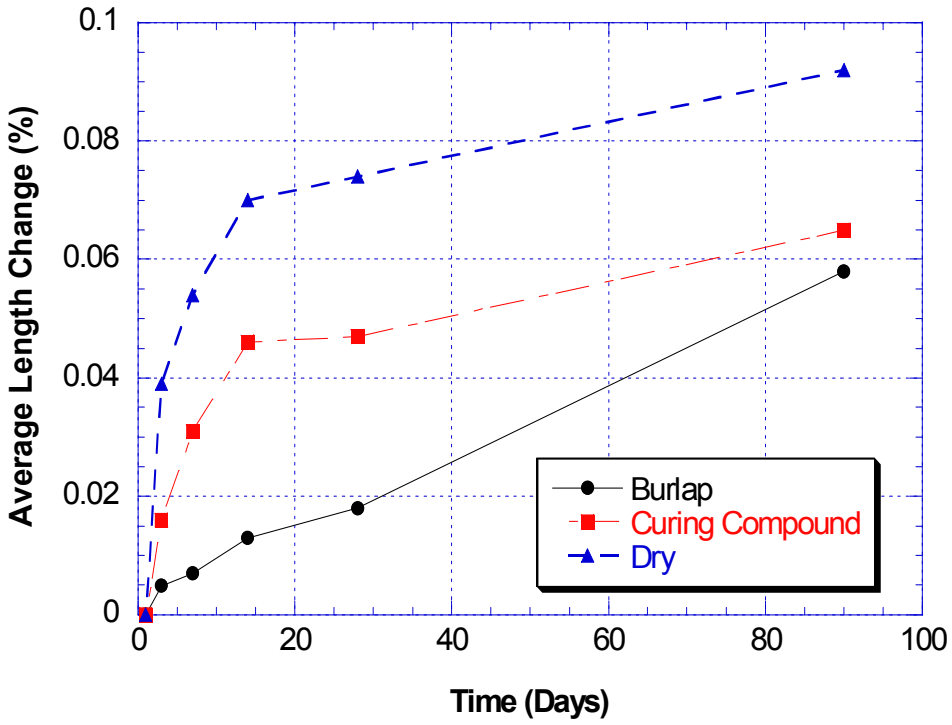

Figure 106. Effect of curing methods on drying shrinkage of mix M3

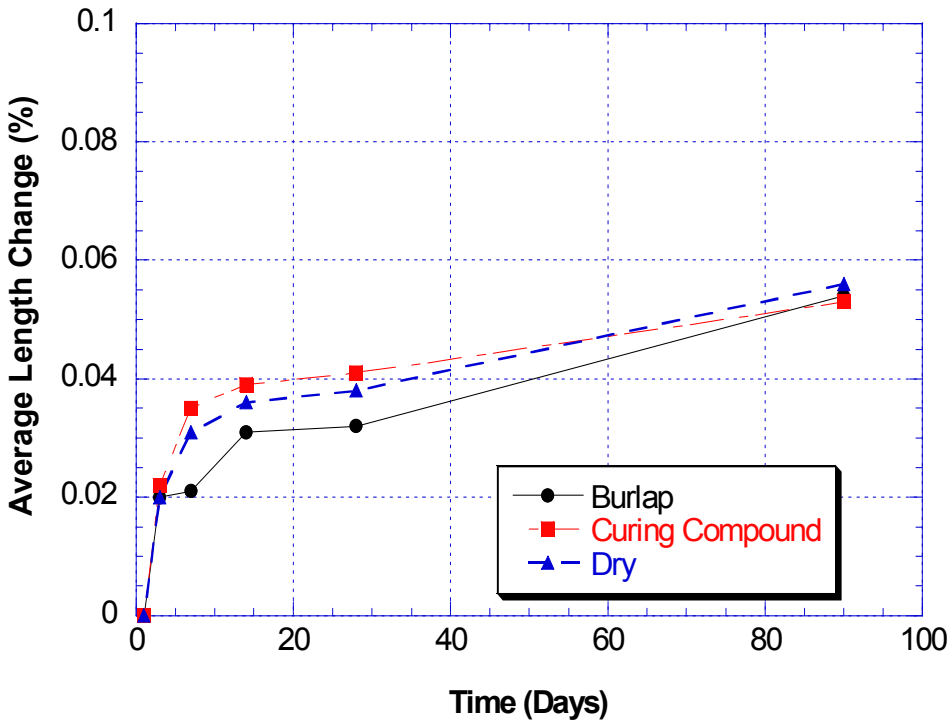

Figure 107. Effect of curing methods on drying shrinkage of mix M4

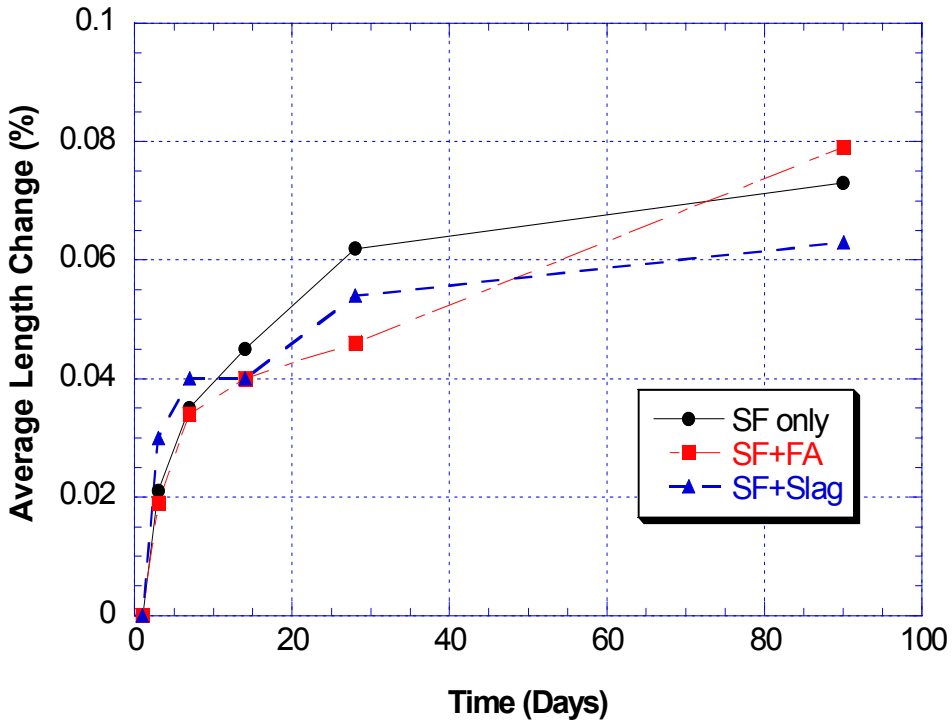

Figure 108. Effect of pozzolans on drying shrinkage with dry curing

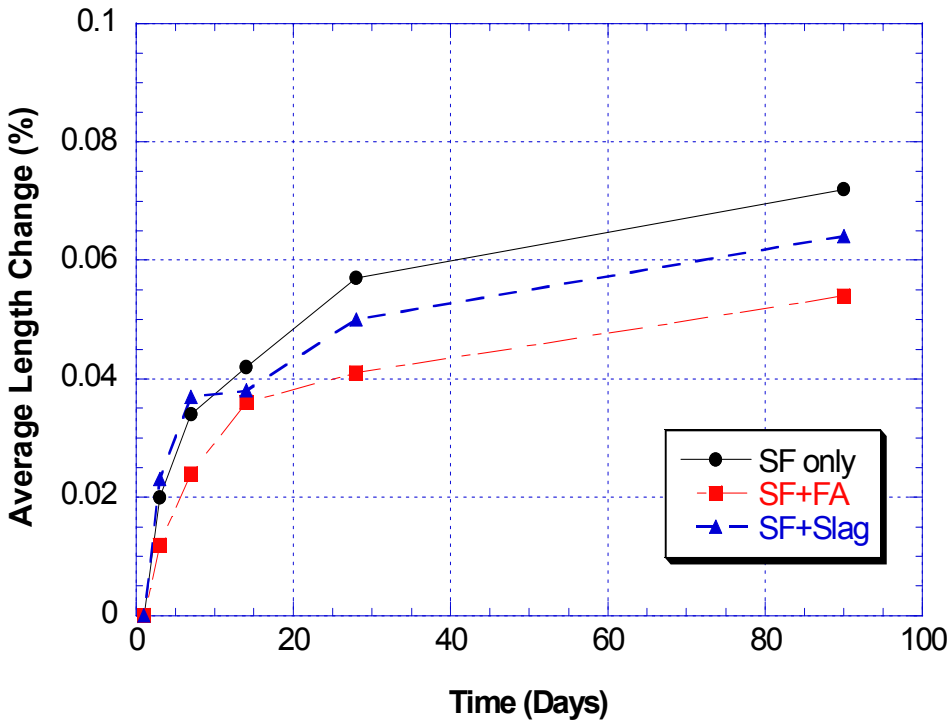

Figure 109. Effect of pozzolans on drying shrinkage with curing compound

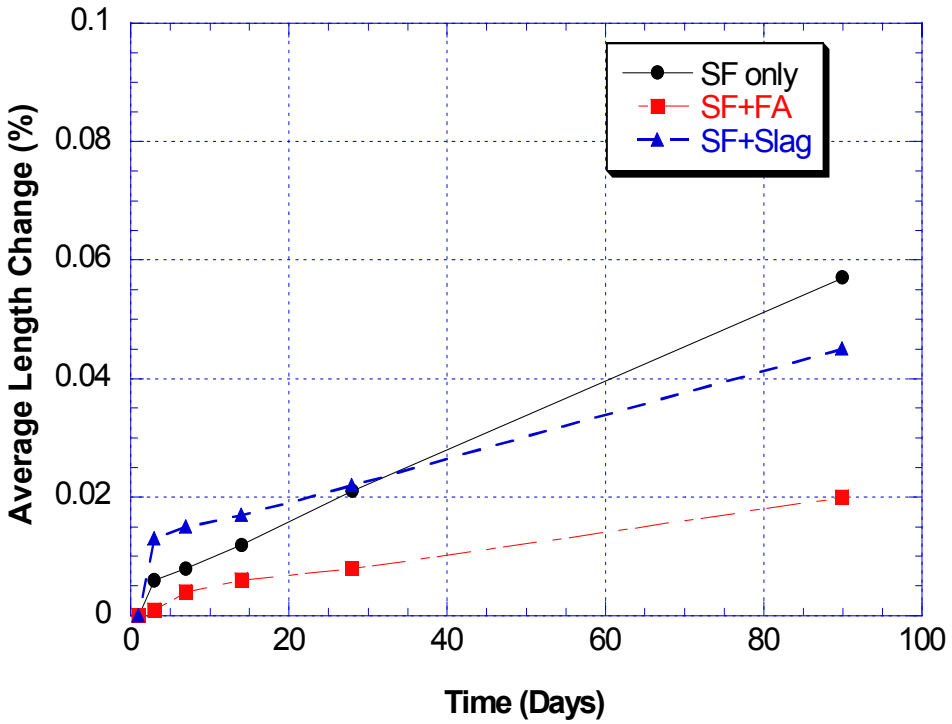

Figure 110. Effect of pozzolans on drying shrinkage with burlap curing

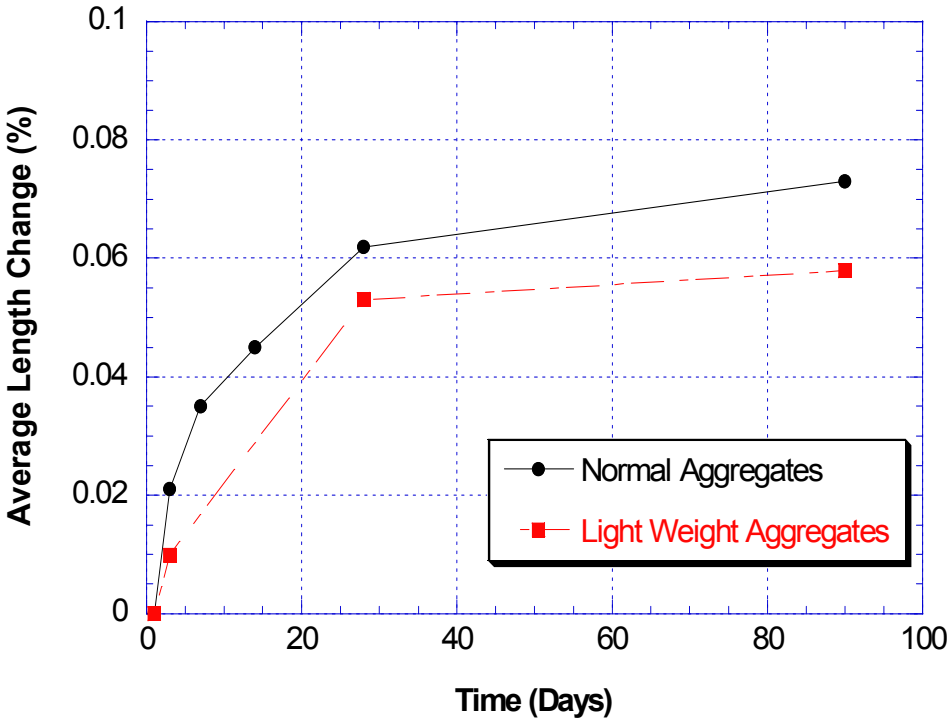

Figure 111. Effect of aggregates on drying shrinkage with dry curing

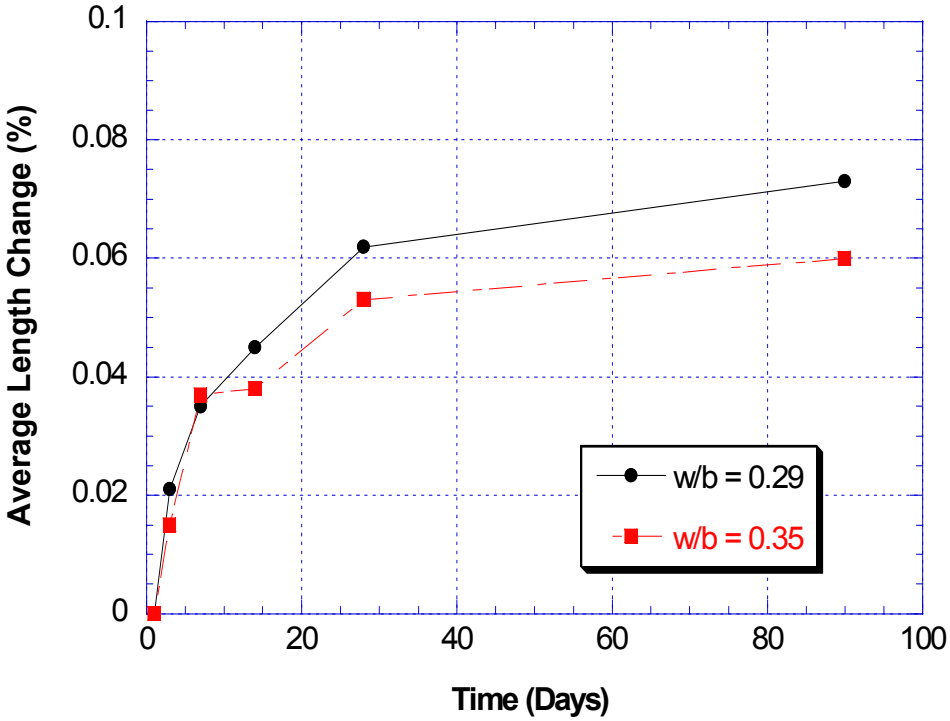

Figure 112. Effect of w/b on drying shrinkage with dry curing

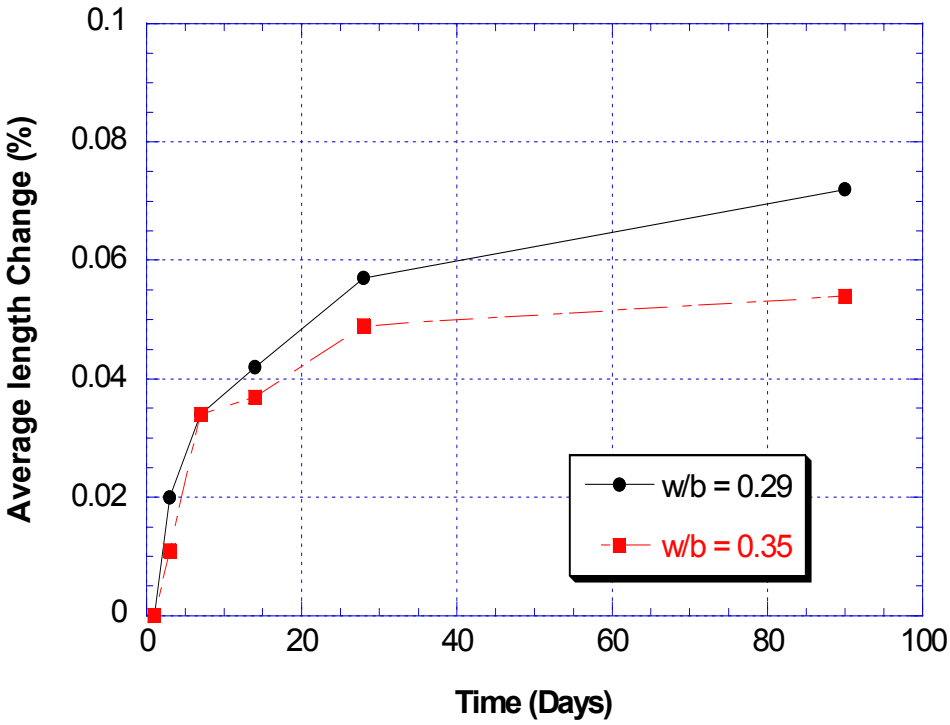

Figure 113. Effect of w/b on drying shrinkage with curing compound

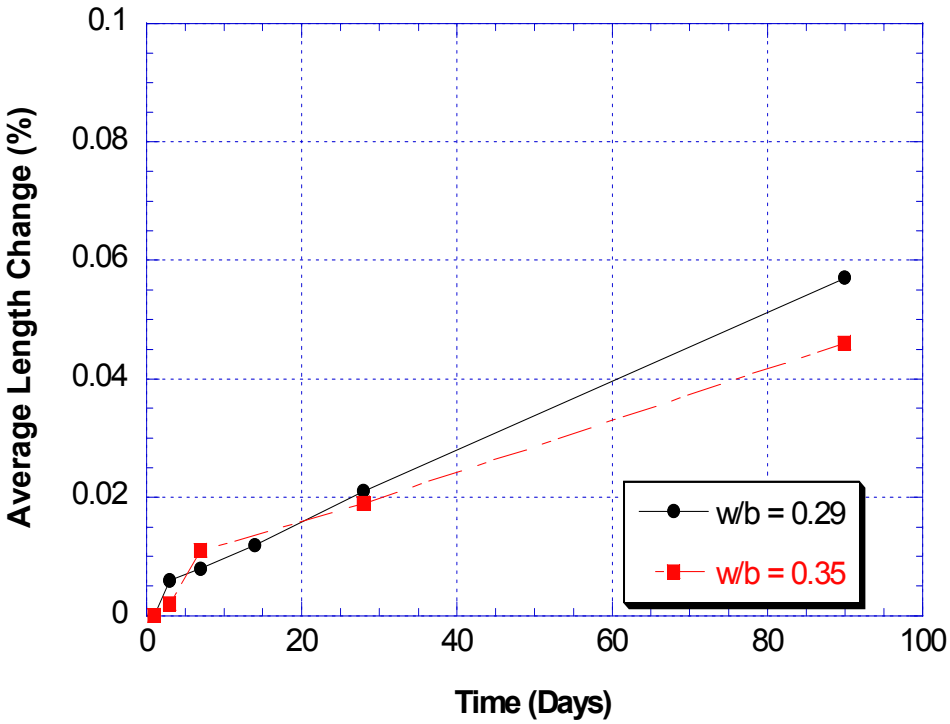

Figure 114. Effect of w/b on drying shrinkage with burlap curing

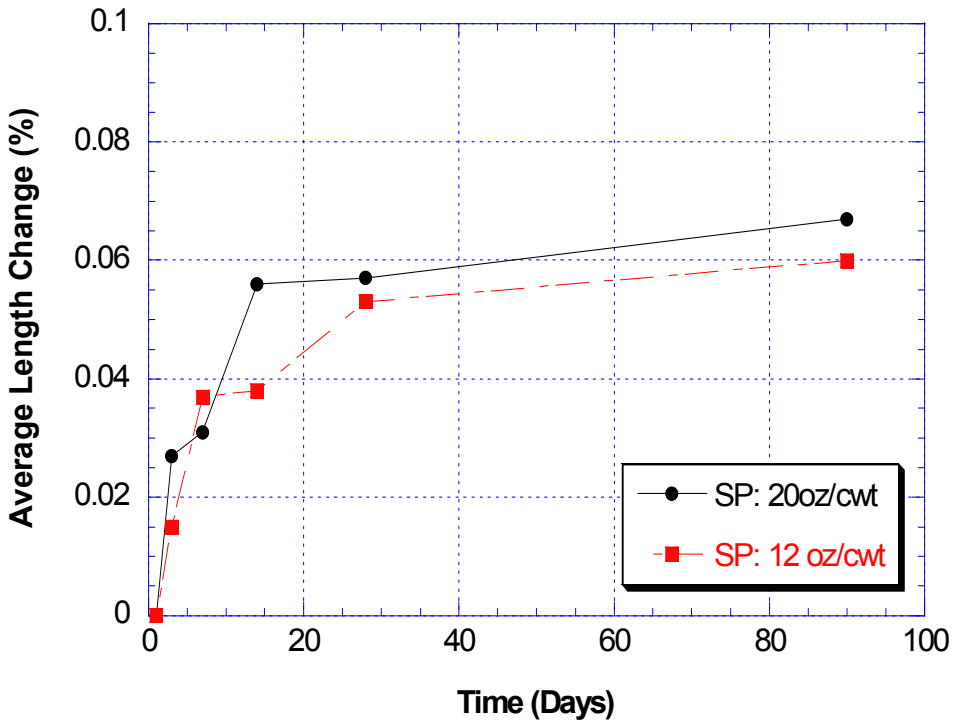

Figure 115. Effect of amount of superplasticizer on drying shrinkage with dry curing

REFERENCES

1) Annual Book of ASTM Standard, Volume 04.02, Concrete and Aggregate, 1996
2) Minnick, L. J., Webster, W. C., and Purdy, E. J., "Prediction of the Effect of Fly Ash in portland Cement Mortar and Concrete," J. of Materials (ASTM), Vol. 6, No.1, 1971, pp. 163-187.
3) Mehta, P. K., "Pozzolanic and Cementitious Byproducts as Mineral Admixtures for Concrete – A Critical Review," ACI, SP-79, 1983, pp. 1 – 46.
4) Sturrup, V. R., Hooton, R. D., Clendenning, T. G., "Durability of Fly Ash Concrete," ACI, SP-79, 1983, pp. 71 – 86.
5) Samarin, A., Munn, R. L., Ashby, J. B., "The Use of Fly Ash in Concrete – Australian Experience," ACI, SP-79, 1983, pp. 143 – 172.
6) Dunstan, M. R. H., Thomas, M.D.A., Cripwell, J.B., and Harrison, D.J., "Investigation into the Long-Term In-Situ Performance of High Fly Ash Content Concrete Used for Structural Application," ACI, SP-132, 1992, pp. 1 – 20.
7) Berry, E. E., Hemmings, R. T., Langley, W.S., and Carette, G. G., "Beneficiated Fly Ash Hydration, Microstructure, and Strength Development in Portland Cement Systems," ACI, SP-114, 1989, pp. 241 – 273.
8) Carette, G. G., Bilodeau, A., Chevrier, R. L., and Malhotra, V. M. "Mechanical Properties of Concrete Incorporating High Volumes of Fly Ash From Sources in the U.S.," ACI Materials Journal, Nov-Dec 1993, Vol. 90, No. 6, pp 535-544.
9) Costa, U., and Massazza, F., "Some Properties of Pozzolanic Cements Containing Fly Ashes," ACI, SP-79, 1983, pp. 235 – 254.
10) Gebler, S. Klieger, P., "Effect of Fly Ash on the Air-Void Stability of Concrete," ACI, SP-79, 1983, pp. 103 – 142.
11) Sivasundaram, V., Carette, G. G., Malhotra, V. M., "Properties of Concrete Incorporating Low Quantity of cement and High Volumes of Low-Calcium Fly Ash," ACI, SP-114, 1989, pp. 45 – 71.
12) Gebler, S. H., and Klieger, P., "Effect of Fly Ash on the Durability of Air-Entrained Concrete," ACI, Sp-91, 1986, pp. 483 – 519.
13) Roy, D. M., "Fly Ash and Silica Fume Chemistry and Hydration," ACI, SP-114, 1989, pp. 117 – 138.
14) Gautefall, O. and Havdahl, J., "Effect of Condensed silica fume on the Mechanism of Chloride Diffusion into Hardened Cement Paste," ACI, SP – 114, 1989, pp. 849 – 860.
15) Gagné, R., Pigeon, M., Revertégat, E., and Aïtcin, P.C., "Chloride-Ion Attack on Low Water-Cement Ratio Pastes Containing Silica Fume," ACI, SP – 132, 1992, pp. 1471 – 1490
16) Mehta, P. K., "Pozzolanic and Cementitious By-Products in Concrete – Another Look," ACI, SP 114, 1989, pp. 1 – 44.
17) Lamond, J. F., "Twenty-five Years' Experience using Fly Ash in Concrete," ACI, SP-79, 1983, pp. 47 – 70.
18) Gebler, S. H., Klieger, P., "Effect of Fly Ash on Physical Properties of Concrete," ACI, SP-91, 1986, pp. 1 – 50.

19) Tse, E. W., Lee, D. Y., and Klaiber, F. W., “Fatigue Behavior of Concrete Containing Fly Ash,” ACI, SP-91, 1986, pp. 273 – 290.
20) Nasser, K. W., and Al-Manaseer, A. A., “Shrinkage and Creep of Concrete Containing 50 Percent Lignite Fly Ash at Different Stress-Strength Ratios,” ACI, SP-91, 1986, pp. 433 – 448.
21) Swamy, R. N., and Mahmud, H. B., “Mix Proportions and Strength Characteristics of Concrete Containing 50 Percent Low-Calcium Fly Ash,” ACI, SP-91, 1986, pp. 413 – 432.
22) Nasser, K. W., and Marzouk, H. M., “Properties of Concrete Made with Sulfate Resisting Cement and Fly Ash,” ACI, SP-79, 1983, pp. 383 – 396.
23) Ukita, K., Ishii, M., Yamamoto, K., Azuma, K., and Kohno, K., “Properties of High Strength Concrete Using “Classified Fly Ash,”” ACI, SP-132, 1992, pp. 37 – 52.
24) Bilodeau, A., and Malhotra, V.M., “Properties of high-Volume Fly Ash Concrete Made with High Early-Strength ASTM Type III Cement,” ACI, SP-153, 1995, pp. 1 – 23.
25) Freeman, R.B., Carrasquillo, R.L., “Effects of Interfrinding Fly Ash on the Sulfate Resistance of Fly Ash Concrete,” ACI, SP-132, 1992, pp. 281 – 297.
26) Whiting, D., “Deicer Scaling Resistance of Lean Concretes Containing Fly Ash,” ACI, SP-114, 1989, pp. 349 – 372.
27) Nasser, K. W., Lai, P.S.H., “Resistance of Fly Ash Concrete to Freezing and Thawing,” ACI, SP-132, 1992, pp. 205 – 226.
28) Carette, G. G., Malhotra, V. M., Bedard, C., De Benedictis, V., Plumat, M., “Development of Heat-Curing Cycles for Portland Cement-Fly Ash Concrete for the Precast Industry,” ACI, SP-91, 1986, pp. 249 – 272.
29) Killoh, D. C., Parrott, L. J., and Patel, R. G., “Influence of Curing at Different Relative Humidities on the Hydration and Porosity of a Portland/Fly Ash Cement Paste,” ACI, SP-114, 1989, pp. 157 – 174.
30) Thomas, M. D. A., Matthews, J. D., Haynes, C. A., “The Effect of Curing on the Strength and Permeability of PFly Ash Concrete,” ACI, SP-114, 1989, pp. 191 – 217.
31) Barrow, R. S., Hadchiti, K. M., Carrasquillo, P. M., and Carrasquillo, R. L., “Temperature Rise and Durability of Concrete Containing Fly Ash,” ACI, SP-114, 1989, pp. 331 – 347.
32) Vandewalle, L., and Mortelmans, F., “The Effect of Curing on the Strength Development of Mortar Containing High Volume of Fly Ash,” ACI, SP-132, 1992, pp. 53 – 63.
33) Luther, M. D. and Hansen, W., “Comparison of Creep and Shrinkage of High-Strength Silica Fume Concretes with Fly Ash Concretes of Similar Strengths,” ACI, SP-114, 1989, pp. 573 – 591.
34) Marusin, S.L., “Influence of Fly Ash and Moist Curing Time on Concrete Permeability,” ACI, SP-132, 1992, pp. 257 – 269.
35) Bilodeau, A., and Malhotra, V.M., “Concrete Incorporating High Volumes of ASTM Class F Fly Ashes: Mechanical Properties and Resistance to Deicer Salt Scaling and to Chloride-Ion Penetration,” ACI, SP-132, 1992, pp. 319 – 349.

36) Ramachandran, S., Ramakrishnan, V., and Johnston, D., “The Role of High Volume Fly Ash in Controlling Alkali-Aggregate Reactivity,” ACI, SP-132, 1992, pp. 591 – 613.
37) Thomas, M.D.A., Mukherjee, P.K., Sato, J.A., and Everitt, M.F., “Effect of Fly Ash Composition on Thermal Cracking in Concrete,” ACI, SP-153, 1995, pp. 81 – 98.
38) Hindy, E. E., Miao, B., Chaallal, O., and Aitcin, P.C., "Drying Shrinkage of Ready-Mixed High-Performance Concrete" ACI Materials Journal, May-Jun 1994, Vol. 91, No. 3, pp 300-305.
39) Charif, H., Jaccoud, J-P., and Alou, F. "Reduction of Deformations with the Use of Concrete Admixtures" Admixtures for Concrete: Improvement of Properties, Proceedings of the International Symposium held by RILEM, May 14-17, 1990, Barcelona, Spain; Ed. by E. Vazquez; Chapman and Hall, London, 1990, pp 402-428.
40) Al-Khaja, Waheeb A. “Strength and time-dependent deformations of silica fume concrete for use in Bahrain,” Construction & Building Materials, v 8 n 3, Sept 1994, p 169-172
41) Wiegrink, Karl. Marikunte, Shashidhara. Shah, Surendra P. “Shrinkage cracking of high-strength concrete,” ACI Materials Journal, v 93 n 5, Sep-Oct 1996, p 409-415.
42) Koveler, K., Igarashi, S., and Bentur, A., “Tensile Creep Behavior of High Strength Concretes at Early Ages,” Materials and Structures, V32, June 1999, pp. 383-387.
43) Kanstad, T., Bjøntegaard, O., Sellevold, E.J., Hammer, T.A., and Fidjestøl, P., “Effect of Silica Fume on early age crack sensitivity of High Performance Concrete,” RILEM Proceeding 17: Shrinkage of Concrete-‘Shrinkage 2000’.
44) Persson, B. “Correlating laboratory and field tests of creep in high-performance concrete,” Cement & Concrete Research, v 31 n 3, March 2001, p 389-395.
45) Alexander, M G. “Deformation properties of blended cement concretes containing blast furnace slag and condensed silica fume,” Advances in Cement Research, v 6 n 22, Apr 1994, p 73-81.
46) Khatri, R P. Sirivivatnanon, V. Gross, W. “Effect of different supplementary cementitious materials on mechanical properties of high performance concrete,” Cement & Concrete Research, v 25 n 1, Jan 1995, p 209-220
47) Li, H., Wee, T. H., and Wong, S.F., “Early-Age Creep and Shrinkage of Blended Cement Paste,” ACI Materials Journal, V. 99, No. 1, Jan –Feb 2002.
48) Berke, N.S., “Resistance of Microsilica Concrete to Steel Corrosion, Erosion, and Chemical Attack,” ACI, SP – 114, 1989, pp. 861 – 886.
49) ACI 211.4R.93. “Guide for Selecting Proportions for High –Strength Concrete with Portland Cement and Fly Ash,” ACI Manual of Concrete Practice. Part 1. American Concrete Institute, Detroit, 1994.
50) The New Hampshire Department of Transportation, The University of New Hampshire, and The Federal Highway Administration, “SHRP High Performance Concrete Showcase”, September 22-23, 1997
51) Transportation Inspector Reference Package, Publication CP – 31
52) Yamato, T., Sugita, H., “Shrinkage and Creep of Mass Concrete Containing Fly Ash,” ACI, SP-79, 1983, pp. 87 – 102.
53) Berke, N.S., “Resistance of Microsilica Concrete to Steel Corrosion, Erosion, and Chemical Attack,” ACI, SP – 114, 1989, pp. 861 – 886.

54) Helmuth, R.A., " Water-Reducing Properties of Fly Ash in Cement Pastes, Mortars, and Concretes: Causes and Test Methods," ACI, SP-91, 1986, pp. 723 – 740.
55) Wiegrink, K., Marikunte, S., and Shah, S.P., "Shrinkage Cracking of High Strength Concrete," ACI Materials Journal, V93, No. 5, Sep-Oct 1996.
56) Igarashi, S., Bentur, A., Kovler, K., "Autogenous shrinkage and induced restraining stresses in high strength concretes," Cement and Concrete Research. v 30 n 11 Nov 2000, pp. 1701-1707.
57) Kohno, K., Okamoto, T., Isikawa, Y., Sibata, T., Mori, H., "Effects of artificial lightweight aggregate on autogenous shrinkage of concrete," Cement and Concrete Research. v 29 n 4 1999, pp. 611-614.
58) Lura, P. Van Breugel, K. Maruyama, I., "Effect of curing temperature and type of cement on early age shrinkage of High Performance Concrete", Cement and Concrete Research. v 31 n 12 December 2001.p 1867-1872.
59) Sakata, K. and Ayano, T., "The Effect of Ambient Temperature on Creep and Shrinkage of Concrete," Presented at the 1997 Fall Convention, ACI, Atlanta, Georgia, USA, Nov. 9-14, 1997.
60) ACI Committee 209, "Prediction of Creep, Shrinkage, and Temperature Effects in Concrete Structures", Report No. ACI 209R-82, ACI, SP-76, 1982, pp. 193-300.
61) Branson, D.E., and Christiason, M.L., "Time-Dependent Concrete Properties related to Design-Strength and Elastic Properties, Creep, and Shrinkage," Design for Effects of Creep, Shrinkage, and Temperature in Concrete Structures, ACI Publication SP-76, pp. 257-277.
62) CEB-Bulletin d'Inforamtion No. 203/204/205: CEB-FIP Model Code 1990, Final Draft 1991. Commite Euro-International du Beton (CEB), Lausanne, 1991.
63) Muller, H.S. and Hillsdorf, H.K., "CEB Bulletin d' information, No. 199, Evaluation of the Time Dependent Behavior of Concrete, Summary Report on the work of general Task Group 9," Sept. 1990, pp.290.
64) Muller, H.S., "New Prediction Model for Creep and Shrinkage of Concrete," ACI Publication SP-135, pp. 1-18.
65) Bazant, Z.P., and Baweja, S. "Creep and Shrinkage Prediction Model for Analysis and Design of Concrete Structures – Model B3," Materials and Structures, 1995, Vol. 28, pp. 357-365, 415-430, 488-495.
66) Gardner, N.J., and Marty Lockman, "Design Provisions for Drying Shrinkage and Creep of Normal – Strength Concrete," ACI Materials Journal, Mar-Apr 2001 Vol. 98, pp. 159-167.
67) Miyazawa, S. and Tazawa, E., "Prediction model for shrinkage of concrete including Autogenous shrinkage," Proc. of the 6th International Conference CONCREEP6@MIT- Creep, Shrinkage and Durability mechanics of concrete and other quasi-brittle materials, 2001, pp. 735-740.